Rapid Damage Detection in Buildings Through ARMAX Analysis of Wind Induced Vibrations

by

Gregory Patrick Gislason

A thesis submitted in partial fulfillment of the requirements for the degree of

Master of Science

in

Structural Engineering

Department of Civil and Environmental Engineering

University of Alberta

Abstract

After a seismic event, it is imperative that critical structural members that are damaged within a building are identified and analyzed as soon as possible to ensure proper remedial measures can be taken. Failure to detect damage or correctly analyze the severity of damage within the building could have catastrophic consequences. When a reinforced concrete building is subjected to a damaging event, the standard method for identifying and analyzing structural damage currently involves extensive surface-level visual inspections which often result in inconclusive and inconsistent damage analysis. Structural Health Monitoring (SHM) is a rapidly developing field which is vastly improving the way damage is assessed within buildings and other major infrastructure. In this thesis, an automated SHM Damage Detection Model (DDM), specifically tailored for buildings, is developed that uses time series analysis along with sensor clustering techniques to detect damage in a building from its vibration response due to ambient wind loading. The specific time series analysis methodology used throughout this thesis is an Auto-Regressive Moving Average model with eXogenous inputs (ARMAX). To validate the ARMAX DDM, a detailed wind simulation model that applies forces based on actual wind behaviour is created along with a numerical damage model applicable to reinforced concrete buildings. To evaluate the effectiveness of the proposed DDM in locating and quantifying damage at storey-level precision, six different buildings are modelled in SAP2000. The results from the numerical modelling proved the effectiveness of the ARMAX DDM at accurately locating and quantifying the degree of damage from wind induced floor vibrations at storey-level precision. The limitations of the DDM in its current state and recommendations for future work are discussed to conclude the thesis.

Acknowledgements

I would first like to express my sincerest gratitude to my supervisor, Dr. Mustafa Gul, who has been a constant pillar of support throughout my graduate studies at the University of Alberta. Through his guidance, I was introduced to a field of civil engineering that is more exciting than anything I could have imagined prior to starting my degree. His support and mentorship was invaluable and my research could not have been completed without it.

I would like to thank the committee members of my MSc defense, Dr Ali Imanpour and Dr Douglas Tomlinson, for their time and helpful feedback.

I would also like to thank the other members of Dr Gul's research group, including Qipei Mei, Riasat Azim and Do Ngoan in particular, who was always willing to take time out of his busy schedule to assist me with my research and give me guidance.

Finally, I would like to thank my friends and family. Most of all, I would like to thank Lisa Cruthers, whose unconditional love and support helped me in more ways than can possibly be imagined. I could not have completed this master's degree without her and am forever grateful to have her in my life.

Table of Contents

List of Tables

List of Figures

List of Abbreviations

ANN	Artificial Neural Network
AR	Auto-Regressive model
ARMA	Auto-Regressive Moving Average model
ARMAV	Auto-Regressive Moving Average Vector model
ARMAX	Auto-Regressive Moving Average model with eXogenous inputs
ARX	Auto-Regressive model with eXogenous inputs
ASCE	American Society of Civil Engineers
B-J	Box-Jenkins model
CG	Correlation Generator
DDM	Damage Detection Model
DF	Damage Feature
DOF	Degree of Freedom
DR	Damage Ratio
DSF	Damage Senstive Feature
FE	Finite Element
FEMA	Federal Emergency Management Agency
MA	Moving Average model
MAC	Modal Assurance Criterion
MD	Mahalanobis Distance
MDOF	Multi-Degree-Of-Freedom
MIF	Multiple Impulse Force
MOM	Method of Moments
OMA	Operational Modal Analysis
PDF	Probability Density Function
RANS	Reynolds-Averaged Navier-Stokes
RC	Reinforced Concrete
SDF	Stiffness Damage Feature
SHM	Structural Health Monitoring
SR	Slope Ratio
TSA	Time Series Analysis
VAR	Vector Auto-Regressive model

CHAPTER 1: INTRODUCTION

When a building undergoes a seismic event, the typical method for locating and analyzing any potential structural damage involves lengthy surface-level visual inspections by structural engineers where each critical member is classified in a damage category based on visual inspections and the engineer's judgement. Such an arbitrary inspection method often leads to inconclusive and inconsistent damage analysis.

This thesis presents an automated Structural Health Monitoring (SHM) system based on Time Series Analysis (TSA) capable of rapidly providing engineers with the location and degree of damage at storey-level precision from the building's vibration due to ambient wind forces. This model aims to complement lengthy visual inspections and subjective scaling constants to provide a more efficient, consistent and accurate damage assessment.

The following section introduces the field of SMH, various damage detection methods and existing seismic damage analysis methods.

1.1. Introduction to Structural Health Monitoring

Structural Health Monitoring refers to the process of implementing a damage identification strategy and condition assessment for aerospace, civil and mechanical structures (Farrar & Worden, 2007). The domain of SHM in this thesis refers specifically to monitoring the damage and change in structural properties (i.e. stiffness, mass, damping coefficients, boundary conditions) of a building before and after an earthquake has occurred. SHM has seen substantial progress due to the rapid development of advanced technologies in the areas of computer science and electrical engineering; it is now more convenient and cheaper to acquire large amounts of data. Despite this abundant data, the proper way to detect damage is still a big challenge. In existing literature, widely available technologies have spawned a range of SHM techniques applicable to both buildings and other infrastructure (Dharap et al., 2006; Hearn et al., 1991; Im et al., 2013; Moaveni et al., 2013; A.K. Pandey et al., 1991). One of the most important factors in a successful SHM system is to be able to detect damage regardless of operational or loading conditions (Bernal et al., 2004; Fan et al., 2011; J.P. Lynch et al., 2006). Note that SHM techniques are not limited to only buildings, SHM systems have been applied to all kinds of civil infrastructures in real-world scenarios

(Carpinteri et al., 2006; Chae et al., 2012; Dharap et al., 2006; Ko et al., 2005; Koo et al., 2013;; VanZwol et al., 2008; Wong, 2004).

1.2. Introduction to Damage Detection Techniques and Time Series Analysis

Damage detection is one of the most vital components of SHM, as the existence and location of damage must be determined before any mitigation measures can be undertaken. In general terms, damage refers to the changes introduced into a structure which lead to a decrease in its current and future performance. When considering seismic damage in reinforced concrete (RC) buildings, this will be primarily related to the changes in the material properties which will decrease the lateral stiffness of the structure.

According to Rytter (1993), any damage detection should focus on the following four objectives: 1) identifying the existence of damage; 2) localizing the damage; 3) determining the severity of damage; 4) estimating the remaining useful life. Among the numerous damage detection techniques available in the literature, objectives 1, 2, and 3 have attracted a great deal of attention as identifying and locating any potential damage is paramount to complete any critical remedial work.

Damage detection methods (DDMs) can be divided into two distinct categories, local methods and global methods (Johnson et al., 2004). Local methods focus on detecting damage in a relatively small area using techniques such as ultrasonic waves and X-ray detection (Kessler et al., 2002a; Hola and Schabowicz, 2010; Cheng and Tian, 2012). The local methods are considered a different subject area and are not directly related to this thesis. Despite not being directly related, the ARMAX DDM presented in this thesis can potentially be used as a tool to locate damage at storey-level precision which can then be followed up with local damage detection methods to further analyze the damage.

Global damage detection methods, also known as vibration-based methods, assess the condition of the entire structure through its dynamic response. The vibration based methods are categorized as either parametric or non-parametric methods. The general idea behind parametric techniques is that local changes in stiffness, mass or damping will influence the global properties of the structure such as the natural frequencies, mode shapes, and damping parameters (Shiradhonkar and Shrikhande, 2011; Siebel et al., 2012; Hamze et al., 2014). Developing such physics based methods require detailed knowledge and significant experience and these methods tend to struggle when

handling large amounts of unrefined data. In addition, due to operational and environmental conditions, applying such techniques to real structures poses a significant challenge (Catbas et al 2007).

In recent decades, Time Series Analysis has seen a substantial amount of use in the field of SHM. A time series is a sequence of well-defined data points measured at consistent time intervals over a specified period of time. Time series modelling is the use of statistical methods to model time series data and extract the meaningful characteristics. As most of the time series methods do not explicitly define modal or other structural parameters as damage features, it is considered a non-parametric method. Some commonly used time series models include the Auto-Regressive (AR) model, the Moving Average (MA) model, the Box-Jenkins (B-J) model and the Auto-Regressive Moving Average model with eXogenous inputs. Recent technical papers have demonstrated the effectiveness of such techniques in detecting damage (Gul et al., 2009; Monroig et al., 2006; Nair et al., 2006; Hoon Sohn & Farrar, 2001; Trendafilove et al., 2008). These papers, along with a variety of other damage detection techniques are explored further in the Literature Review section.

1.3. Introduction to Seismic Damage Analysis

The Canadian standard procedure for analyzing seismic damage on a concrete structure is based off the *Guidelines for Seismic Evaluation of Existing Buildings* (NRCC, 1993). These guidelines are heavily based on the extensive research completed in the United States by the Federal Emergency Management Agency (FEMA), the American Society of Civil Engineers (ASCE) and the Applied Technology Council (ATC).

When a structure undergoes a seismic event, the concrete members are visually inspected as per *ATC-20-1: Procedures for Post-earthquake Safety Evaluation of Buildings* (ATC, 2005). The procedure guides the damage inspector in assigning a post-earthquake status through extensive checklists and the structure's occupancy status is assigned based on the estimated potential of the structure to undergo an identical seismic event without collapse. The degree of damage is determined by inspecting the width of the cracks, the buckling of reinforcement and spalled concrete cover in the damaged concrete members.

After the structure is inspected, the results from the ATC-20-1 report are analyzed with standards created in *ASCE 41-17: Seismic Evaluation and Retrofit of Existing Buildings* (ASCE, 2017). The standards issued by the ASCE with regards to concrete structures are specified in *FEMA 306-308:*

Evaluation of Earthquake Damaged Concrete and Masonry Wall Buildings (FEMA, 1998). These documents state that to determine the capacity of a member under seismic loading, dynamic analysis must be undertaken. The dynamic analysis procedure involves first creating a force deformation envelope for an undamaged column or wall through hysteric testing, as shown in Figure 1-1. This is done either through numerical simulations or using approximate dynamic analysis methods.

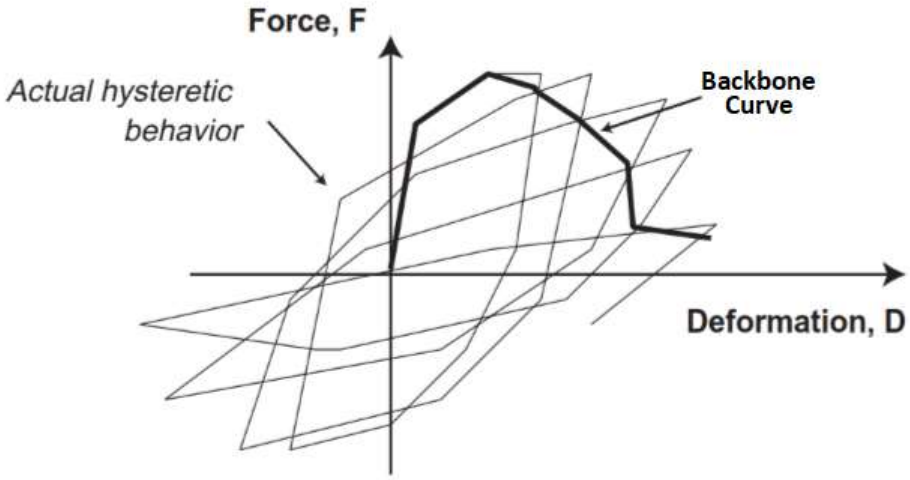

Figure 1-1 Force Deformation Envelope (Adapted from FEMA 306, 1999)

Once an undamaged force deformation envelope is created, the envelope is then reduced by empirical scaling factors (λ) to account for the damage as per Figure 1-2. The degree of the reduction factors are primarily based on shear and flexural crack widths and the presence of spalling. This new force deformation envelope represents the capacity of the shear wall post-earthquake.

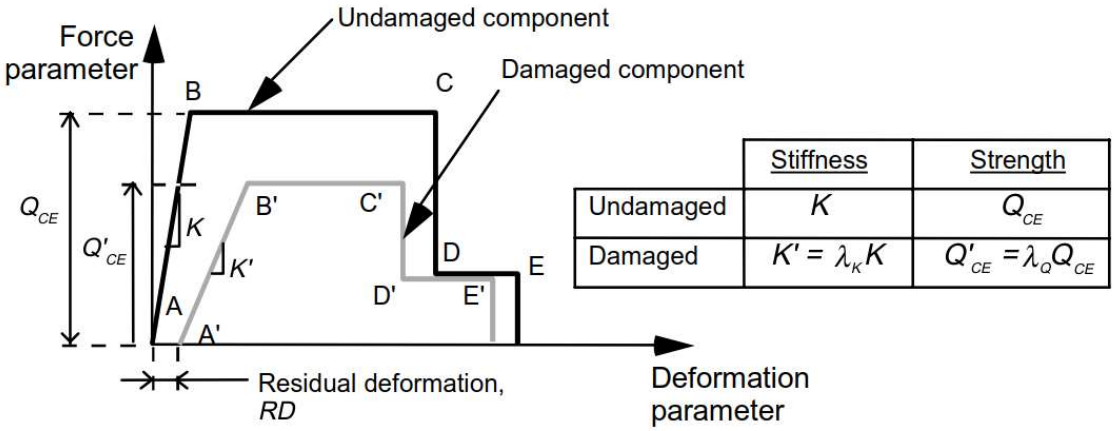

Figure 1-2 Undamaged and Damaged Force Deformation Envelopes (FEMA 306, 1999)

The common limitation of these visual inspections is that the final judgement on safety relies largely on the inspector's opinion, and as a result, a uniform evaluation between multiple inspectors cannot be guaranteed (Yazgan, 2009). Another prevalent issue is that it relies heavily on crack widths. This is not ideal as although a two-millimetre wide crack in a wall panel on the verge of shear-brittle failure is a very serious condition, in a flexural controlled panel, it may be insignificant with regard to future seismic performance (FEMA, 1999). To rely so heavily on crack widths to determine the new capacity of a member is not always a reliable solution.

In using time series analysis and determining an exact loss in stiffness for each story, a model can be created which would require no visual inspection and no arbitrary scaling constants to determine the new stiffness of a damaged member resulting in a more efficient, consistent and accurate damage assessment.

1.4. Objectives and Scope

The objective of this thesis is to create a damage detection model capable of rapidly locating and quantifying the degree of damage in a concrete frame structure through time series analysis of its dynamic response to ambient wind forces. To verify the validity of this DDM, numerical damage simulations are undertaken on a variety of building models.

To the best of the author's knowledge, this is the first time that a structure's response to ambient wind had been utilized to rapidly detect damage in a building at storey-level precision with

information on severity. When relating this damage detection methodology to the objectives presented by Rytter (1993), it satisfies the first three steps.

1.5. Organization of Thesis

The thesis is organized as follows:

Chapter 2 presents a review of damage detection methods available in literature with a focus on the recent achievements in damage detection techniques using time series models. Following that, the chapter will explore the past work done towards simulating wind speeds and location dependent pressure coefficients. The final section looks at different commonly used damage modelling techniques in reinforced concrete structures for numerical modelling.

Chapter 3 provides an overview on how, using the acceleration response of a structure with sensor clustering, this DDM is capable of detecting damage in a multi-story structure using ARMAX time series analysis. The wind force simulation model is then presented, which first involves calculating the wind speed at a reference level, followed by an interpolation of that data to generate wind speeds at all other levels. The wind pressure coefficient model to account for the location and surrounding characteristics of a building is then explained. The final section introduces the damage modelling technique used throughout the numerical modelling simulations of the structure.

Chapter 4 tests the capability of the proposed ARMAX DDM through numerical modelling of five different buildings using SAP2000 v14. Each structure is subjected to damage cases of varying severity and through wind induced vibrations the ARMAX DDM is used to calculate the location and severity of damage for each case.

Chapter 5 completes the thesis with the summary and conclusions. The prominent issues and possible future work towards improving the model are mentioned.

CHAPTER 2:LITERATURE REVIEW

In this chapter, a literature review of important and recent publications in SHM is presented starting with an overview of some classical methods in damage detection. Following this, a review of applicable work done in simulating wind forces are presented and the final section explores recently used seismic damage analysis modelling methods.

2.1. Literature Review of Structural Health Monitoring

SHM is a multi-disciplinary subject involving many different components, including experimental testing, sensors, data acquisition systems, signal processing, and damage detection methods. For the completeness of this review, an introduction to the widely used parametric damage detection methods is presented in Section 2.1.1. Section 2.1.2 reviews the history and latest accomplishment in damage detection methods based on time series analysis.

2.1.1. Literature Review of Parametric Methodologies

2.1.1.1. Natural Frequency Methods

During the early stages of SHM, changes in basic modal properties such as natural frequencies, modal damping, and mode shape vectors were the most commonly used parameters as damage features. In the following paragraphs, a literature review on modal frequencies-based damage detection and the inherent limitations of produced from these methodologies are explored.

Hearn et al. (1991) conducted non-destructive inspection of structures via modal analysis of the vibration response of structures. The stiffness damage detection was determined by the change of natural frequencies and modal damping coefficients. This analysis was verified with two experimental tests, the first test involved fatigue loading a steel frame structure, and the second test involved saw cutting wire ropes. The derived change in the equation of motion and subsequent change in natural frequencies successfully determined the location and severity of the damage.

Ju at al. (1988) used the modal frequency method to determine the location and damage of a cantilever beam in which the damage was limited to the mid length of the beam. The authors identified the location and severity of damage based on their analytical theory involving a spring loaded “fracture hinge”. This method was independent of the loading strength, frequency of vibration and damage location. Through testing, the method identified the location of damage to within one percent and the intensity of the damage within four percent.

Additional information regarding the use of natural frequencies in damage detection can be found in a comprehensive technical review done by Salawu in 1997, in which the author thoroughly explored the inherent advantages and disadvantages. The reason that the natural frequency method was so commonly used in the earliest methodologies of SHM was due to its simplicity. The main drawback however, was that results pertaining to the severity of damage were often inaccurate and inconsistent. Also, many experimental structures were found to have an insensitivity regarding damage and a change to their natural frequencies (Doebling et al., 1998). For these reasons, researchers have been producing new methodologies which expand on natural frequencies to include other parameters to create new damage features (J. -T. Kim et al., 2003; Maity et al., 2005; Zhong et al., 2008).

2.1.1.2. Modal Shape Methods

One major issue with the natural frequency is that natural frequencies cannot provide any spatial information for a structure. To alleviate this issue, mode shape based methods, which could account for spatial information became a better solution for damage. The introduction of Modal Assurance Criterion (MAC) (Allemang et al. in 1982) became a common tool to compare mode shapes.

West (1984) was one of the first researchers to employ mode shape parameters to detect damage. The author analyzed empirical modal models of structural components within the Space Shuttle Orbiter's aft bulkhead. By correlating the mode shapes at the undamaged state and the damaged stages after acoustic loading. A subdivision of the modal vector was done and followed by a computation of the MAC for each part to localize the changes.

Ahmadian et al. (2000) proposed a different method for damage localization using mode shapes information. When damage occurs in a substructure, its mode of vibrations change however the modes of the other substructures did not. By assuming that higher modes will not participate in the deflections of undamaged substructures, the author formulated two damage location indicators which were successfully applied to a numerical example.

Siebel et al. (2012) conducted Operational Modal Analysis (OMA) on numerical and experimental studies of a wind turbine to develop a system that detects and locates damage based on the wind turbines's vibration response to wind. The mode shapes which are found with OMA are evaluated by two damage detection algorithms. The Modal Strain Energy method and the Gapped Smoothing

Technique. Various types of damage are investigated, with the two main sources being tower damage and a change in foundation stiffness. The comparisons between the numerical and experimental results conclude that locating damage with this approach is feasible.

Although mode shape based damage detection have shown significant improvements over natural frequency based methods, there are still drawbacks when using this method. One disadvantage is that high mode shapes, which are particularly sensitive to minor damage, are not easy to excite with ambient vibration. Also, environmental effects can modify a structures mode shapes and thus, faulty mode shapes and faulty detections can be made.

2.1.1.3. System Identification Methods

Recent developments in SHM damage features have undertaken more complex methods which greatly expand on the use of natural frequencies and mode shapes to identify specific characteristics of a structure such as stiffness or damping. Zhang and Johnson (2013) proposed a system identification model focusing on shear-type structures. Their technique involved dividing a structure into simple substructures. Equations of motion were built for each substructure and the equations were used to calculate each story's stiffness and damping by solving the optimization problem. To limit the error in the stiffness and damping coefficients, the authors applied least-square method. A numerical five storey shear structure validated the effectiveness of their substructure technique.

A system identification for shear bending models was introduced by Kuwabra et al. (2013) in which the authors determined the story shear and bending stiffness's from the floor accelerations just below and above the specified storey. This was done using a set of closed-form expressions for the stiffness's in terms of the limited floor accelerations and through introducing an Auto-Regressive model with eXogenous input (ARX).

Ikeda et al. (2014) created a smart system identification method which solely relies on the horizontal floor accelerations. By combining the use of Auto-Regressive model with eXogenous inputs (ARX), Taylor Series and Transfer functions, the authors found that their numerical shear bending system could reasonably simulate the vibration records. Numerical modelling found that the natural frequencies and stiffness's of super high rise buildings could be accurately estimated during the 2011 Tohoku earthquake. Minami et al. (2012) used a similar system identification

method to calculate damage detection using time series models on the same super high rise buildings during the 2011 Tohoku earthquake.

Kaya et al. (2015) created a simplified methodology to identify and calibrate analytical models of multi storey buildings from their vibration responses. This approach is based on the Transfer Matrix formulation which requires vibration reading from every storey. In most cases, vibration responses are not recorded for every storey so the authors developed a methodology to estimate the vibrations of the unrecorded floors based on the linear approximation of the mode shapes or shear and bending beams. By starting from the top storey and using the Transfer Matrix formulation, the authors identified the frequency of each storey. If the mass is already known, the approach was capable of identifying the storey stiffness. This approach was validated through a numeric model of a seven storey building and the earthquake records from the UCLA Factor building.

2.1.1.4. Model Updating Methods

In parametric methods, some researchers utilized finite element models and numerical formulations are used in conjunction with measured vibration data to detect damage. This type of model is categorized as the model updating method. The method aims to intensively modify the finite element model or mathematical models to create accurate baseline and damaged structures by comparing the simulated and measured vibrations. Once the model captured the behaviour of the structure, the inverse problem was solved to define the damage.

Box et al. (1994) conducted a survey regarding how the model updating method was being utilized in structural dynamics. The authors defined model updating as a process which incrementally improves the finite element models to obtain vibration results which match as close as possible to measured vibration results. This was done using a variety of algorithms which changed the constraints and mesh sizing. One example using the model updating method involved comparing the stiffness matrices of the FE model to locate and quantify damage.

Ching et al. (2006) created a new Bayesian model updating approach which could be used for linear structural models. The basis of the model is from the Gibbs sampler method, a simulation method which can decompose the uncertain model parameters into three groups, creating a more practical methodology. Although the authors have shown that this method can be applied on

various SHM problems in which there is incomplete modal data, it requires a large amount of monitored locations for optimal results.

Shiradhonkar et al. (2011) completed a study aimed at detecting and locating damage in a beam in a FE moment resisting frame. The response at unmonitored degrees of freedom (DOFs) were calculated by interpolating recorded vibration responses in the time domain. The modal parameters are identified by using frequency domain decomposition and empirical transfer functions. These identified modal parameters are then treated as the damage features. Although the study has shown reasonable accuracy, the method requires much time, effort and expertise to properly update the FE model. There is still some uncertainty in the model, however, as the FE is entirely modified based on measured vibration data, which can be drastically affected by noise or other operational and environmental factors.

Link et al. (2012) applied their model updating methodology to detect damage on the Gaertnerplatz Bridge in Germany. They first created a finite element model of the bridge and continuously updated it based on the monitored vibration data to create a healthy state. The data was taken over a period of three years and after considering temperature effects and noise, the authors concluded that there was no structural degradation over the three years. Their process, like so many other model updating techniques, required much effort, time and knowledge in order to simulate an accurate FE model. Although FE models give researchers useful information on the state of structures, their abilities to detect damage are greatly hampered by the extensive effort and time required to closely reveal and diagnose any symptoms of damage in a real structure.

2.1.1.5. Other Parametric Methods

Other prevalent parametric damage detection methods which were not mentioned include the Principal Component Analysis based damage detection (De Boe et al., 2003; Kullaa, 2003; Mujica et al., 2014; Hoon Sohn et al., 2000), the Frequency Domain Analysis, e.g. the Wavelet Analysis (Kim et al., 2004; Reda Taha, 2010), Frequency Response Functions (Lee at al., 2002; Pandey et al.,1994; Park et al., 2003; Sampaio et al., 1999), Singular Value Decomposition, and the Complex Mode Indicator Function (CMIF) (Catbas et al., 2006; Liu et al., 2014; Shih et al., 1988).

2.1.2. Literature Review of Time Series Based Damage Detection Methods

Non-parametric methods and statistical pattern recognition techniques such as Artificial Neural Networks (ANN) (Sohn et al., 2002; Zhao et al., 1998) and Time Series Modelling (Gul et al., 2009, 2011a; Nair et al., 2006; Nair et al., 2007; Sohn & Farrar, 2001) have gained significant momentum in the field of SHM due to their ability to deal with massive data and their capability to improve reliability by accounting for the variations in the recorded data. Among the different statistical pattern recognition techniques, Time Series Analysis is chosen as the basis of damage detection in this thesis. An exclusive literature review on time series models is presented as follows.

Time series analysis is used to analyze time dependent data sets to understand their statistical characteristics. In their infancy, time series models were not used for structural analysis purposes. They were initially used in a variety of fields such as population modelling, electrical engineering, long term weather predictions, and stock price prediction. In the following papers, the coefficients of time series models are used as damage sensitive features. Damage was found by comparing the changes in the coefficients from the undamaged models and the damaged. The first instance of employing time series modelling for SHM purposes was undertaken by Anderson (1997) in the system identification of civil structures in which the author employed vector auto-regressive-moving-average (ARMA) vector models.

Bodeux et al. (2000) introduced the application of auto-regressive with moving average vector (ARMAV) models for both system identification and damage detection. Their approach utilized a prediction error method which assumed a zero mean Guassian white noise. The method was tested on the "Steel-Quake" benchmark proposed in the framework of COST Action F3 "Structural Dynamics". The tests showed a good correlation for the modal parameters and for detecting damage based on the modal parameter uncertainties, however the location of the damage was not properly identified.

Y Lei et al. (2003) implemented a modified ARX approach in which they considered the effects of excitation variation and the ARX models' orders. Similar to other related papers, the damage features were constructed by comparing the residual errors in the unknown cases and the undamaged cases. Their method was tested on the numerical ASCE benchmark structure and both medium and severe damage was detected and localized successfully.

Monroig et al. (2006) presented a decentralized method in which second order ARX models were built based on the equation of motion and a dense array of wireless sensors. The model was applied to numerical data from a building model similar to the ASCE benchmark and it was shown that damage on individual elements could be identified and located, however there were some false-positives and false-negatives.

Gul and Catbas (2011) implemented a novel damage detection process which involved creating a damage detection model which combined time series modelling and a novel sensor clustering technique. The authors created ARX models for different sensor clusters by using the free response of the structure and each sensor cluster output was treated as an input for the ARX model. The methodology was shown to successfully identify and locate damage on both numerical and experimental vibration data even when noise is considered.

To improve on the methodologies presented in the previous section, researchers began combining the time series modelling with a variety of statistical pattern recognition methods. Gul and Catbas (2009) used time series modelling in conjunction with Mahalanobis distance (MD) based outlier detection algorithms to identify a variety of structural changes on different test structures. What makes this model unique is in its use of a random decrement function to eliminate the effects of exogenous inputs. The authors tested their methodologies on a simply supported steel beam and a highly redundant steel grid structure. Their methodology was successful in detecting changes in stiffness and boundary conditions for both test specimens, however there were still issues such as threshold determination which must be considered when creating automated SHM systems.

Nair et al (2006) introduced a new damage sensitive feature (DSF) which is a function of the first Auto Regressive (AR) component and the vibration signals obtained from sensors are modeled as ARMA time series. The authors found that the mean values of the DSF for the damaged and undamaged signals were different, so a statistical summarization, i.e. a t-test, was implemented to obtain a confident damage decision. Numerical and experimental vibration data from the ASCE benchmark was used to validate the method and the results showed that both minor and major damage could be precisely detected and located.

Lautour and Omenzetter (2010) combined AR models with an Artificial Neural Network for damage detection in structures. AR models are used to fit acceleration time history data and the coefficients, which are considered to be DSF are used as an input into an artificial neural network.

The ANN was trained to both classify damage cases and estimate the remaining structural stiffness. The authors tested this on two experimental structures and the methodology performed well at classifying and estimating the remaining stiffness using a small number of DSF and limited sensors.

Xing and Mita (2012) proposed a substructure approach for damage detection of a shear structure which only required three sensors to identify damage in any story. The authors divided a structure into several substructures, enabling damage detection in each substructure which allowed the authors to detect damage at each substructure independently. A five storey building was employed to validate their methodology both numerically and experimentally and the researchers successfully identified and located damage. The drawback to their methodology, however, is that an excitation source must be provided.

Noman et al. (2012) presented a method of damage detection using statistical pattern recognition which focuses on the long term degradation in structures. Their experiments centred on long term acceleration and strain measurements taken from the Portage Creek Bridge in Victoria, British Columbia which were used in to fit three AR model coefficients. The authors implements two statistical pattern recognition techniques: statistical pattern comparison and statistical model development. Throughout their research they found that the bridge was in relatively good condition, however there was slight degradation noticed towards the end of the period. This study demonstrated the feasibility of statistical pattern recognition techniques in assessing the conditions of a practical structure.

Mosavi et al. (2012) presented a statistical pattern method for damage detection in an idealized steel bridge girder using only the ambient vibration measurements. Their experimental two span continuous steel beam was subjected to ambient vibrations via a hydraulic actuator and the damage was induced by cutting parts of the flange at two locations. AR models were fitted to the vibration response history and a Stiffness Damage Feature (SDF) was proposed by applying Mahalanobis Distances (MD) to the coefficients of the vector AR models to compare the differences between the healthy and damaged cases. In addition, Fisher criterion was used to evaluate the variance in the damage features where the location of damage is made based on the sensor with the highest variation in their damage feature. Experimental results showed a high sensitivity to identifying damage location even when the damage was very small. Although the results are promising, there

are issues within their methodology such as the high density of sensors required and the effects of adverse loading conditions.

Huang et al. (2013) presented a damage detection method for transmission towers based on the use of Vector Auto Regressive (VAR) Model. Vibration data from both the undamaged and damaged cases were divided into smaller segments, respectively, in order to build the VAR coefficient matrix in which the diagonal elements are extracted and used to construct MD which is used as a DSF. The mean and variance of the MD values for sensors near any damage are expected to change from their baseline condition. This method was tested on a 6-DOF numerical system and a transmission model and in both cases, damage was accurately identified and detected but the severity was not very well defined.

Yao and Pazkad (2014) completed a performance evaluation and comparison study between two damage features: the Mahalanobis distance of AR coefficients and the Cosh distance of AR model spectra. The effectiveness of each method is illustrated on a numerical 10 DOF bridge model with respect to their sensitivity to structural damage and measurement noise level. The comparison showed that both DFs are sensitive to local damage and noise levels and the authors concluded that both DFs are effective for structures under stable operating conditions.

Roy et al. (2015) proposed a set of 4 ARX model based DSF for damage detection and localization when no input excitation data is made available. This was done by assuming that one of the output responses in a multi-degree-of-freedom (MDOF) system is assumed as an input whereas the rest are taken as the output. The damage features are based on ARX model coefficients, Kolmogorov-Smirnov test statistical distance, and the model residual error. The authors' methodology was tested on both numerical and experimental structures and the results show that the DSF could both localize and quantify the stiffness degradation, however, in cases where there are multiple locations of damage, one of the DSFs was unable to clearly quantify the amount of stiffness degradation.

Lakshimi and Rao (2014) created a novel output-only damage detection technique based on time series analysis which accounted for environmental variability and measurement noise. The authors applied Principle Component Analysis to transform the large amount of data in order to reduce the data size, thereby improving computational efficiency. Their Probability Density Functions (PDFs) of damage features were obtained from the variance in prediction errors when comparing

the healthy and damaged data which was processed using AR and ARX models. The authors tested their methodology on a numerical simply supported beam and an experimental three storey framed bookshelf benchmark structure. Results from the experiments indicate that the method can detect and locate damage, however the measurement of the severity of damage should be further examined.

Bao et al. (2013) proposed a damage detection technique for subsea pipelines which could account for various loading conditions. The authors first partitioned and normalized the acceleration data, then used auto-correlation functions and partial-correction functions to compute the ARMA models inputs and their orders respectively. The AR parameters served as the damage feature vector and the damage indicators were based on the MD between the ARMA models which were used for damage detection and localization. A finite element model of a subsea pipeline under ambient excitations was numerically simulated to verify the authors' methodology, and the results show that it can successfully detect and locate damage even with noise effects.

This thesis expands on a methodology created by Do (2015) which has been shown in both numerical and experimental tests to successfully detect changes in stiffness in damaged building structures. Do (2015) improved upon a methodology which was originally based on an ARMAX damage detection model created by Mei and Gul (2014). Do's methodology, which will be further discussed in Section 3, was expanded upon and used throughout this thesis to detect various degrees of damage within a multi storey building when random wind excitation is applied to the building.

2.1.3. Literature Review of Damage Detection Methodologies in Buildings

One of the critical problems after an earthquake is building damage assessment. The traditional methods of visual inspections by people at every site is both unreliable and inefficient. Due to these issues, a variety of remote sensing techniques have been explored to help with building damage assessment in which no person is required at a building to determine its damage state.

Dong and Shan (2013) performed a comprehensive study comparing the multitude of spaceborne and airborne remote sensing building damage assessment techniques including SAR (Synthetic Aperture Radar) and LIDAR (Light Detection and Ranging). When using SAR or LIDAR, heavy damage grades such as total collapse are easily detectable; however, the identification of lower

damage grades which may only involve slight or moderate structural damage was a challenge even when using 0.5m resolution (Ehrlich et al., 2009; Yamazaki et al., 2005; Kerle, 2010). More accurate results were obtained with methodologies that utilized both pre earthquake and post-earthquake data as opposed to the methods which only utilized post-earthquake results (Dong and Shan, 2013). Through Geographic Information Technologies (GIS), Menderes et al. (2015) developed a Normalized Digital Surface Model which measures the difference in elevations at the earth surface from before and after an earthquake. Judging by the degree in which the elevation changed, the authors could accurately determine whether a building collapsed, although it did not attempt to identify any buildings which may have undergone seismic damage without collapsing. Overall, spaceborne and airborne remote sensing techniques are best utilized for rapid damage assessment for first response and not for evaluation of slight or moderate seismic damage in buildings.

De Lautour and Omenzetter (2006) analyzed the vibrations of a multi storey building due to ground motion to detect seismic damage within the building. Their simple numerical 3-storey structure was subjected to random ground motion and the resulting vibrations at each storey were fit to an AR time series model. The AR coefficients were then used as the inputs for an Artificial Neural Network (ANN). The ANN was trained to detect any changes in the AR coefficients from before and after damage to identify and quantify the damage at each storey. The results from their numerical case study proved that their methodology could successfully detect damage in a simple numerical structure even in the presence of noise and changes in operating conditions.

Shiradhonkar and Shrikhande (2011) developed a finite element model updating technique to detect seismic damage in a moment resisting frame. Their methodology is based on tracking changes in the structural parameters of a building (natural frequencies, modal damping, mode shapes) by analyzing the vibration signals due to strong seismic ground motion at a limited number of degrees of freedom. The authors used piecewise cubic hermite interpolating polynomial to construct the missing vibration data from degrees of freedom which weren't measured along with the Curvature Mode to identify damage at any building storey in their numerical simulations.

Ji et al. (2011) conducted a series of full scale tests at the E-Defense shaking table facilities to simulate realistic seismic damage in a high-rise steel building. In conducting these full scale tests, the authors could evaluate the effectiveness of vibration-based damage diagnosis methodologies

using real life vibration data. The vibration data from each floor was fit by the frequency response curve-fitting method and the ARX method. As the seismic damage increased, the natural frequencies of the structure decreased as expected. The modal shapes, however did not change as the damage was distributed evenly over the height of the structure. Note that these results only apply to steel high rise structures and it is expected that different results would occur if a different type of structure was used, such as a concrete moment frame or shear wall structure.

Koo et al. (2010) created a vibration induced damage detection technique for simple shear type buildings through a modal flexibility model. A new load concept; positive shear inspection load; which is defined as a load producing positive shear forces on all floors was utilized along with analytical investigations on the damage-induced inter-story deflection to successfully detect damage on either a single floor or at multiple locations. Both numerical and experimental studies on a 5-storey shear structure were undertaken to test the validity of the model. It was found that the modal flexibility model could successfully identify and locate damage for most damage cases, however it was found to miss some damage on multiple storey damage cases.

Vafaei et al. (2012) created a seismic damage detection model which focused solely on concrete shear walls. First, a FE model of an existing 5-storey shear wall was generated and then a modal pushover analysis was applied to the model. The inter story drift ratios and plastic hinge rotations were recorded as input and output data sets respectively for conditioning an ANN which, after training, could properly predict the plastic hinge rotation in the shear wall under numerous damage cases.

M.P. Limongelli (2014) developed a method for identifying and localizing seismic damage in a multistory building through the interpolation method. The basis for this methodology is to analyze the interpolation error related to the use of a spline function for modelling the operational deformed shapes of the structure. The variations within the interpolation error between the undamaged and damaged state indicate the presence and location of damage. The author's methodology was validated through testing it on the UCLA factor building, a densely instrumented multistory steel building and it was found that the methodology could localize both single and multiple locations of damage even in the presence of measurement noise. Note that this methodology requires a dense network of measurement instruments to function and high quality signals must be recorded to detect slight damage.

Pierdicca et al. (2015) created a seismic damage model which identifies, and localizes damage while also estimating the remaining life of a structure to gauge its post-earthquake performance. A two-storey industrial structure in Italy was re-created as a numerical model in which time history nodal forces; representing seismic ground motion; were applied and the displacement, velocity and acceleration of the structure were calculated. To identify and locate damage, a ductility damage index was created which is based off the displacements of the structure's members beyond their elastic threshold. To calculate the remaining life of a structure, the structure underwent a displacement global control analysis to see which regions of the structure would reach their ultimate displacement first. Those regions then underwent a traditional pushover analysis to determine the ultimate capacity curves of the governing regions of the structure.

Valdes-Gonzalez et al. (2014) conducted experimental tests on a two-storey reinforced concrete frame in which the frame was progressively damaged up to a point of significant damage. The frame was damaged by using a testing pendulum which simulated the effects of a growing intensity earthquake. The authors measured the acceleration signals from the structure at all intermediate stages to estimate the dynamic properties of the structure through each stage of damage. It was found that the correlation coefficient between the frequency response function of the undamaged and damaged states could help identify the presence of structural damage and could help identify whether the damage was due to yielding or not. For this methodology to function properly, the FRF from the undamaged state must be known beforehand.

2.2. Literature Review of Wind Force Simulation

In order to test the damage detection model to validate whether it can be applied to ambient wind forces, a program must be calculated which can generate a wind load at storey by storey-level. The typical approach for wind loading simulations on structures is to generate a synthetic wind velocity field in time domain and then transform that velocity field into a pressure field through approximate pressure coefficients (Rossi et al. 2004). The following literature review presents the work done by previous researchers with regards to generating a wind load.

Rossi et al. (2004) conducted a study of common stochastic wind velocity simulation techniques and directly compared the performance of AR, ARMA and Shinozuka-Deodats approaches based on the authors' quality indices. Through their scalar quality indices, it was found that the Shinozuka-Deodats method gives the best results in terms of overall quality of the signal. The

ARMA techniques behave better than the AR methods, however both time series techniques had difficulty simulating accurate propagation effects. Throughout their simulation tests, the authors found that length of turbulence is very sensitive and large error bounds are considered acceptable.

Wang et al. (2004) studied the turbulent transport and dispersion of wind in the urban atmospheric boundary layers. The authors monitored the wind field around the urban centre of Oklahoma City using Doppler Lidar and sonic anemometers. The analysis of their results indicate that there are significant differences in the mean, turbulence intensity, and spatial integral length scale over urban and suburban domains. The authors found that the average wind speed was lower over the urban areas, however the turbulence was much higher.

Ubertini and Giuliano (2010) investigate methods to improve one of the most commonly used wind velocity field simulations which uses waves superposition (WAWS). Although the WAWS method has been shown to create accurate wind simulations, its computational time and effort are significant so the authors used the WAWS method as a basis for calibrating two other much simpler methods, the Proper Orthogonal Decomposition and the AR filtering method. These calibrated simpler methods could complete the wind field simulations with a small reduction in accuracy compared to the WAWS, however the computational time and effort were both drastically reduced as shown through their two numerical examples.

Villanueva et al. (2012) presented a new method which included correlation and autocorrelation in simulations of randomly generated wind speed distributions which keeping the wind speed distribution in a Weibull form. The authors based their methodology off the work mentioned previously from Feijoo et al (1999). Instead of operating directly with Weibull or Rayleigh distributions, correlations were induced over a set of normally distributed variables and then transformed from normal to Weibull distributions after. The purpose of their updated method was to solve the economic dispatch problem, which looks at minimizing the cost of producing power generation by optimizing the dispatching of power between available generators. Their method concluded that correlation must be taken into account in wind simulations in order to properly model real life scenarios.

Shamshad et al. (2005) utilized hourly wind speed time series data from meteorological stations in Malaysia to create an hourly wind speed simulation using first and second order Markov chain processes. The first and second order Markov wind speed simulations had their statistical

information compared with real life wind data. The main statistical properties measures were mean, standard deviation, median percentiles, Weibull distribution parameters, autocorrelations, and spectral density of the wind speed values. The comparison shows that the Markov simulations have statistical characteristics which satisfactorily simulate real life data.

Feijoo and Villanueva (2015) gathered and reviewed a multitude of wind speed simulation methods. The authors found that if no chronological features are necessary, then using evolutionary algorithm methods and methods which induce Spearman rank correlations were found to be acceptable. The most accurate method for non-chronological features was the method presented above from Villanueva et al. (2012). When chronological requirements are part of the constraints, autoregressive methods which incorporate either first order or second order Markov processes (refer to the work presented above by Shamsad et al (2005)) and autocorrelation methods were both found to be acceptable.

Wai Hong Lau (2016) created a wind velocity field simulation which improves on the commonly used Reynolds-averaged Navier-Stokes (RANS) equation. The author found that the RANS methodology did not properly simulate the fluctuating behaviour of wind velocity, so he improved on it by implementing a stochastic Kinematic Simulation (KS) to the RANS results. The author found that the RANS-KS yielded excellent spatial correlation results when compared to wind tunnel measurements.

Fernandez and Alonso (2017) created a model which could simulate wind speeds using a drastically reduced number of inputs. The authors created a low frequency component (hourly wind speed changes) based on a conditional probability density function and a high frequency component based a Beta probability density function and a simple rescaling feature. Their methodology was compared with real speed wind data and the results showed excellent correlation.

2.3. Literature Review of Numerical Damage Analysis and Residual Stiffness Techniques

This thesis will only involve numerical simulations to detect damage in structures. As such, a proper damage model must be utilized to validate the ARMAX DDM. The type of structures tested in this thesis will be primarily concrete moment frames and as such, the following research focuses heavily on the effects of damage on reinforced concrete members.

A commonly used damage analysis technique to determine the degree of damage in a structure is the stiffness degradation method, which compares the stiffness slope of an undamaged structural member to the reloading stiffness slope after the member / structure is subjected to a seismic event. This type of damage model pairs excellently with the time series analysis as the analysis focuses on the change in stiffness in a structure.

Roufaiel and Meyer (1981) and Toussi and Yao (1983) were some of the first researchers to utilize such a measurement to determine seismic damage in a structure. Roufaiel and Meyer (1981) utilized a Flexural Damage Ratio which compared the initial stiffness to the reduced secant stiffness at the maximum displacement. Toussi and Yao (1983) create a Slope Ratio (SR) method which is defined as the ratio of the slope of the loading branch of the force displacement diagram to the slope of the unloading branch and compared the SR to the degree of damage in the structure. Ghobarah et al. (1999) gathered and critically evaluated these two methods along with a multitude of other commonly used damage indices. Following this review, the authors introduced a practical method based on the static pushover analysis to estimate the expected damage to structures which are subjects to earthquakes of varying intensities.

Yazgan and Dazio (2012) presented an improved post-earthquake damage assessment that primarily accounts for the residual deformations of the structure post-earthquake. This method accounted for both the displacements and rotation of the structure, eliminating uncertainties pertaining to both the excitation and the damaged structure. The methodology relates their residual displacement to the residual stiffness of the structure, providing the researchers with a reliable way of measuring the residual stiffness of a structure post-earthquake. A trial application which excited a structure excited via shaking table confirmed the capability of their method to determine both the residual displacements and the residual stiffness.

Jianguang et al. (2016) created a multi-level damage model to evaluate seismic damage in reinforced concrete frame structures. The methodology involved creating a deformation-based continuum damage model with stiffness degradation and establishes a deformation equivalent relationship between the concrete and steel reinforcement. The model can detect multi-level damage, signifying that it can associate damage to many performance levels based on its severity (immediate occupancy, life safety, collapse prevention). Numerical modelling (finite element

method) utilizing the proposed damage model produces results in good agreement with previously tested damaged structures.

Zongming et al. (2016) developed a stiffness degradation-based damage model for reinforced concrete members which can be applied to performance-based earthquake applications. The damage model was developed using fiber beam-column elements to model both the concrete and the reinforcing steel. The model initially incorporates the material changes at a member by member level, and then each section member was modified accordingly to create storey by storey lateral stiffness changes which in turn models the structures lateral stiffness in its entirety. The damage model was applied to various reinforced concrete columns and members and was able to accurately predict the magnitude of the damage and estimate the storey by storey damage.

CHAPTER 3:METHODOLOGY

The methodology is broken down into three main sections:

Section 3.1 outlines how ARMAX time series analysis is used in conjunction with sensor clustering to detect damage in a structure from its acceleration responses.

As this thesis is based on damage detection from wind induced vibrations, Section 3.2 outlines the procedure for generating a wind force model for a multi storey building which reflects the real life behaviours of wind.

Section 3.3 elaborates on how a simplified numerical damage model was implemented in SAP2000 in order to perform damage trials to test the ARMAX DDM.

3.1. Outline of the Time Series Based Method for Damage Detection

3.1.1. Background to Time Series Models

A time series is a sequence of well-defined data points measured at uniform time intervals over a specified period. Time series modelling is the use of statistical methods to model the measured time series data in an attempt extract meaningful characteristics. This section provides a brief discussion about the Auto-Regressive Moving Average model with eXogenous inputs (ARMAX), which is used throughout this thesis to detect damage. This ARMAX model is based on work completed previously by Mei and Gul (2014). More discussions about time series model theories can be found in the following literature (Lu & Gao, 2005; Omenzetter & Brownjohn, 2006; Hoon Sohn et al., 2001).

ARMAX modelling was the specific time series model used in this thesis. Its general form is given in Equation 3.1.

$$\begin{aligned} y(t) + a_i y(t-\Delta t) + \cdots + a_{n_a} y(t-n_a\Delta t) \\ = b_1 u(t-\Delta t) + \cdots + b_{n_b} u(t-n_b\Delta t) + e(t) \\ + d_1 e(t-\Delta t) + \cdots + d_{n_c} e(t-n_c\Delta t) \end{aligned} \tag{3.1}$$

In Eq. 3.1, $y(t)$ is the output, $u(t)$ is the input of the model, $e(t)$ is the error term, and a_i, b_i, d_i are the parameters of the model. The model orders are given in terms of n_a, n_b, n_d. A general form of the ARMAX equation can be written as Equation 3.2.

$$A(q)y(t) = B(q)u(t) + D(q)e(t) \tag{3.2}$$

The terms $A(q)$, $B(q)$ and $D(q)$ are polynomials in delay operators q^j as shown in Eq. 3.3.

$$\begin{aligned} A(q) &= 1 + a_1 q^{-1} + \cdots + a_{n_a} q^{-n_a} \\ B(q) &= b_1 q^{-1} + b_2 q^{-2} + \cdots + b_{n_b} q^{-n_b} \\ D(q) &= 1 + d_1 q^{-1} + \cdots + d_{n_c} q^{-n_c} \end{aligned} \tag{3.3}$$

The ARMAX model considers exogeneous inputs $u(t)$ as shown in Equation 3.2. For better understanding, a block diagram of an ARMAX model is shown in Figure 3.1:

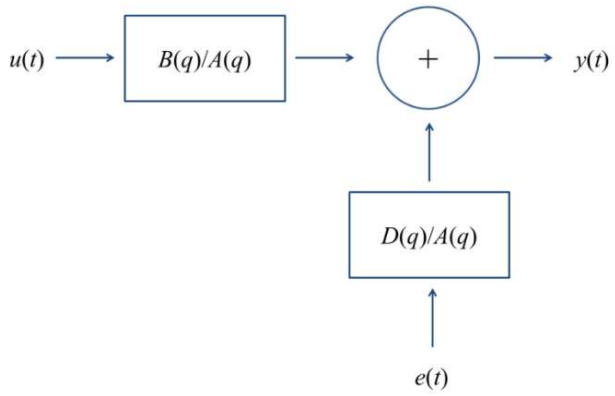

Figure 3-1 ARMAX Block Model (Ljung, 1999)

From Equation 3.3, it is simpler to understand the meaning of the delay operator. For example, a data set $x(t)$ at time multiplied by q^j is equal to $x(t\text{-}j\Delta t)$. From the general form of the ARMAX models (Eq. 3.2), different time series models can be created by changing the order of $A(q)$, $B(q)$ and $D(q)$. For example, Auto Regressive (AR) process is created with only n_a while n_b, and n_c are set to zero. The Moving Average (MA) process sets n_a and n_b to zeros and a non-zero value to n_c. The ARX model is defined as setting n_c to zero. As previously stated, the focus of this thesis will be solely on ARMAX modelling.

3.1.2. ARMAX Models for Different Sensor Clusters

The equation of motion, which governs the dynamic responses (accelerations, velocities and displacements) of structures, is described herein. Eq. 3.4 below represents the general equation of motion for an N degree of freedom system.

$$\mathbf{M}\ddot{\mathrm{x}}(\mathrm{t}) + \mathbf{C}\dot{\mathrm{x}}(\mathrm{t}) + \mathbf{K}\mathrm{x}(\mathrm{t}) = \mathbf{f}(\mathrm{t}) \tag{3.4}$$

In which M, C and K represent the N by N mass, damping and stiffness matrices of the system. The vectors $\ddot{x}(\mathrm{t})$, $\dot{x}(\mathrm{t})$, and $x(\mathrm{t})$ represent the acceleration, velocity and displacement at a certain time t. The external forcing vector is denoted by $f(\mathrm{t})$ which, in the context of this thesis, is considered a wind force. For better visualization, Eq. 3.4 can be written in matrix form with the order NxN degree of freedom, as shown in Eq. 3.5.

$$\begin{bmatrix} m_{11} & \cdots & m_{1N} \\ \vdots & \ddots & \vdots \\ m_{N1} & \cdots & m_{NN} \end{bmatrix} \begin{Bmatrix} \ddot{\mathrm{x}}_1 \\ \vdots \\ \ddot{\mathrm{x}}_N \end{Bmatrix} + \begin{bmatrix} c_{11} & \cdots & c_{1N} \\ \vdots & \ddots & \vdots \\ c_{N1} & \cdots & c_{NN} \end{bmatrix} \begin{Bmatrix} \dot{\mathrm{x}}_1 \\ \vdots \\ \dot{\mathrm{x}}_N \end{Bmatrix} + \begin{bmatrix} k_{11} & \cdots & k_{1N} \\ \vdots & \ddots & \vdots \\ k_{N1} & \cdots & k_{NN} \end{bmatrix} \begin{Bmatrix} x_1 \\ \vdots \\ x_N \end{Bmatrix} = \begin{Bmatrix} f_1 \\ \vdots \\ f_N \end{Bmatrix} \tag{3.5}$$

The vibration of a structure is strongly dependent on time, the prior state of the structure, and external inputs. By modelling the vibration data as a time series sequence, statistical characteristics of the time series which represents the behaviour of the structure can be extracted. This vibration data can be gathered by installing a pair of bi-axial sensors in perpendicular directions at each storey. The focus of this research centres on the change in stiffness which represents damage within the lateral resisting members of a structure.

Equations 3.6 – 3.14 outlines the steps for how the EOM can be transformed so that it can be represented as an ARMAX model. For clarity, one storey (represented as a single degree of freedom) is considered as a single i^{th} row in Eq. 3.5 is shown in Eq. 3.6 below.

$$\begin{aligned} \left(m_{i1}\ddot{\mathrm{x}}_1(\mathrm{t}) + \cdots + m_{iN}\ddot{\mathrm{x}}_N(\mathrm{t})\right) + \left(c_{i1}\dot{\mathrm{x}}_1(\mathrm{t}) + \cdots + c_{iN}\dot{\mathrm{x}}_N(\mathrm{t})\right) \\ + \left(k_{i1}\mathrm{x}_1(\mathrm{t}) + \cdots + k_{iN}\mathrm{x}_N(\mathrm{t})\right) = f_i(t) \end{aligned} \tag{3.6}$$

Rearranging Eq. 3.6 to isolate the acceleration on the left-hand side results in Eq. 3.7.

$$\ddot{x} = \frac{f_i}{m_{ii}} - \frac{m_{i,1}\,\ddot{x}_1 + \cdots + m_{i,i-1}\,\ddot{x}_{i-1} + m_{i,i+1}\,\ddot{x}_{i+1} + \cdots + m_{i,N}\,\ddot{x}_N}{m_{ii}} - \frac{c_{\,i,1}\,\dot{x}_1 + c_{\,i,2}\,\dot{x}_2 + \cdots + c_{\,i,N}\,\dot{x}_N}{m_{ii}} - \frac{k_{\,i,1}x_1 + k_{\,i,2}x_2 + \cdots + k_{\,i,N}\,x_N}{m_{ii}} \tag{3.7}$$

It can be assumed in shear type building modelling that the mass of each degree of freedom is entirely lumped into the centre of the degree of freedom. Any mass values which aren't in the diagonal are assumed to be zero and can be removed. For simplicity, the damping terms in the equation can be removed due to their miniscule contribution to the equations balance. As such, Eq. 3.7 can be simplified to Eq. 3.8 below.

$$\ddot{x} = \frac{f_i}{m_{ii}} - \frac{k_{\,i,1}x_1 + k_{\,i,2}x_2 + \cdots + k_{\,i,N}\,x_N}{m_{ii}} \tag{3.9}$$

Taking the second derivative of Eq. 3.9 results in Eq. 3.10 below.

$$\dddot{x} = \frac{\ddot{f}_i}{m_{ii}} - \frac{k_{\,i,1}\ddot{x}_1 + k_{\,i,2}\ddot{x}_2 + \cdots + k_{\,i,N}\,\ddot{x}_N}{m_{ii}} \tag{3.10}$$

The goal of taking the second derivative of Eq. 3.10 is to create an equation in which the right-hand side is only dependent on acceleration values. Measuring the displacement and velocities of a structure under light ambient wind loading may result in measurement errors due to the miniscule values involved. By applying the forward difference technique (Levy & Lessman, 1961) as shown in Eq. 3.11 the left side of Eq. 3.10 can be transformed to create a new equation solely based on acceleration values as shown in Eq. 3.12.

$$\dddot{x} = \frac{\ddot{x}_{\boldsymbol{i}}(t+\Delta t) - \ddot{x}_{\boldsymbol{i}}(t)}{\Delta t}$$
$$\dddot{x} = \frac{\frac{\ddot{x}_{\boldsymbol{i}}(t+2\Delta t) - \ddot{x}_{\boldsymbol{i}}(t+\Delta t)}{\Delta t} - \frac{\ddot{x}_{\boldsymbol{i}}(t+\Delta t) - \ddot{x}_{\boldsymbol{i}}(t)}{\Delta t}}{\Delta t} \tag{3.11}$$

$$\frac{\frac{\ddot{x}_i(t+2\Delta t)-\ddot{x}_i(t+\Delta t)}{\Delta t}-\frac{\ddot{x}_i(t+\Delta t)-\ddot{x}_i(t)}{\Delta t}}{\Delta t} = \frac{f_i(t)}{m_{ii}}-\frac{k_{i,1}\ddot{x}_1(t)+k_{i,2}\ddot{x}_2(t)+\cdots+k_{i,N}\ddot{x}_N(t)}{m_{ii}} \tag{3.12}$$

One issue with the newly transformed Eq. 3.12 is that the acceleration $\ddot{x}$(t) exists on both sides of the equation, which could lead to trivial solutions. To eliminate this possibility, a new sequence y_i(t) is introduced to represent the left components in Eq. 3.12. The final transformation of the equation of motion is shown in Eq. 3.13.

$$\frac{y_i(t+\Delta t)-y_i(t)}{\Delta t^2} = \frac{f_i(t)}{m_{ii}}-\frac{k_{i,1}\ddot{x}_1(t)+k_{i,2}\ddot{x}_2(t)+\cdots+k_{i,N}\ddot{x}_N(t)}{m_{ii}} \tag{3.13}$$

This newly transformed equation can be represented as an ARMAX function (Eq. 3.1) provided that y_i(t) and $\ddot{x}_i$(t) are considered the output and input terms, respectively. The error term in the ARMAX model is represented by damping, excitation force and ambient noise. When Do and Gul (2015) developed their ARMAX model, it was found that an order of 1 for both the n_a and n_b terms and an order of 3 for the n_c term was sufficient to account for these influences. The ARMAX model for the ith row of the equation of motion of a multi DOF system can be expressed as in Eq. 3.14 below.

$$\begin{aligned} y_i(t+\Delta t)+a^i y_i(t) &= b_1^i\ddot{x}_1(t)+b_2^i\ddot{x}_2(t)+\cdots+b_N^i\ddot{x}_N(t)+e(t) \\ &+ d_1 e(t-\Delta t)+d_2 e(t-\Delta t) \end{aligned} \tag{3.14}$$

3.1.3. Sensor Clustering

Due to the nature of shear structures, it can be assumed that the signal of a DOF can only affect the DOFs located directly above or below. With this assumption, the time series models can be constructed in a more concise way where each model only incorporates the neighbouring DOFs. These models are referred to as a sensor cluster.

Based on the ARMAX model built for the equation of motion of a DOF, vibration at one sensor is chosen to fit the part at the left side of the equation, which is considered the reference channel.

The vibration data from the neighbouring sensors represent the right part of the equation. For an N-DOF structure, there are N ARMAX models with outputs as the reference channel and inputs only from the adjacent channels.

The ARMAX model is solely reliant on the sensor clusters, and not the readings of each individual sensor. This sensor clustering technique, which was previously developed by Gul and Catbas (2011), greatly reduces the complexity of the equation of motion for an N DOF. A simplified four storey structure is presented in Figure 3-2 to help illustrate this sensor clustering technique.

The first sensor cluster created to build the ARMAX model incorporates the first and second storey and the first storey is chosen as the reference channel. The reference channel of the second cluster is the second storey, and the two neighbouring storeys (first and third) are included. The third sensor cluster has the third storey as its reference channel and includes the two adjacent storeys: the second and the fourth. The final sensor cluster incorporates both the third the fourth storeys, with the fourth storey being the reference channel.

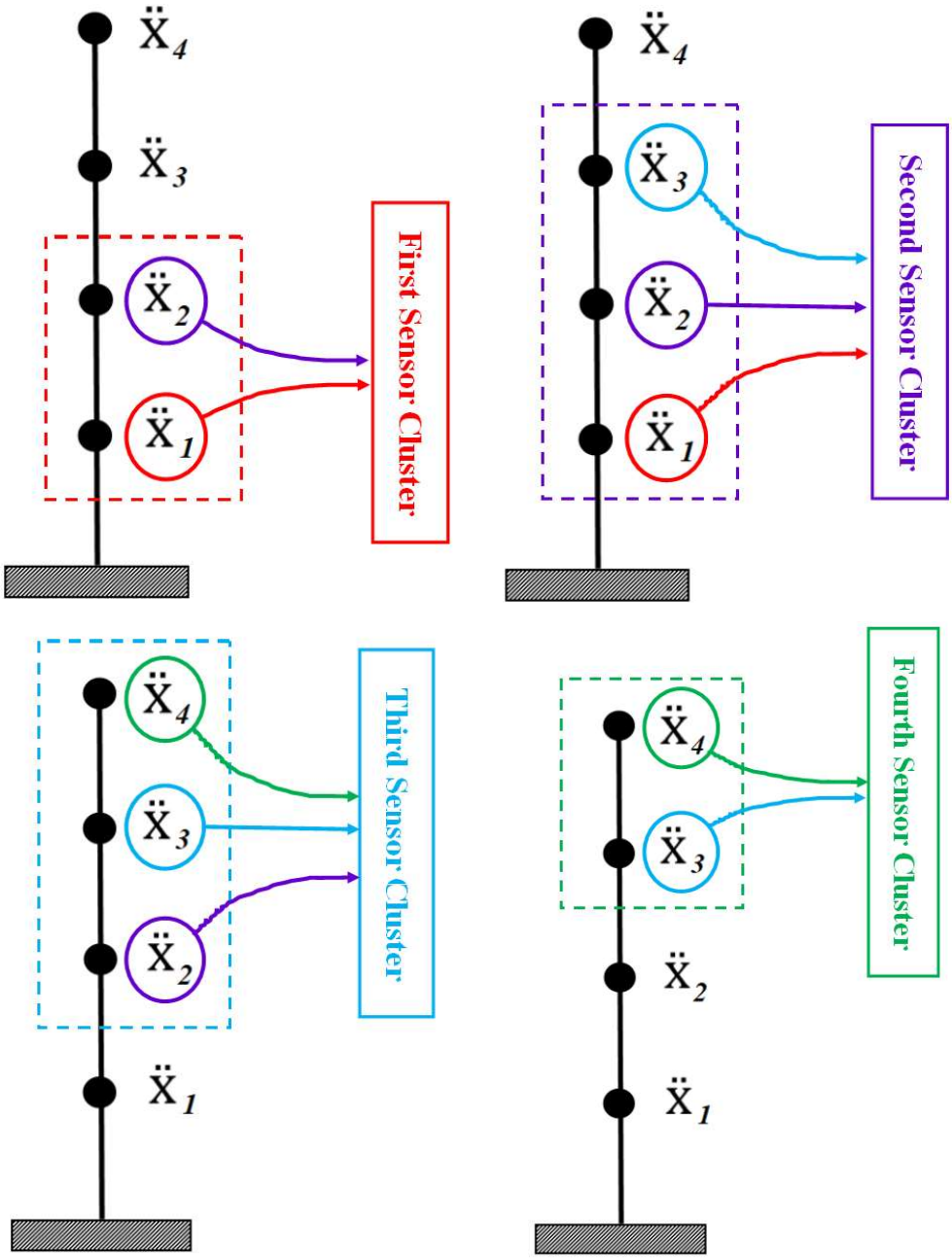

Figure 3-2 Sensor Clustering of 4 DOF Structure

3.1.4. Building Damage Features

Do and Gul (2015) expanded on the mathematical transformations from Section 3.1.2 and the sensor clustering technique from Section 3.1.3 to isolate the stiffness damage features as described herein.

The B(q) terms in the ARMAX model (Eq. 3.14) represents the terms $\frac{k_{ij}}{m_{ii}}$ in the equation of motions of each sensor cluster. The baseline case matrix is defined in Eq. 3.15 and the matrix representing the unknown case (i.e. damaged case) is represented by Eq. 3.16.

$$b^i_{j,baseline} = \begin{bmatrix} b^1_1 & b^1_2 & \dots & b^1_n \\ b^2_1 & b^2_2 & \dots & b^2_n \\ \vdots & \vdots & \ddots & \vdots \\ b^n_1 & b^n_2 & \dots & b^n_n \end{bmatrix} \cong \begin{bmatrix} \frac{k_{11}}{m_{11}} & \frac{k_{12}}{m_{11}} & \dots & \frac{k_{1n}}{m_{11}} \\ \frac{k_{21}}{m_{22}} & \frac{k_{22}}{m_{22}} & \dots & \frac{k_{2n}}{m_{22}} \\ \vdots & \vdots & \ddots & \vdots \\ \frac{k_{n1}}{m_{nn}} & \frac{k_{n2}}{m_{nn}} & \dots & \frac{k_{nn}}{m_{nn}} \end{bmatrix} \tag{3.15}$$

$$d^i_{j,damaged} = \begin{bmatrix} d^1_1 & d^1_2 & \dots & d^1_n \\ d^2_1 & d^2_2 & \dots & d^2_n \\ \vdots & \vdots & \ddots & \vdots \\ d^n_1 & d^n_2 & \dots & d^n_n \end{bmatrix} \cong \begin{bmatrix} \frac{k'_{11}}{m'_{11}} & \frac{k'_{12}}{m'_{11}} & \dots & \frac{k'_{1n}}{m'_{11}} \\ \frac{k'_{21}}{m'_{22}} & \frac{k'_{22}}{m'_{22}} & \dots & \frac{k'_{2n}}{m'_{22}} \\ \vdots & \vdots & \ddots & \vdots \\ \frac{k'_{n1}}{m'_{nn}} & \frac{k'_{n2}}{m'_{nn}} & \dots & \frac{k'_{nn}}{m'_{nn}} \end{bmatrix} \tag{3.16}$$

During seismic events, the property of the structural members which is most severely impacted is the change in stiffness. As such, this thesis focuses only on the loss of stiffness in a structure to determine damage and the mass is assumed to have not changed significantly during the seismic event. Therefore, the denominators in Eq. 3.16 can be changed from m'_{ij} to m_{ij} to produce a new matrix as shown in Eq. 3.17, where the stiffness terms are the only ones which change between the baseline case and the unknown case.

$$d^i_{j,damaged} \cong \begin{bmatrix} \frac{k'_{11}}{m_{11}} & \frac{k'_{12}}{m_{11}} & \dots & \frac{k'_{1n}}{m_{11}} \\ \frac{k'_{21}}{m_{22}} & \frac{k'_{22}}{m_{22}} & \dots & \frac{k'_{2n}}{m_{22}} \\ \vdots & \vdots & \ddots & \vdots \\ \frac{k'_{n1}}{m_{nn}} & \frac{k'_{n2}}{m_{nn}} & \dots & \frac{k'_{nn}}{m_{nn}} \end{bmatrix} \tag{3.17}$$

The Stiffness Damage Feature (SDF) is presented in Eq. 3.18 as follows.

$$SDFs = \frac{d^i_{j,damaged} - b^i_{j,basline}}{b^i_{j,basline}} \times 100\% \tag{3.18}$$

where i: sensor clusters; j: adjacent sensors

An overall procedure of the ARMAX DDM is presented in Figure 3-3.

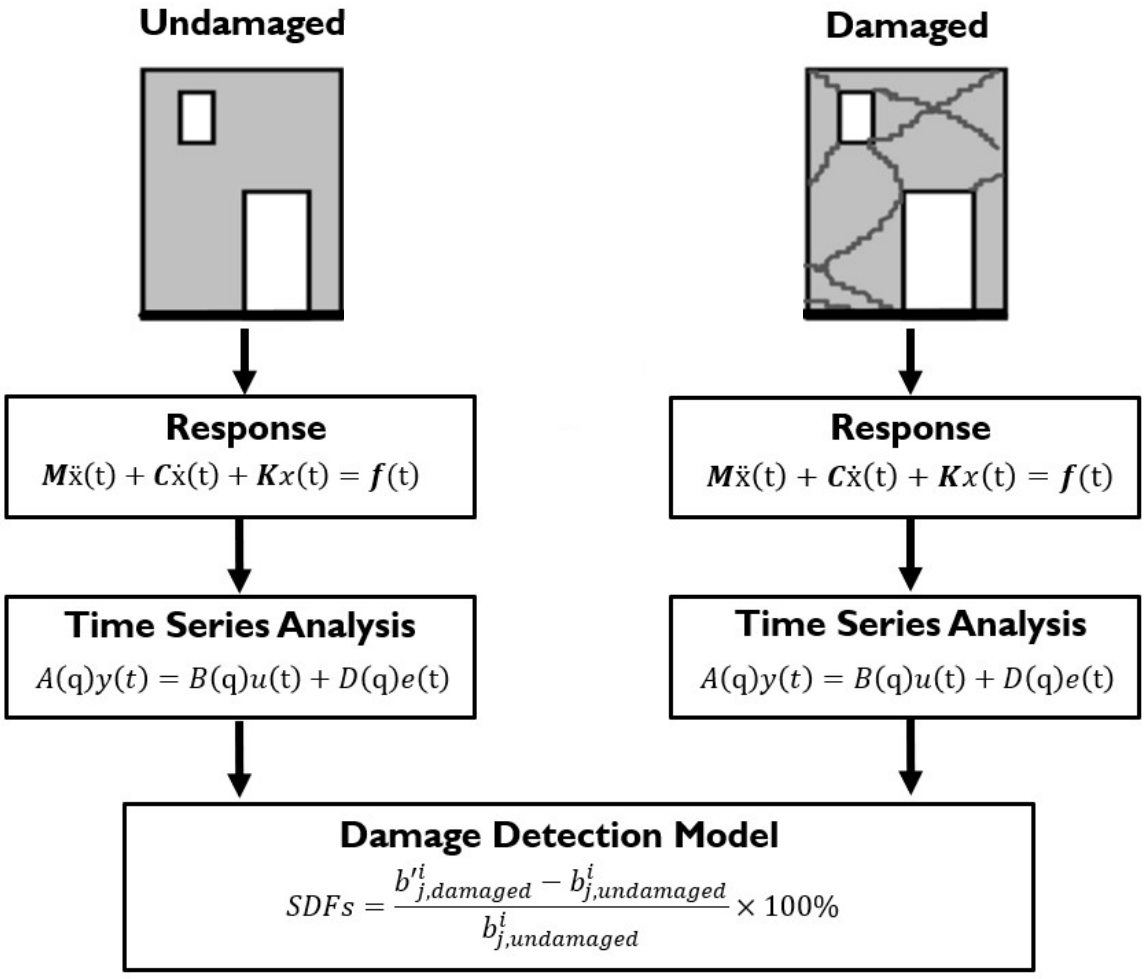

Figure 3-3 ARMAX DDM Procedure (FEMA 306)

3.2. Wind Speed Simulation Model

The ARMAX DDM previously outlined requires acceleration readings at every storey to properly function. As previously stated, the acceleration responses can be gathered by installing one bi-axial sensor per storey in two perpendicular directions. These accelerations are created by a lateral excitation forces acting on the building. The two main lateral excitation forces considered in structural analysis are wind forces acting on the face of the building and seismic forces created from ground motion. The following section outlines the benefits of incorporating wind forces as opposed to seismic forces.

One benefit of wind is that no matter how small of a speed, wind is almost always present which allows lateral acceleration measurements to be taken at any time. Seismic events, on the other hand, are much more sporadic. It is never certain when a building will be excited by ground motions, making seismic excitation forces much less dependable for detecting damage.

As previously described in Section 3.1, the ARMAX damage model functions by taking a set of acceleration measurements during the structure's undamaged state and a set of acceleration measurements in the damaged state. It is assumed that as those measurements are taken, no additional damage occurs on the structure. For example, if a 100 second sample is taken for the damaged case, it is assumed that at the 40 second mark, more damage is not suddenly incurred on the structure. Provided that the wind speeds are not exceedingly high, it can be assumed that the ambient wind forces won't induce additional damage during the 100 second sampling time. Seismic excitation forces, however, may cause damage to the structure as the measurements are taking place which does not fit the ARMAX DDM's assumption.

As previously mentioned in the Literature Review, the typical approach for wind loading simulations on structures involves generating a synthetic wind velocity field in time domain and transforming that velocity field into a pressure field through approximate pressure coefficients (Rossi et al. 2004). Sections 3.2.1, 3.2.2 and 3.2.2.3 detail the process in generating a wind velocity field applicable to the ARMAX DDM and Section 3.2.4 elaborates on how to determine the pressure coefficients pertaining to the location and surrounding characteristics of the building in question.

3.2.1. Wind Speed at Reference Elevation

When simulating a wind speed function, a common technique involves breaking the wind down to two components: the Low Frequency Component (LFC) which represents the average hourly wind speed; and the high frequency component (HFC) which considers the wind speeds at shorter time periods ranging from 10s to 300s (Welfonder et al, 1997; Bayem et al, 2008; Nichita et al, 2002). This can be represented as follows:

$$v(t) = v_{LFC}(t) + v_{HFC}(t) \tag{3.19}$$

Welfonder et al (1997) generated a LFC using a stochastic process based on a Weibull probability density function (PDF). The turbulence component was obtained using white noise as the input from a Von Karman based spectral density function. The model was validated through excellent fitting with real-life data. Bayem et al. (2008) obtained the low frequency component from an ARMA model which was previously developed by Karki et al. (2006). The turbulence component was created using a state equation with white noise as input. This equation was based on the Kaimal SDF from a previous study completed by Eckelund (1994). Validation of Bayem's model was never provided. Nichita et al (2002) obtained the LFC by interpolating the low frequency range of the experimental Van der Hoven power spectral density (Van, 1957). The turbulence component was generated by calculating the convolution of the impulse response of a second order rational transfer function. This method required a great amount of computational effort and the model was never validated with real data.

Fernando and Alonso (2017) created a model which considered both wind components as stochastic variables, greatly simplifying the wind speed simulation process. Their process involved first calculating the wind speed at the start and end of an hour time period (v_{LFC}[i] and v_{LFC}[i+1]) and then calculating the high frequency component at ten second intervals. Their simulation model correlated excellently to real life measurements taken at four separate wind farms.

The reference elevation wind simulation model which is detailed in Section 3.2.1 is based on the work previously done by Fernando and Alonso in 2017. Note that their method focused on wind simulations for wind turbines in open fields, and therefore thorough modifications were applied to the wind simulation model to account for buildings in dense urban areas.

3.2.1.1. Low Frequency Component (V_{LFC})

In order to create a low frequency function which can relate to real-life conditions, the wind speed at the start and at the end of an hour sample is required. It is impossible to predict with absolute certainty what the wind speed will be at the end of an hour based on the starting hourly wind speed, however numerous statistical models have been created to best predict this. Reviews of various statistical models have shown that a forecasting Weibull distribution model could best predict the next hourly wind speeds based on the previous wind speeds (Amri et al., 2015; Gualtieri & Secci, 2012; Carvalho et al., 2014). Figure 3-4 illustrates the general shape and characteristics of a Weibull distribution at different starting hourly wind speeds.

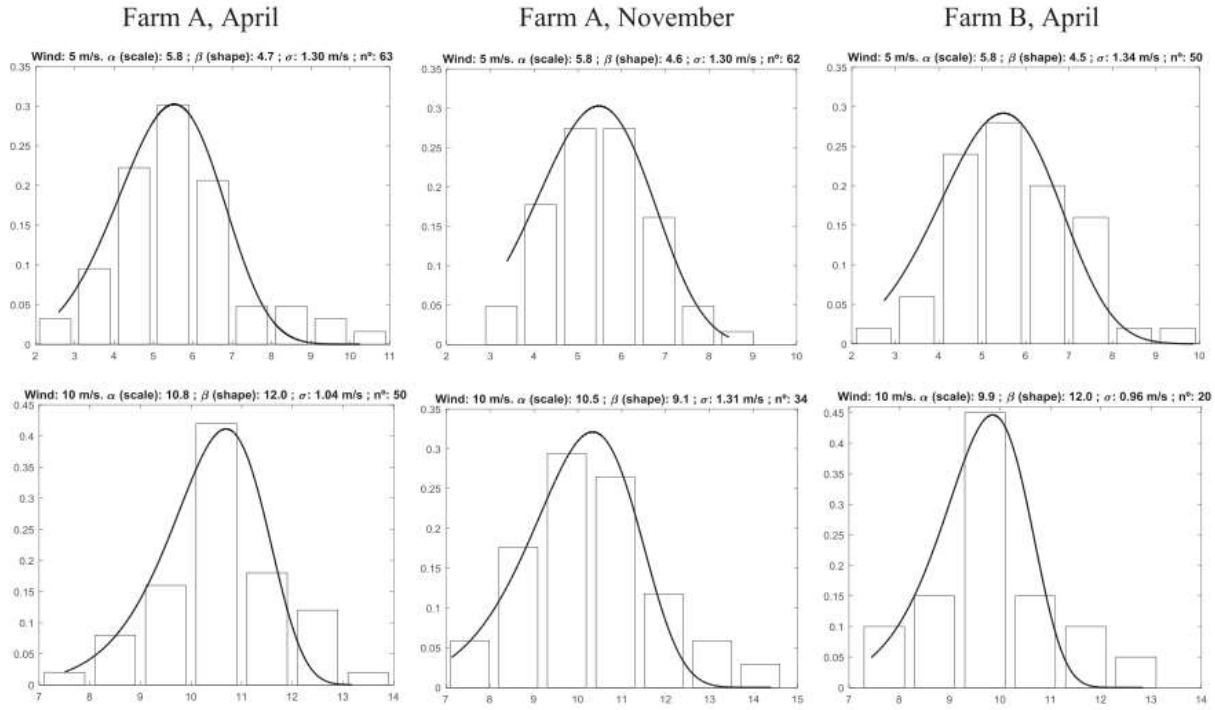

Figure 3-4 Weibull Distribution of Wind at Various Wind Farms (Fernando and Alonso, 2017)

To generate a forecasting Weibull distribution model, the first parameters required include the previous hourly wind speed and a corresponding standard deviation. Karki et al. (2012) studied the relationship between previous hourly wind speeds and the standard deviation and presented their results. For clarity the results are presented in both Table 3-1 and Figure 3-5.

Table 3-1 Relationship Between Previous Hourly Wind Speed and Future Standard Deviation

Previously Hourly Mean Wind Speed (m/s)		Standard Deviation for Wind in the Next Hour
Very Low	2.78	1.22
Low	4.19	1.28
Average	5.42	1.31
High	6.78	1.35
Very High	8.12	1.42

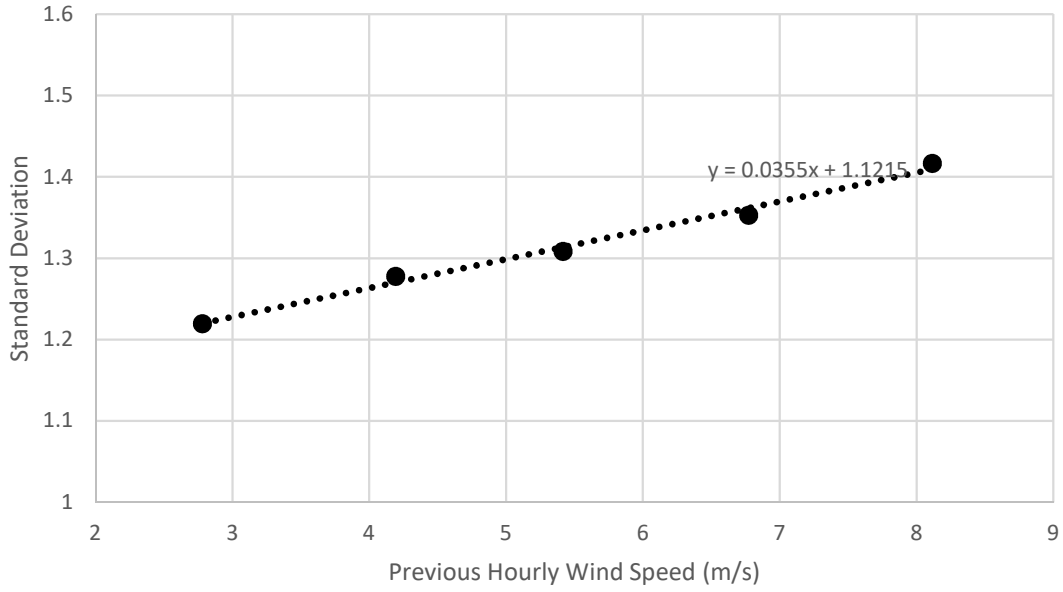

Figure 3-5 Relationship Between Previous Hourly Wind Speed and Future Standard Deviation

Figure 3-5 illustrates how the relationship between the previous hourly wind speed and next hourly wind standard deviation can be represented as a linear relationship as presented in Eq. 3.20.

$$\sigma = (0.0355 \times U_{SPEED}) + 1.1215 \tag{3.20}$$

With an hourly wind speed known from measurements and the standard deviation calculated from Eq. 3.20, the only other requirements to create a forecasting Weibull distribution are a scale and shape parameter.

There are a multitude of numerical methods to calculate the scale and shape parameter of a Weibull Distribution solely based on the mean and standard deviation values. These methods include the maximum likelihood method, energy pattern factor method, graphical method, equivalent energy method, and the method of moments (MOM). Direct comparison studies between the numerical methods consistently show that the MOM performed best with any given Weibull distribution parameters (Rocha et al, 2012; Y. Lei, 2008; Azad et al, 2014). The MOM relates the mean (v) and standard deviation (σ) of hourly wind speed to the shape (k) and scale (c) factors as follows:

$$\begin{aligned} v &= c\Gamma(1+1/k) \\ \sigma &= c[\Gamma(1+2/k) - \Gamma^2(1+1/k)]^{1/2} \\ \text{where } \Gamma(k) &= \int_0^\alpha y^{x-1} \times e^{-y} dy \end{aligned} \tag{3.21}$$

Although the MOM has been proven to accurately calculate the Weibull distribution parameters, it is computationally heavy due to the Gamma function in both the mean and standard deviation equations. Some mean and standard deviation combinations yielded trivial solutions with negative shape and scale parameters. To avoid any trivial solutions, Azad et al. (2014) found that the shape factor can be approximated as follows:

$$k = \left(\frac{0.9874}{\frac{\sigma}{v}} \right)^{1.0983} \tag{3.22}$$

This approximation eliminated the need for a Gamma function in the shape function equation, greatly simplifying the process and eliminating any trivial possibilities. The accuracy of the approximation was within 0.5% when considering low and moderate shape parameters. This approximation was applied throughout this thesis' wind simulation function.

By inputting any previous hourly wind speed, using the standard deviation relationship as shown in Eq. 3.20, the MOM as shown in Eq. 3.21 and the approximation in Eq. 3.22, a Weibull Distribution model could be created which can accurately simulate the behaviour of wind speed at the end of the hour. With the wind speeds at the start (v_{LFC}[i]) and end (v_{LFC}[i+1]) of an hour, the mean hourly wind speed, which represents V_{LFC}, was calculated as follows:

$$v = \frac{v_{LFC}[i] + v_{LFC}[i+1]}{2} \tag{3.23}$$

3.2.1.2. High Frequency Component (V_{HFC})

3.2.1.2.1. Overview

With the V_{LFC} determined, the next step involved calculating the high frequency component (V_{HFC}). The model used to generate the HFC presented below is based on work originally completed by Fernandes-Bernal (2012) which was then then modified further by Fernando and Alonso (2017). This thesis introduces modifications to the HFC to ensure that the wind simulation can be applied at any reference elevation and in any type of terrain.

In this thesis, the high frequency component sample size is 10 seconds. To generate wind speeds at these 10 second intervals, a random number was generated based on a Beta probability density function with a range of [0,1]. This random number is then scaled to an appropriate range [v_{MIN}, v_{MAX}] based on V_{LFC} which was previously calculated. This newly scaled random number is labelled as V_{HFC} [n]. This process is then repeated 360 times to calculate one hour's worth of wind speed values. This process is outlined below in Eq. 3.24 and in Figure 3-6.

$$\begin{aligned} v_{HFC}[0] &= v_{LFC}[i] \\ v_{HFC}[n] &= \xi(a,b) \times (v_{MAX}[n] - v_{MIN}[n]) + v_{MIN}[n] \\ &\qquad (n = 1 \;\; to \;\; N) \\ v_{HFC}[N+1] &= v_{LFC}[i+1] \end{aligned} \tag{3.24}$$

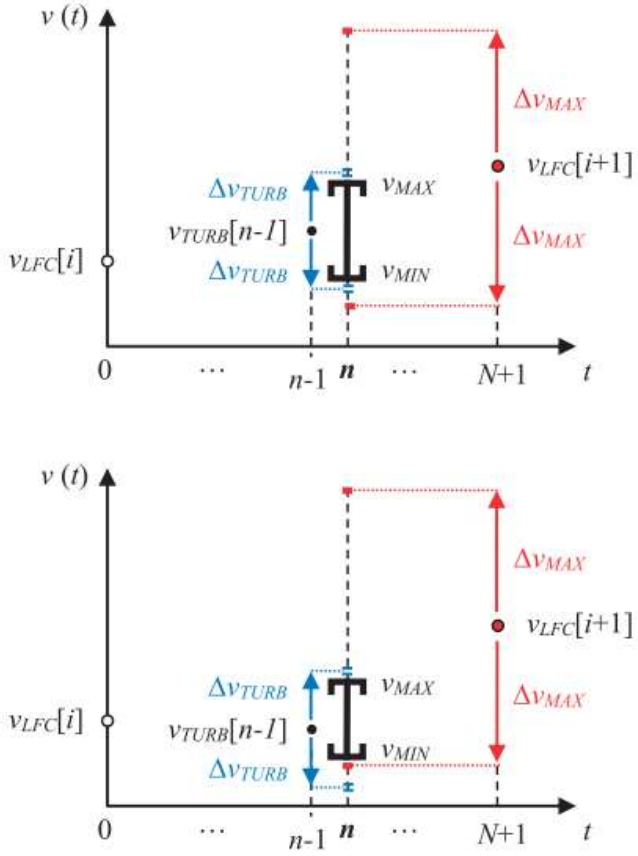

Figure 3-6 Overview of Wind Speed Simulation Model (Fernando & Alonso, 2017)

The integral part of this simulation is correctly calculating the [v_{MIN}, v_{MAX}] range which determined the limits of the Beta PDF. The Beta PDF has a mean of 0.5 to ensure symmetry, a standard deviation of 0.2 and shape parameters $a = b = 2.625$. Previous work completed by Fernando and Alonso (2017) shows that these parameters best reflect the properties of wind from measured data at multiple sites. Figure 3-6 illustrates how the [v_{MIN}, v_{MAX}] is limited by both the Δv_{TURB} and Δv_{MAX}, both of which are constant throughout the hour time period. The values for v_{MIN} and v_{MAX} are defined in Eq. 3.25 as follows.

$$\begin{aligned} v_{MIN}[n] &= MAX\{v_{TURB}[n-1] - \Delta v_{TURB}[i], v_{LFC}[i+1] - \Delta v_{MAX}[i], 0\} \\ v_{MIN}[n] &= MIN\{v_{TURB}[n-1] + \Delta v_{TURB}[i], v_{LFC}[i+1] \\ &\quad + \Delta v_{MAX}[i], v_{LIM}[i]\} \end{aligned} \tag{3.25}$$

The following section details how to obtain the Δv_{TURB} and Δv_{MAX} required to create the $[v_{MIN}, v_{MAX}]$ range.

3.2.1.2.2. Calculating Δv_{TURB} and Δv_{MAX}

To calculate ΔV_{TURB}, the standard deviation of the turbulence component was first determined using Eq. 3.26 below:

$$\sigma_{TURB}[i] = \kappa[i] \times \left(\frac{v_{LFC}[i] + v_{LFC}[i+1]}{2}\right) \qquad (3.26)$$
$$where\ \kappa[i] = turbulence\ component$$

The turbulence component is dependent on the location of the wind speed generation and is generally much higher in "rough" terrain such as heavily urban areas and much lower in "smooth" terrain such as open fields. Terrain types can be classified into five categories as illustrated in Figure 3-7 below.

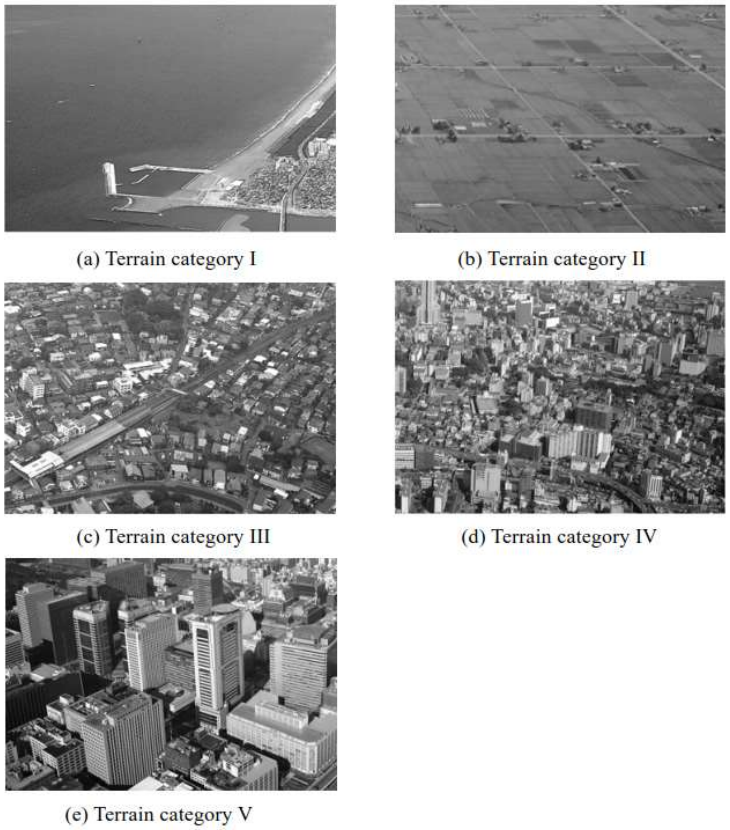

Figure 3-7 Terrain Categories (Holmes, 2015)

Goto et al. (2002) conducted full scale turbulence measurements in each terrain category listed above in Figure 3-7. The authors found that the turbulence can be related to the terrain category and reference elevation as per the interpolated lines in Figure 3-8.

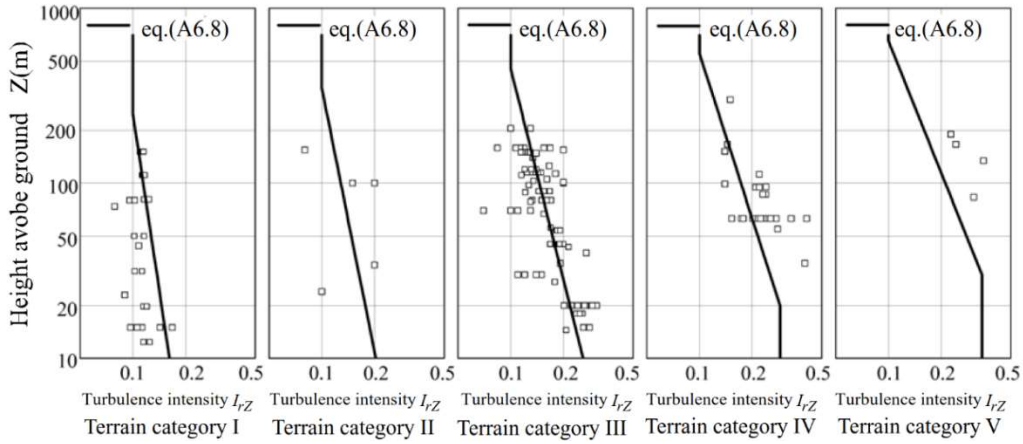

Figure 3-8 Turbulence Intensity Values for Varying Terrain Categories (Goto et al., 2002)

With the terrain category and reference elevation chosen, the standard deviation of the 10 second interval wind speeds was calculated as shown in Eq. 3.27.

$$\Delta v_{TURB}[i] = k_{SAMPLE} \times \sigma_{TURB}[i]$$
$$where\ k_{SAMPLE} = 3.25 - 0.3 \times \ln(N) \tag{3.27}$$

Note that Δv_{TURB} is dependent on the sampling time used as shown in k_{SAMPLE} where N represents the total number of samples taken in the hour time period. For example: T_{SAMPLE} = 10 s (N=360), T_{SAMPLE} = 300 s (N=12). The k_{SAMPLE} equation was determined experimentally based on the comparison between the multiple simulations and real life wind data. Extensive trials have shown that this factor combined with others in the turbulence algorithm give excellent fitting with experimental results.

The process for calculating Δv_{MAX} is shown in Eq. 3.28. The factor of 1.25 in Eq. 3.28 was found to best fit the real life wind behaviour of wind at multiple sites. The second condition assures that the simulation generates no trivial solution where v_{MIN} becomes greater than v_{MAX}.

$$\Delta v_{MAX}[i] = MAX\{1.25 \times \Delta v_{TURB}[i], |v_{LFC}[i+1] - v_{LFC}[i]| \tag{3.28}$$

With Δv_{TURB} and Δv_{MAX} both calculated, the wind simulation model can be generated at 10 second intervals. Eq 3.29 presents the order for the loop calculations which include all the factors previously listed.

$$
\begin{aligned}
&v_{TURB}[0] = v_{LFC}[i] \\
&\sigma_{TURB}[i] = \kappa[i] \times \left(\frac{v_{LFC}[i] + v_{LFC}[i+1]}{2} \right) \\
&\Delta v_{TURB}[i] = k_{SAMPLE} \times \sigma_{TURB}[i] \\
&\Delta v_{MAX}[i] = MAX\{1.25 \times \Delta v_{TURB}[i], |v_{LFC}[i+1] - v_{LFC}[i]| \\
&v_{MIN}[n] = MAX\{v_{TURB}[n-1] - \Delta v_{TURB}[i], v_{LFC}[i+1] - \Delta v_{MAX}[i], 0\} \\
&v_{MIN}[n] = MIN\{v_{TURB}[n-1] + \Delta v_{TURB}[i], v_{LFC}[i+1] + \Delta v_{MAX}[i], v_{LIM}[i]\} \\
&v_{TURB}[n] = \xi(a,b) \times (v_{MAX}[n] - v_{MIN}[n]) + v_{MIN}[n] \quad ; \quad n = 1 \ \ to \ \ N \\
&v_{TURB}[N+1] = v_{LFC}[i+1]
\end{aligned}
\tag{3.29}
$$

With this loop calculation methodology, a wind speed simulation can be created pertaining to the speed at one reference elevation only. For the ARMAX DDM, wind forces are required for every storey, not just at one reference elevation. This loop process cannot simply be repeated at every elevation as the inherent randomness would lead to no correlation between the wind speeds at each elevation which in turn does not reflect real life scenarios. As such, a novel correlation function was created to generate wind speeds at every elevation based on the reference elevation wind speed calculated in Eq. 3.29.

3.2.2. Wind Speeds at Other Elevations

When generating the wind speed functions for elevations other than the reference storey elevation, two factors must be considered: the mean wind speed at the given elevation and the correlation with regards to the neighbouring storey wind speeds.

3.2.2.1. Wind Speed – Elevation Relationship (Power Law)

In general, wind speeds increase at higher heights. A variety of wind speed profiles in different terrain types illustrating this phenomenon are shown in Figure 3-9.

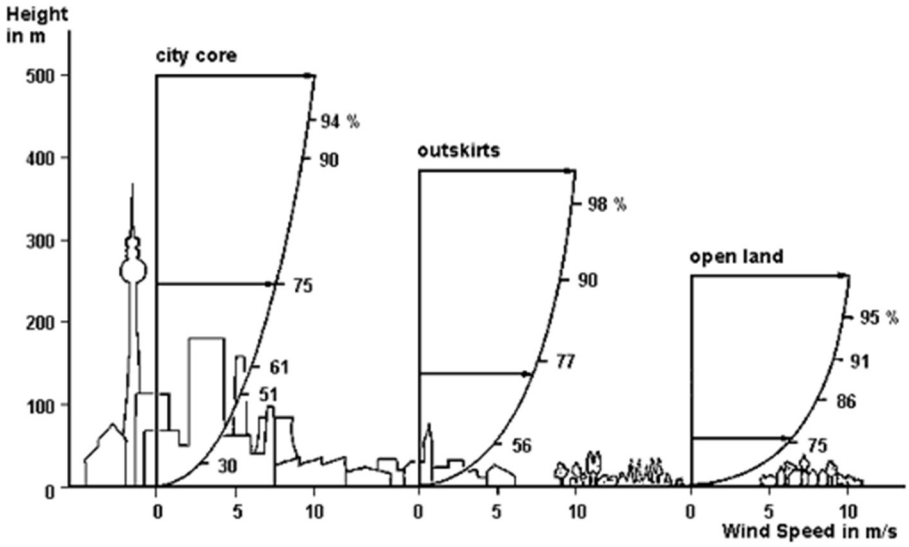

Figure 3-9 Wind Speed Profiles in Multiple Terrain Categories (Baumbach, 1994)

Previous studies have shown that the mean wind speed profiles shown in Figure 3-9 can be represented most accurately with the Power Law at heights below 200m (Peterson & Hennessey, 1978).

$$U(z) = U_r \times \left(\frac{z}{Z_r}\right)^{\alpha} \tag{3.30}$$

This equation can relate the mean wind speeds at any elevation to the mean wind speed which was calculated at the reference elevation (U_r) in Section 3.2.1. The exponent α is an empirically derived landscape coefficient that ranges from 0.10 for smooth, flat terrain to 0.40 for cities with high rise buildings (Bañuelos-Ruedas et al., 2010).

3.2.2.2. Wind Speed Correlation

Correlation is defined as the real number in the range [-1, 1] that measures how two variables (i.e. wind speeds) at different elevations evolve with each other. If both variables change in a similar way, i.e. they increase simultaneously or decrease simultaneously, they are considered strongly correlated and the value will be close to 1. If the variables change in the opposite way, i.e. the wind speed at one storey decreases while the wind speed at another increases, then they are considered strongly correlated in a negative sense and the value will be close to -1. If the variables have a

correlation value of 0, then they are considered uncorrelated. The Pearson correlation equation, which is used to measure correlation of two variables is defined in Eq 3.31.

$$\rho_{xy} = \frac{\sigma_{xy}^2}{\sigma_x \sigma_y} \tag{3.31}$$

It is without question that there exists a positive correlation between wind speeds at different elevations. The correlation generally ranges from 0.50 – 0.80 depending on site characteristics and wind speeds. Kim and Yoon (2009) studied the various equations which have been previously created to represent the coherence of wind speeds at different elevations of a building. They looked at nine different equations and compared them directly with wind tunnel data to determine which methodologies had the most accurate results. Through their comparison, they found that a methodology presented by Kim et al. (2009) best reflected real-life measurements.

$$\begin{aligned}
&C_{12}(r_y, r_z, n) = e^{(-r^* \times n^*)} \\
&r^* = \frac{\sqrt{(k_y r_y)^2 + (k_z r_z)^2}}{L_x(z_m)} \\
&n^* = \sqrt{1 + \left(\frac{n L_x(z_m)}{k_2 U(z_m)}\right)^2} \\
&z_m = \sqrt{z_1 \times z_2} \\
&r_z = z_2 - z_1 \\
&where\ k_y = 0.5,\ \ k_z = 0.5,\ \ k_2 = 0.06
\end{aligned} \tag{3.32}$$

In Eq. 3.32 listed above, the only inputs required are the vertical and horizontal distances between two points (r_z and r_y respectively) and the frequency at which wind speeds are taken (i.e. T_{SAMPLE}=10s, n=0.1). With the power law and correlation effects accounted for, a wind speed model was generated in the following section which accounts for any elevation as it relates to the wind speed created in Section 3.2.1.

3.2.2.3. Wind Speed Generation Model (Any Elevation)

The first step in creating a wind speed at any elevation was to generate the wind speed at the reference elevation (first storey) as shown in Section 3.2.1, as that reference elevation speed is the

baseline for the second storey wind speed. With the baseline wind speed generated, each storey's wind speed was built in ascending order while accounting for the power law and wind speed correlation.

Section 3.2.2.3 outlines the procedure for generating the wind speed at the second storey based on the previously calculated wind speed of the first storey. The example structure in question involves a multi storey structure with 3.25m height storeys in unsheltered terrain. Looking at the sample structure, the mean wind speed at the second floor (6.50 m elevation) is predicted to be 1.07 higher than the mean wind speed of the second floor (3.25 m elevation) as illustrated in Figure 3-10.

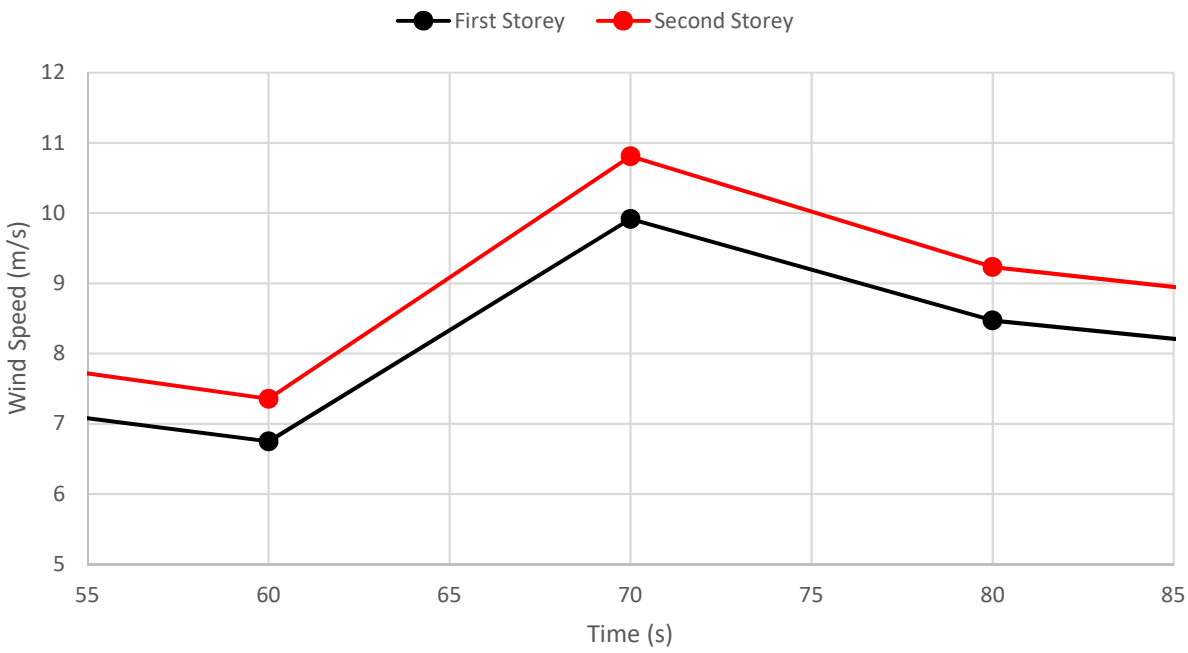

Figure 3-10 Wind Speed Correlation = 1.0

Note that this figure represents two winds speeds with a perfect correlation value of 1.0. The correlation of real life wind speeds, however, will not be equal to one as shown by Kim et al. (2009). Therefore, a Correlation Generator (CG) was incorporated to induce some randomness by either increasing or decreasing the wind speed from its baseline value as shown in Figure 3-11. The numbers were bounded by a normal distribution with varying limits to create wind speed trials with varying correlation values. Figure 3-11 illustrates the wind speeds previously shown in Figure 3-10 with a CG in which the limits were set to -0.9 to +0.9 m/s.

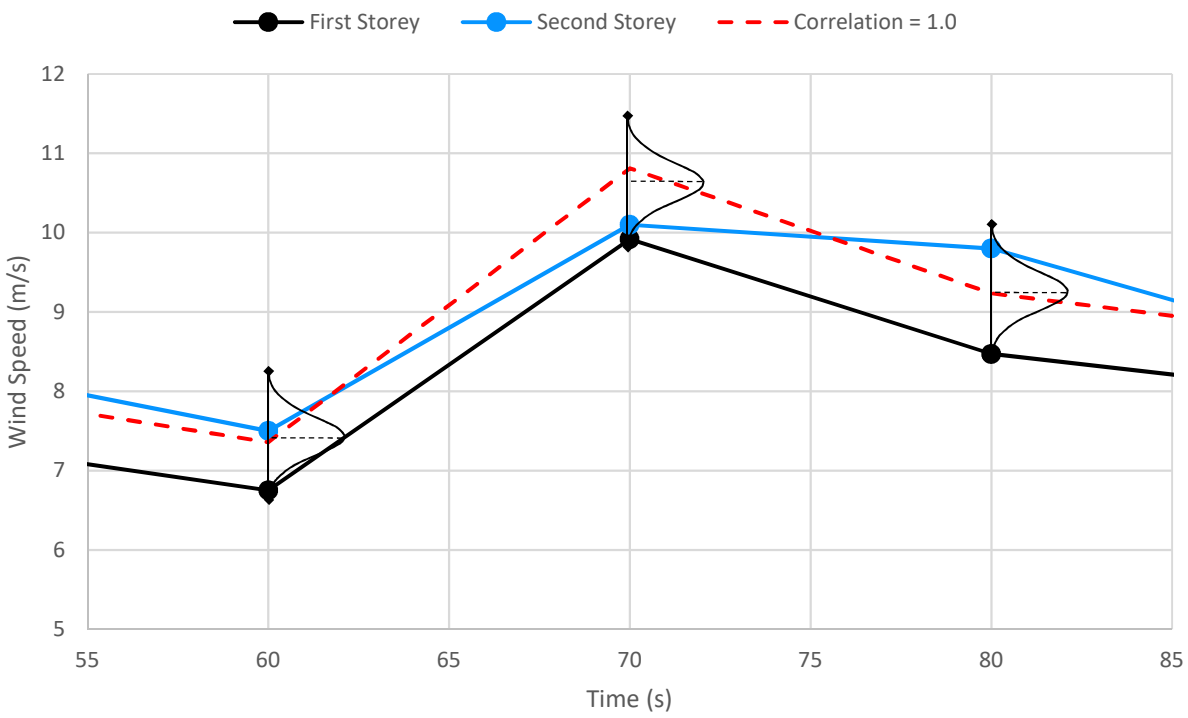

Figure 3-11 Wind Speed Correlation = 0.933

By incorporating a CG with the limits above, the correlation was lowered to 0.933 in one trial. Using the Kanda Coherence method, the coherence between the first and second stories of our sample building is predicted to be 0.695, therefore larger limits must be imposed on the CG to decrease the correlation value. Figure 3-12 illustrates the effect that larger limits have on the CG.

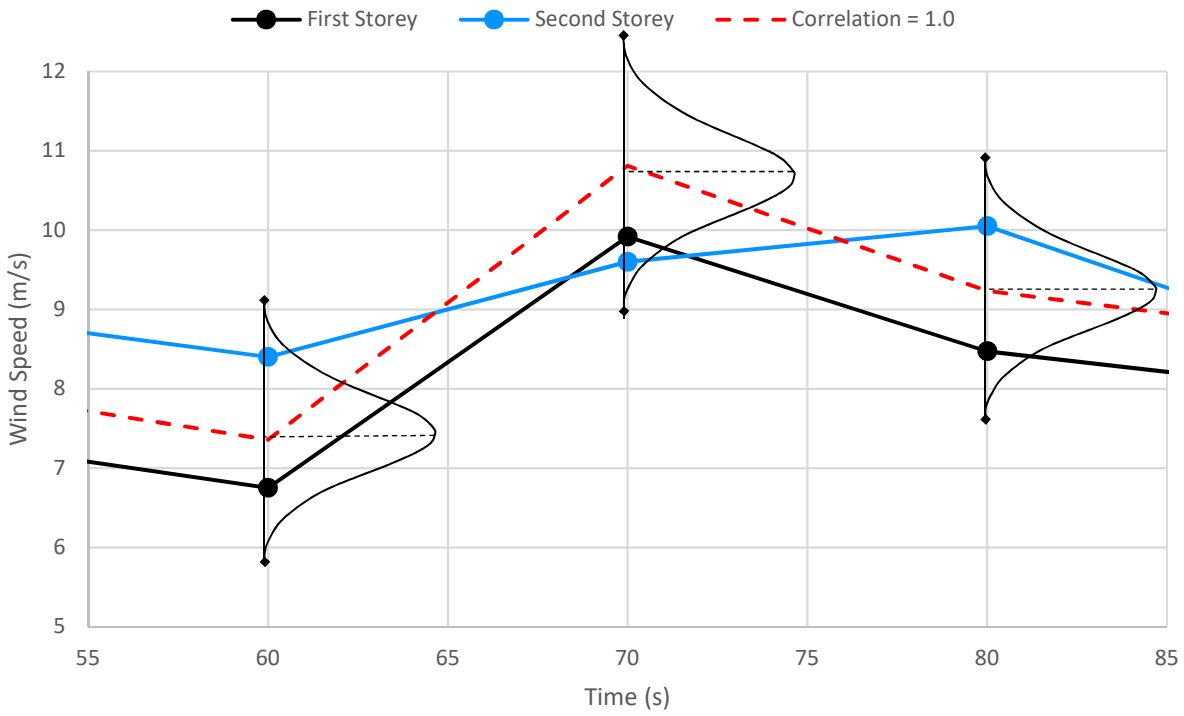

Figure 3-12 Wind Speed Correlation = 0.694

With the limits presented in Figure 3-12, the correlation drops to 0.694 which is nearly identical to the target correlation value of 0.695. As this CG process is randomized, it is not known what exact trial and corresponding limits will yield the wind speed closest to the target value. As such, an iterative program was created which simulates several wind speed trials with different limits and then checks which trial yielded the optimal correlation value.

With the second storey wind speed generated, the wind speed is then generated for the third floor using the same CG procedure with the second storey as the new reference elevation speed. This process is repeated for each storey until each floor has a wind speed which corresponds to the Power Law mean speed and appropriate correlation.

3.2.3. Turbulence Effects

Although the wind speed simulation can accurately generate wind speeds at 10 second intervals, the simulation must be refined further to account for turbulence at a one second wind speed samples. It is unrealistic to assume that wind speeds can be accurately reflected with linear slopes

that change every 10 seconds as shown in Figure 3-10, Figure 3-11 and Figure 3-12. As such, a white noise function is incorporated which creates turbulence at one second intervals.

An example final version of wind speeds at 10 separate storeys is shown below in Figure 3-13 which represents wind speeds with a strong average starting hourly wind speed of 4m/s (~11 km/hr) at the first storey.

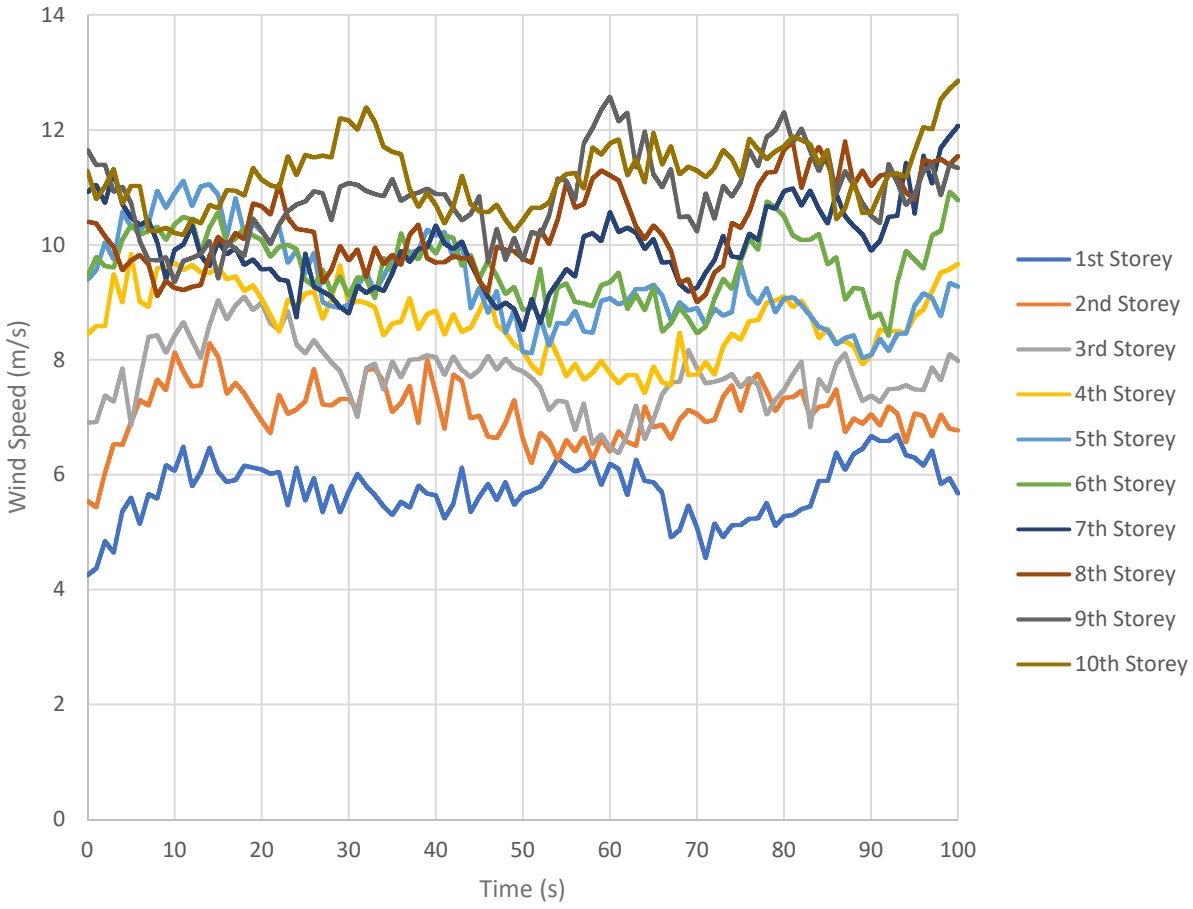

Figure 3-13 Sample Wind Speeds at Ten Storeys

3.2.4. Wind Pressure Coefficients

With the wind speeds calculated for each floor, the next step involved creating a function which converts the wind speeds into a pressure force acting upon a building. As wind hits a building, it does not all hit it straight on due to bluff body aerodynamics which lead to wind dispersion on impact (Baines, 1963). Figure 3-14 illustrates the typical pressure coefficients from wind directly hitting the face of a tall unsheltered building.

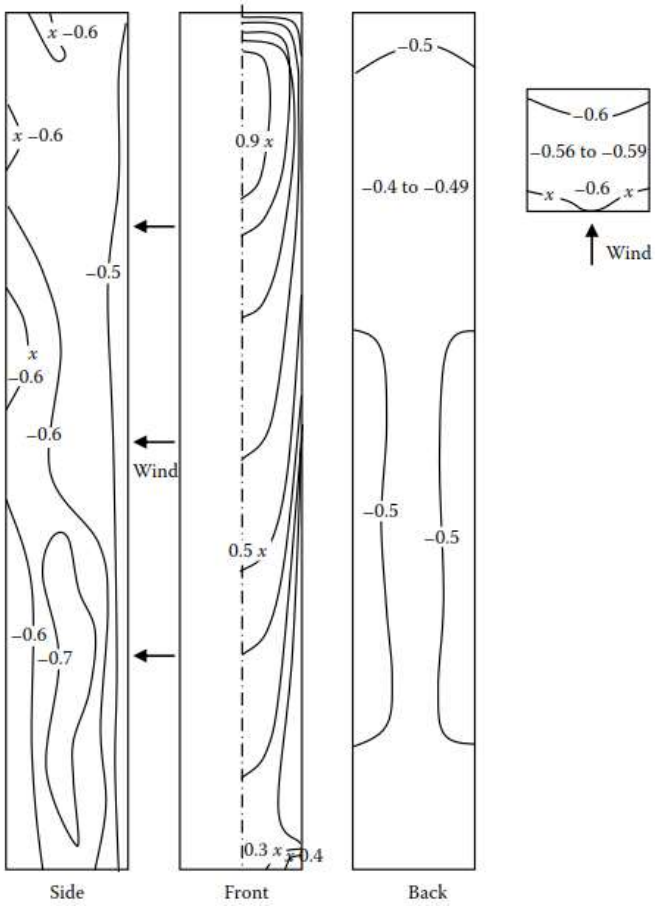

Figure 3-14 Typical Pressure Coefficient Values on a Tall Building (Baines, 1963)

Most buildings, however, are not typically located in unsheltered areas and wind does not always blow directly against a face. When a building is sheltered by other effects, the coefficients are lowered. Table 3-2 presents all the factors accounted for when creating the wind pressure coefficients model.

Table 3-2 Wind Pressure Coefficient Factors

Factor	Description
Density of surrounding buildings (PAD)	The more nearby buildings present, the higher the sheltering effects are, lowering the pressure coefficient
Relative height of surrounding buildings (RBH):	The taller the surrounding buildings are in relation to the building in question, the higher the sheltering effects are, lowering the pressure coefficient
Surface Roughness (α):	The 'rougher' the terrain category (as explained in 4.1.2.2), the higher the sheltering effects are, lowering the pressure coefficient
Angle of Wind	The more direct the angle of the wind is hitting the surface of the building, the higher the overall pressure coefficients will be.

Mario Grosso (1992) gathered data from multiple studies looking at the pressure coefficients and the effects from the factors listed in Table 3-2. With that data, a parametric model was developed which can accurately simulate pressure coefficients along a building based on all factors. Below are sample location values and the corresponding windward face pressure coefficient distributions with respect to the relative height of the building at the centre of the floors.

Table 3-3 Wind Pressure Coefficient Examples

Location	Surface Roughness	Surrounding Building Density	Relative Building Height
1 – Fully Exposed Building	0	0	0
2 – Tall building in lower density area	0.2	5	.5
3 – Tall building in Urban Area	0.33	10	.8

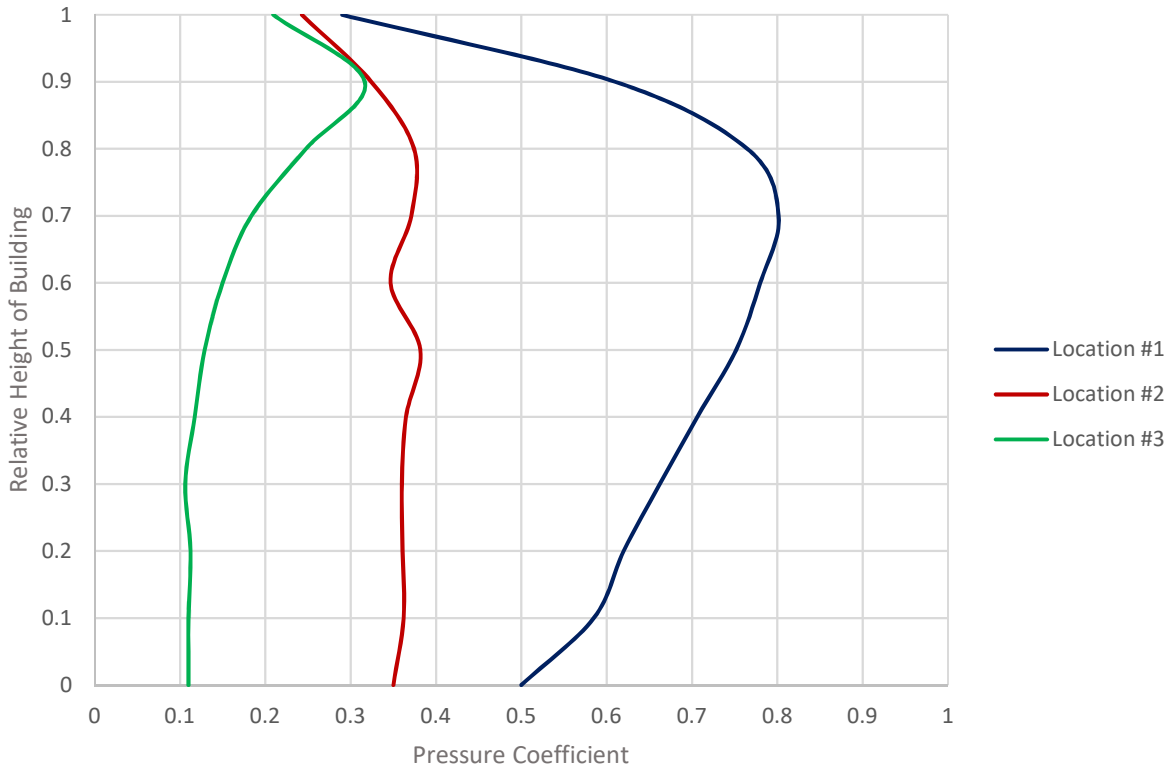

Figure 3-15 Sample Wind Pressure Coefficients

These pressure coefficients along with the previously calculated wind speed functions are used in conjunction to generate storey by storey wind force which can be utilized during the damage detection model. A sample of windward and leeward distributed forces (6m/s average wind speed)

acting on a four storey 16m tall building are presented in Figure 3-16 and Figure 3-17. In both figures, storey #3 has a much larger windward force than storey #4 even though the wind speed at storey #4 is higher. This difference in force is due to storey #4 having a much smaller pressure coefficient along with half the tributary area of all other storeys.

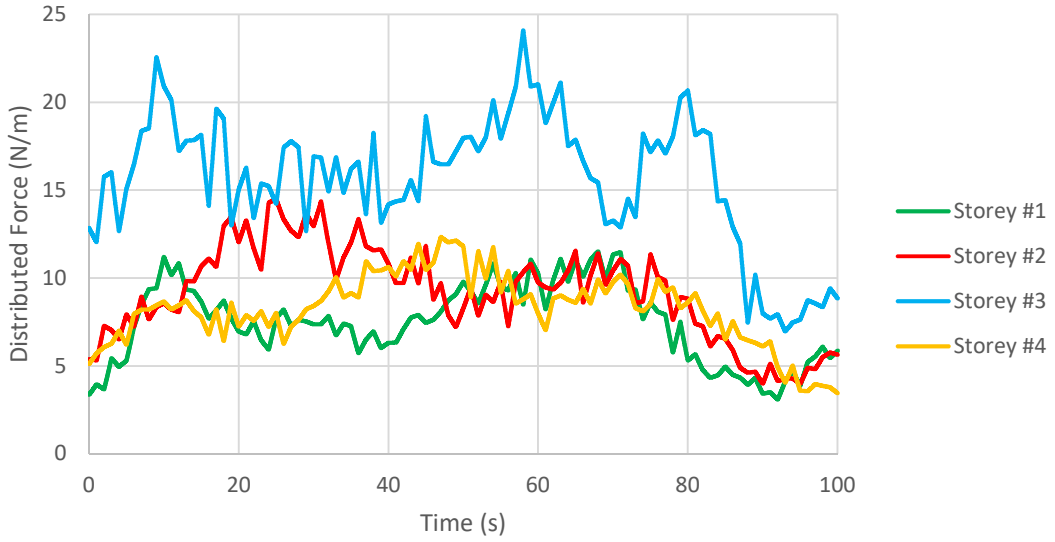

Figure 3-16 Windward Forces Acting on a 4 Storey Building

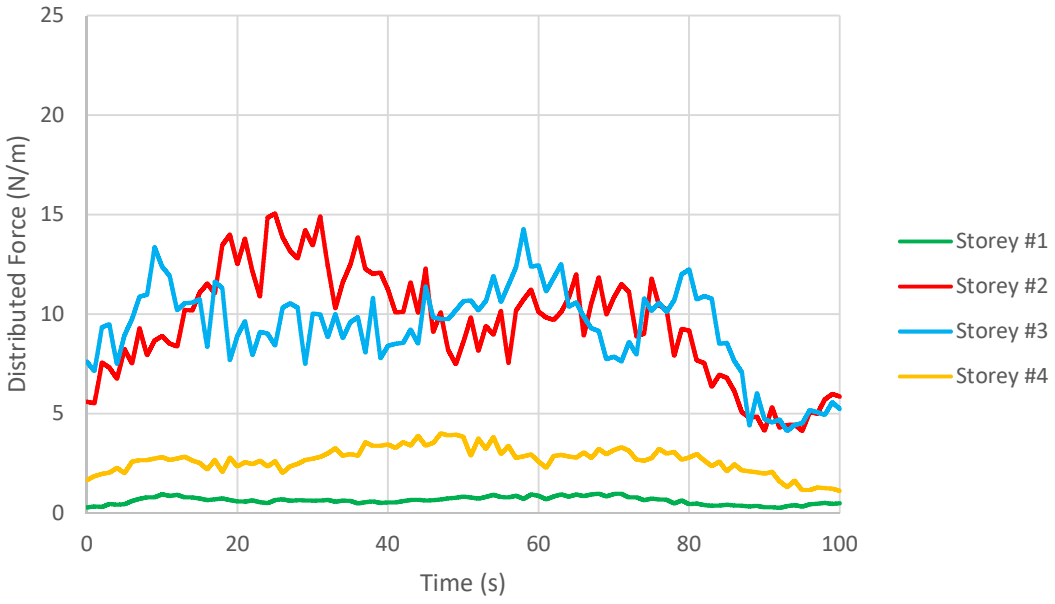

Figure 3-17 Leeward Forces Acting on a 4 Storey Building

3.3. Numerical Damage Modelling Technique

As the proposed method in this thesis is based on its ability to detect damage in numerical building models, it is imperative that the damage properly reflects real life behaviour. As previously mentioned throughout the Literature Review, one of the most commonly used damage analysis technique to determine the degree of damage in a structure is the stiffness degradation method, which compares the initial loading stiffness slope of an undamaged structural member to the reloading stiffness slope after the member / structure is subjected to a seismic event. This stiffness degradation model will be utilized throughout this thesis as it directly relates to the focus of the ARMAX DDM which determines the change in stiffness at a storey by storey-level.

The damage model presented in Sections 3.3.1 and 3.3.2 is a simplified version of the stiffness degradation model created by Zongming et al. (2016) in which stiffness degradation values of reinforced concrete members and structures were converted into damage in concrete and steel material properties using fiber beam elements. To properly reflect damage, both the concrete and steel properties must be modified. Those modifications are presented in the following sections.

3.3.1. Concrete Damage

In the damage model created by Zongming et al. (2016), it was assumed that any stiffness reduction can be attributed to the degradation of the initial reloading modulus of concrete as shown in Eq. 33. This assumption holds true because when the steel bars are unloaded and reloaded, their reloading modulus generally will not change drastically due to the elastic nature of steel, whereas the formation of cracks in concrete due to a seismic event would greatly reduce the reloading modulus. This damage model assumes that the concrete has underwent non-linear damage due to the concrete strain passing its peak strength value (~0.22%) as shown in Figure 3-18. Note that although the concrete has undergone non-linear damage, the ambient wind forces acting on the reinforced concrete afterwards would be of low enough force so that the concrete is behaving in a linear fashion. The damage in the concrete can be represented as Eq 3.33.

$$DR_{Concrete} = 1 - \frac{E_{New}}{E_{Original}} \tag{3.33}$$

Chang and Mander (1994) studied the effects of dynamic and cyclic loading on concrete and they developed a set of equations which can relate the original stiffness ($E_{ORIGINAL}$) to any reloading damaged stiffness (E_{NEW}) while also calculating the new stress and strain capacities. This set of equations proposed by Chang and Mander were adapted to create new concrete capacity curves in which the only inputs required are the original concrete compressive strength, initial flexural stiffness and the target Damage Ratio (DR).

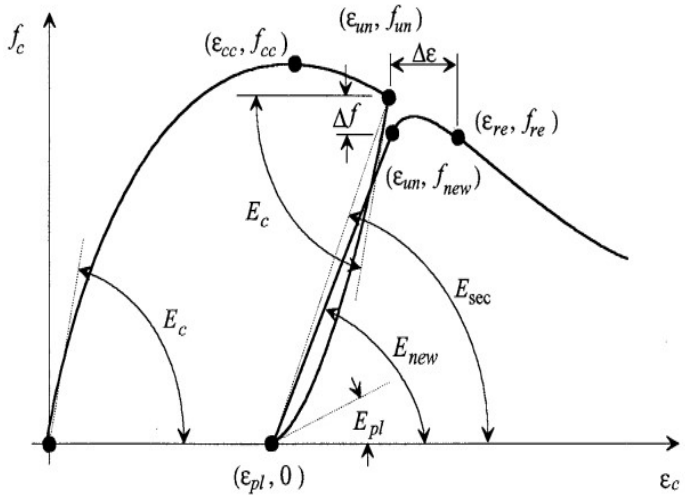

Figure 3-18 Concrete Unloading and Reloading Compressive Curve (Chang & Mander, 1994)

The range of Damage Ratios were tested which range from minor damage (0.40) to critical damage (0.65). Minor damage refers to the point in which cracks become noticeable in the concrete. Critical damage refers to the point just before complete failure of the concrete with zero force capacity as shown by the '**x**' marked on Figure 3-18. These Damage Ratio limits and corresponding degrees of damage were determined previously by Toussi and Yao (1983).

The stiffness, ultimate strength and ultimate strain capacity of the undamaged and damaged 40 MPa concrete used throughout the numerical modelling of this thesis is presented in Table 3-4. It is assumed that the damaged concrete has lost all tensile capacity due to cracking.

Table 3-4 Undamaged and Damaged Concrete Material Properties

Damage Ratio	Undamaged	0.40	0.45	0.50	0.55	0.60	0.65
E (MPa)	32888	19733	18088	16444	14800	13155	11511
σ_{ULT} (MPa)	40	36.66	34.53	31.72	28.19	24.06	19.56
ξ_{ult} (%)	0.220	0.200	0.200	0.200	0.200	0.190	0.180

Figure 3-19 is presented below for better visualization and understanding of how the damaged concrete compressive curves compare to the undamaged concrete. Past a strain value of 0.37%, it is assumed that the concrete will have completely failed (Toussi & Yao, 1983).

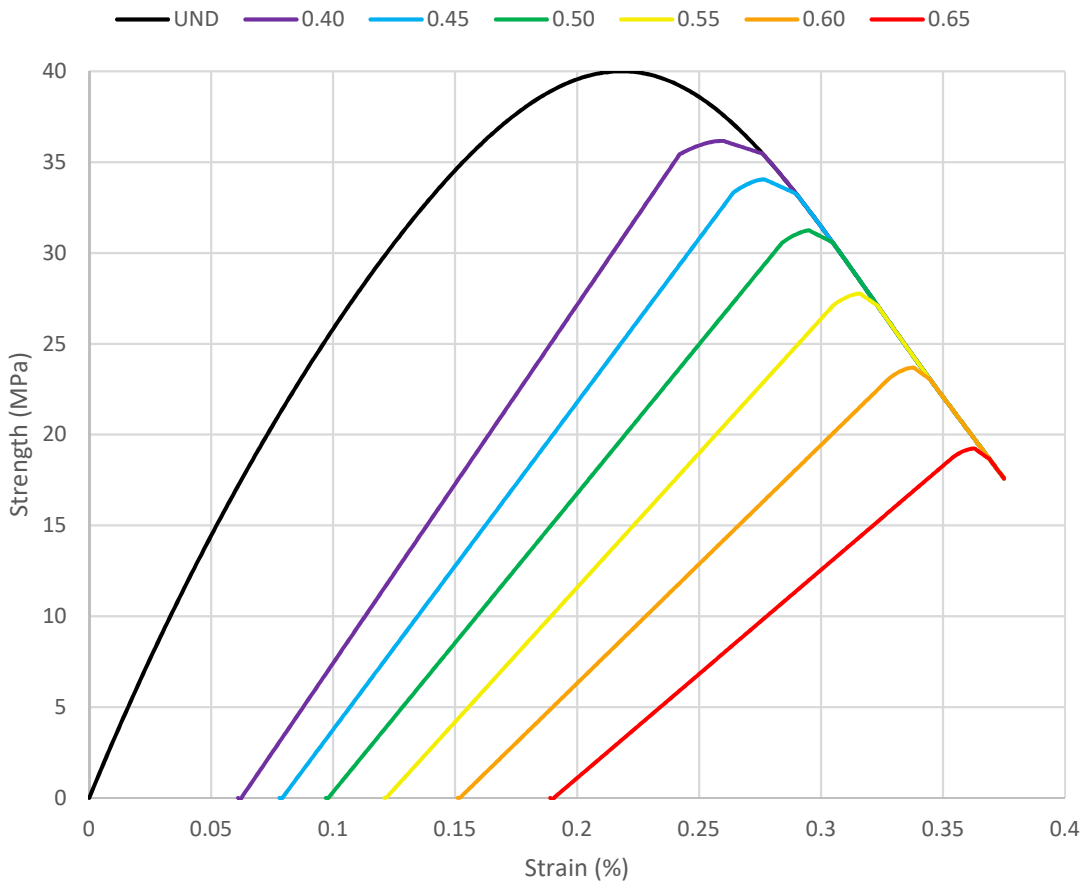

Figure 3-19 Concrete Compressive Strength Curves

3.3.2. Steel Damage

As the steel reinforcing bars undergo cyclic loading, the unloading and reloading modulus of elasticity remains relatively unchanged (Zongming et al, 2016). What does change however, is the ultimate strength of the steel, as the constant cyclic loading has a fatigue loading effect as illustrated in Figure 3-20.

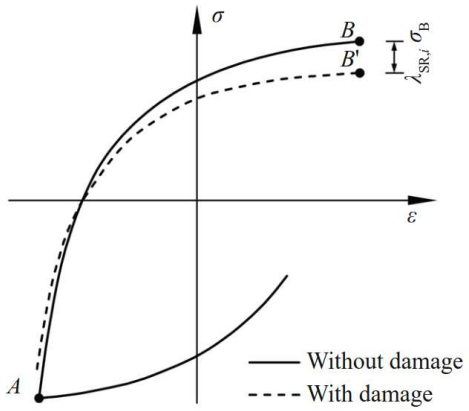

Figure 3-20 Steel Strength Degradation Behaviour (Chang & Mander, 1994)

The DR of the reinforcing steel bars can be calculated as the ratio of the new ultimate strength of the steel compared to its undamaged ultimate capacity and is illustrated in Eq. 3.34 below.

$$DR_{Rebar} = 1 - \frac{\sigma_{Ult.(New)}}{\sigma_{Ult.(Original)}} \tag{3.34}$$

From the numerical work done by Zongming et al. (2016), a relationship between the Damage Ratio of the concrete (loss in stiffness) and the Damage Ratio of the reinforcing steel (loss in ultimate strength) was developed and is presented in Figure 3-22. This numerical damage model was based on applying cycle loading to an experimental symmetric reinforced concrete column and measuring the damage ratios of concrete and steel after each cycle as shown in Figure 3-21.

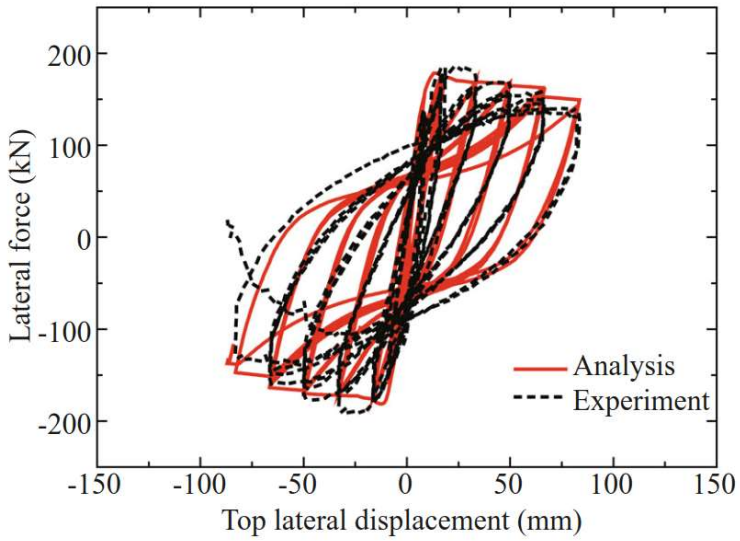

Figure 3-21 Top Lateral Displacements of Numerical and Experimental RC Columns under Cycle Loading

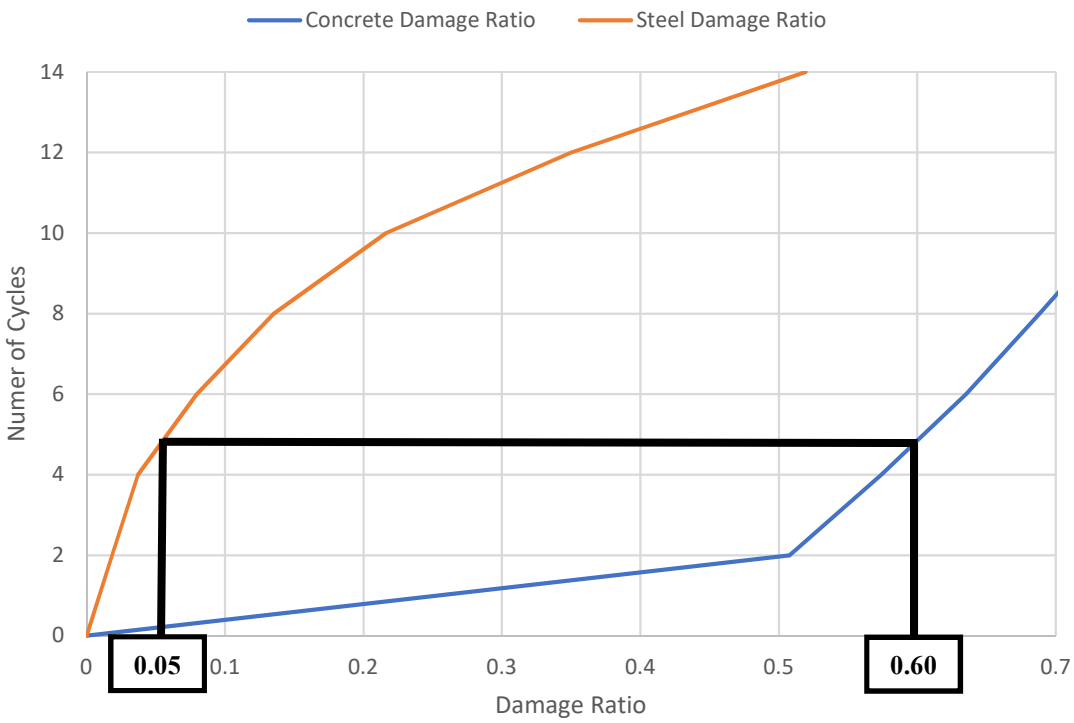

Figure 3-22 Concrete and Rebar DR Relationship

As an example, if a column is severely damaged, it can be assumed that it has a $DR_{Concrete}$ of 0.60 which during the experimental testing corresponds to loading cycles for the experimental columns.

This number of cycles would translate to a DR_{Steel} of 0.05, which signifies that rebar that initially had an ultimate strength of 450 MPa would now have an ultimate strength of 428 MPa.

With these two Damage Ratios along with the relationship shown in Figure 3-22, a simplified damage model can be inputted into the numerical modelling program by updating both the concrete and steel material properties based on the degree of damage.

3.4. Summary and Overview of Damage Detection Model

Chapter 3 can be summarized in three distinct sections. Section 3.1 provided the detailed procedure of the ARMAX DDM that is utilized throughout this thesis. Section 3.2 outlines the steps taken to generate a realistic wind forcing function and Section 3.3 provides a brief overview of the simplified damage model that is used throughout the numerical modelling.

The overview of the entire methodology is presented in Figure 3-23.

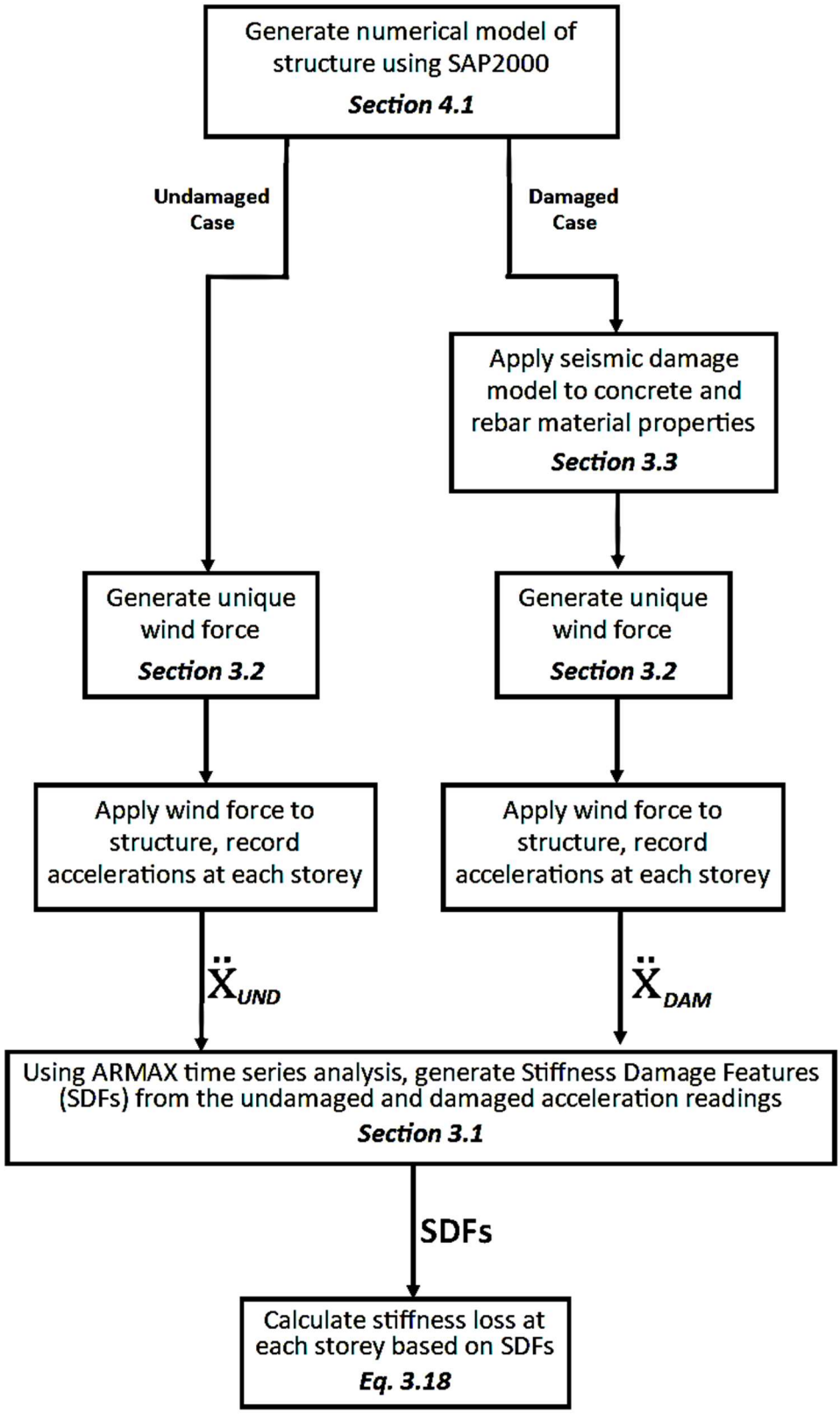

Figure 3-23 Damage Model Overview

CHAPTER 4:ANALYSIS AND RESULTS

To verify the validity of the ARMAX damage detection model, six separate structures were modelled using SAP2000 v14. Each structure was subjected to a variety of damage cases, and the undamaged and damaged models' acceleration responses to ambient wind forces were analyzed and the SDFs were calculated. Those SDFs were then directly compared to the expected SDF results which were obtained from extracting the stiffness matrix from SAP2000.

Two of the structures modeled were steel structures and the other four were reinforced concrete (RC) frames where shear deformation from lateral loading is most prevalent. The ARMAX DDM assumes that the structures can be approximated as shear type structures and therefore flexural deflection are not considered. The material specifications for the structural steel, concrete and rebar are all presented in detail in Appendix A.

Each structure is presented with damage cases which range from minor damage cases (only one storey damaged) to severe damage cases (>70% of storeys damaged). For more detailed results which show the wind speeds used and additional noise levels, refer to Appendix A.

4.1. Testing Parameters

Five of the structures tested were four storeys tall and one structure tested was 10 storeys tall. The four storey buildings were simplified as 4-DOF systems where the stiffness values of k_1 to k_4 are the lateral force resisting stiffness' at each floor and the mass is assumed to be lumped in the floor of each storey. Each numerical building model is treated as a strong beam weak column structure and therefore the beams and slabs were treated as perfectly rigid. The stiffness and mass matrix of the first four buildings are shown in Eq. 4.1 and Eq. 4.2 respectively.

$$K = \begin{bmatrix} K_{11} & K_{12} & K_{13} & K_{14} \\ K_{21} & K_{22} & K_{23} & K_{24} \\ K_{31} & K_{32} & K_{33} & K_{34} \\ K_{41} & K_{42} & K_{43} & K_{44} \end{bmatrix} = \begin{bmatrix} k_1 + k_2 & -k_2 & 0 & 0 \\ -k_2 & k_2 + k_3 & -k_3 & 0 \\ 0 & -k_3 & k_3 + k_4 & -k_4 \\ 0 & 0 & -k_4 & k_4 \end{bmatrix} \tag{4.1}$$

$$M = \begin{bmatrix} m_{11} & 0 & 0 & 0 \\ 0 & m_{22} & 0 & 0 \\ 0 & 0 & m_{33} & 0 \\ 0 & 0 & 0 & m_{44} \end{bmatrix} \tag{4.2}$$

With the stiffness and mass matrices set up as shown, the stiffness damage feature (SDF) matrix was represented as follows. Note that the equation to calculate each SDF is shown in Eq. 3.18.

$$SDF = \begin{bmatrix} SDF_{11} & SDF_{12} & 0 & 0 \\ SDF_{21} & SDF_{22} & SDF_{23} & 0 \\ 0 & SDF_{32} & SDF_{33} & SDF_{34} \\ 0 & 0 & SDF_{43} & SDF_{44} \end{bmatrix} \tag{4.3}$$

This methodology also applies to the 10-storey structure, with the only difference being that the stiffness, mass and SDF matrices are represented as 10x10 matrices as opposed to 4x4 matrices. With the general SDF matrix set up, the overall loss in stiffness at each storey was calculated using Eq. 4.4. Note that 'last storey' refers to the highest storey of the building.

Storey	**Equation Used**
First Storey	$\Delta K_1 = (2 \times SDF_{11}) - \Delta K_2$
Intermediate Storeys (all storeys except the first and last)	$\Delta K_i = \frac{SDF_{i-1,i} + SDF_{i,i-1}}{2}$
Last Storey	$\Delta K_n = \frac{SDF_{n-1,n} + SDF_{n,n-1} + SDF_{n,n}}{3}$

(4.4)

Theoretically, the change in stiffness at each storey (aside from the first) can be gathered by taking a single SDF value, however by averaging the value of two SDF values instead, the experimental errors were mitigated.

To better simulate real life scenarios, environmental and operational conditions were accounted for by adding 5% noise to each storeys acceleration response during the baseline and damaged case. The SDF results presented in the following chapter represent the average SDF values after performing 10 trials with the noisy data.

For each structure, the storey accelerations were measured at the centre of each floor slab. Throughout the numerical modelling simulations, the average starting hourly wind speeds on the first storey ranged from 2m/s (3.6km/hr) to 8m/s (28.8km/hr).

Note that the first five structures were symmetric and therefore the analysis was done in the X-Z plane only. The final building had an asymmetric column layout and therefore it's analysis was not bound by any plane to ensure that torsional movements were incorporated.

The damage in each numerical model was represented as a uniform change in the material properties throughout an entire column. This model is slightly simplified, as it is expected in moment frames that the top and bottom of each column would be the most damaged due to the peak moment forces location. Further work should be done to test the ARMAX DDM with more realistic damage models.

4.1.1. Reinforced Concrete Specific Parameters

For each RC building model, the building reinforcement was designed as per the *Concrete Design Handbook – 4th Edition* with the loads being calculated using the *2015 National Building Code of Canada*. The structures were assumed to be conventional office buildings in Vancouver on Soil Type D. The building reinforcement was verified through SAP2000's automated moment frame design calculations.

The structural response due to wind for each RC model was calculated using Newmark's direct integration method ($\gamma = 0.25$, $\beta = 0.50$) and incorporated proportional damping with a constant 7% damping coefficient for undamaged structures and a 5% damping coefficient for the damaged structures (Newmark & Hall, 1982). The concrete compressive curves were modeled in SAP2000 using Mander's curve.

4.2. Structure #1: Steel Structure

It was imperative that the SAP2000 modelling parameters were properly calibrated to simulate real life structural behaviour. As such, the first structure considered was a replica of an experimental four storey steel structure which was built by Ngoan (2015). The SAP2000 model replica was subjected to identical damage cases to those tested in the experiments to verify that the SAP2000 model parameters used throughout this thesis properly reflect real life damage from previously created experiments. The focus on testing Structure #1 was not to detect seismic damage in a structure, it was to ensure that the numerical modelling parameters reflected real life behaviour.

Details of the experimental steel structure are shown in Figure 4-1 and the structure modeled in SAP2000 is shown in Figure 4-2. As each steel angle column is identical in material properties and dimensions, they are all considered to have identical stiffness values.

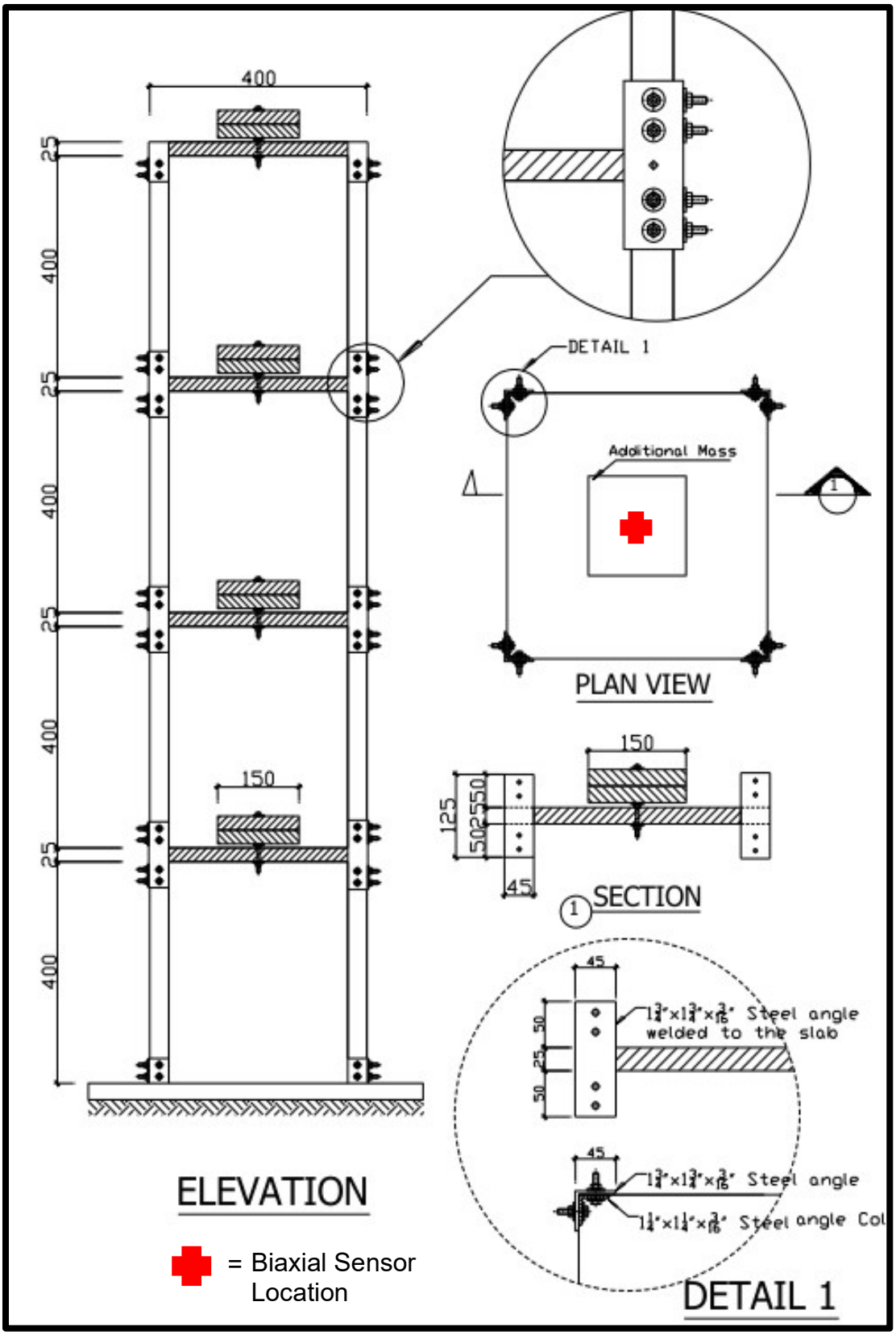

Figure 4-1 Structure #1 (Ngoan, 2015)

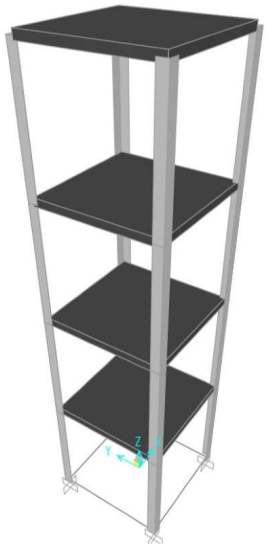

Figure 4-2 Structure #1 SAP2000 Model

To validate that the SAP2000 model can be replicated to match previous experiments, the structure was excited by two pairs of Multiple Impulse Forces (MIF) located at the two corners of the first and third floors. This forcing function was created through randomly generating an impulse force under normal distribution at every 0.1 seconds. A sample of the applied force is shown in Figure 4-3.

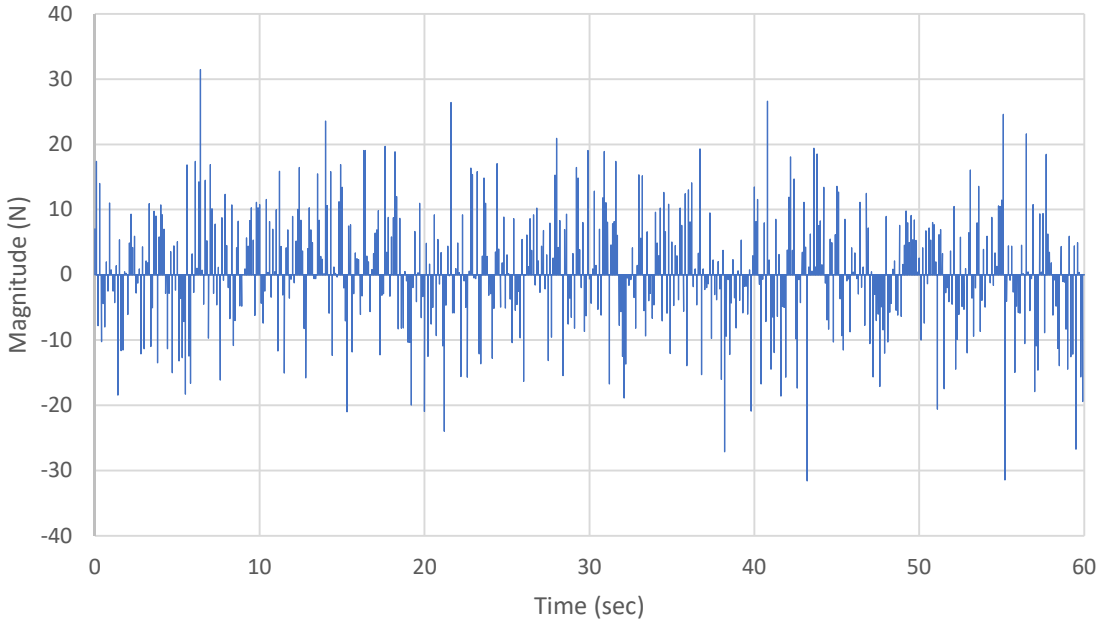

Figure 4-3 Multiple Impulse Force Sample

The acceleration response of the structure from the MIF was recorded at 0.001s intervals. For Structures #1 and #2, the response calculated by SAP2000 was a linear modal response using a constant damping of 2%.

4.2.1. Damage Case 1.1 – Single Storey Damage (4th Storey)

The first damage case tested involved replacing one of the steel angle columns with an identically sized aluminum angle column at the fourth storey as shown in Figure 4-4.

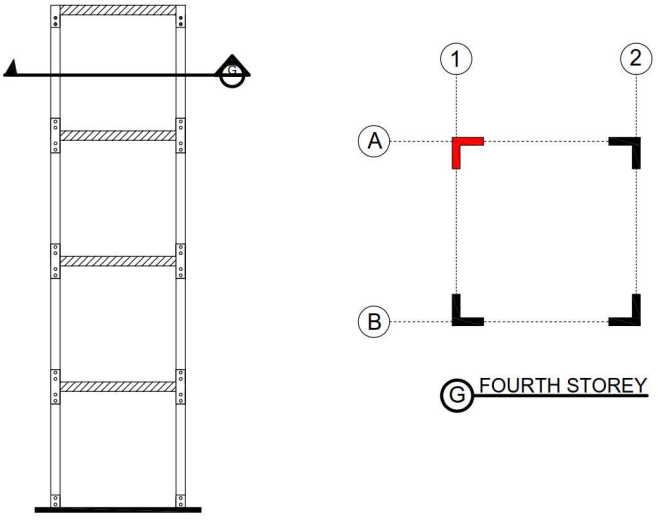

Figure 4-4 Damage Case 1.1

By replacing a 200 GPa steel column with a 63 GPa aluminum column, the Damage Ratio of the single column was 1 – (63/200) = 0.685. Every other column in the structure was unchanged and therefore can be assumed to have Damage Ratio of 0. The overall loss in stiffness on the fourth storey can be calculated as [((3 x 0) – (1 x 0.685)) / 4] = -17.13% which would be reflected in SDF_{34}, SDF_{43}, SDF_{44}; SDF_{33}, which represents the change in combined stiffness of the third and fourth storey can be calculated as [((7 x 0) – (1 x 0.685)) / 8] = -8.56%. Note that the denominator represents the total number of columns that are included in each respective SDF.

To validate this calculation method, each expected SDF is confirmed through extracting the stiffness matrix of the SAP2000 models. The extracted SAP2000 results (also referred to as the 'expected' results) and the ARMAX analysis results; one case with no noise and one with 5% noise added; are presented in Table 4-2 below. Throughout the damage cases, the SDF results

represent the average of 10 trials. Table 4-1 below represents the template for how the SDF results are presented in each damage case.

Table 4-1 SDF Results Template

Damage			SDFs (%) – Average of 10 Trials											
Location	Storey	Damage Ratio	SAP2000 Analysis (Expected)				ARMAX Analysis							
							No Noise				5% Noise			
A1	4	0.685	SDF_{11}	SDF_{12}	-	-	SDF_{11}	SDF_{12}	-	-	SDF_{11}	SDF_{12}	-	-
			SDF_{21}	SDF_{22}	SDF_{23}	-	SDF_{21}	SDF_{22}	SDF_{23}	-	SDF_{21}	SDF_{22}	SDF_{23}	-
			-	SDF_{32}	SDF_{33}	SDF_{34}	-	SDF_{32}	SDF_{33}	SDF_{34}	-	SDF_{32}	SDF_{33}	SDF_{34}
			-	-	SDF_{43}	SDF_{44}	-	-	SDF_{43}	SDF_{44}	-	-	SDF_{43}	SDF_{44}

Table 4-2 - SDF Results (DC 1.1)

Damage			SDFs (%) – Average of 10 Trials											
Location	Storey	Damage Ratio	SAP2000 Analysis (Expected)				ARMAX Analysis							
							No Noise				5% Noise			
A1	4	0.685	0	0	-	-	-0.09	-0.68	-	-	-0.16	-0.50	-	-
			0	0	0	-	-0.76	1.07	1.22	-	1.00	1.24	1.82	-
			-	0	-8.56	-17.13	-	-0.90	-7.52	-14.12	-	-1.60	-7.50	-14.39
			-	-	-17.13	-17.13	-	-	-14.87	-14.80	-	-	-14.71	-14.78

The 5% noise effect did not have a significant impact on the SDF values from the ARMAX analysis. With the SDF matrix set up, the overall loss in stiffness in each storey was calculated as shown in Eq. 4.4 using the 5% noise SDF values. The calculated change in stiffness at each storey from the ARMAX DDM is presented in Table 4-3 as per Eq. 4.4. For brevity, these calculations will not be shown for any other damage case.

Table 4-3 ARMAX Storey Stiffness Loss Calculations (DC 1.1)

Storey	Calculation	Stiffness Change
1	(2 x 0.25) – (-0.16)	- 0.56%
2	((-0.50) + (1.00)) / 2	+ 0.25%
3	((1.82) + (-1.60)) / 2	+ 0.11%
4	((-14.39) + (-14.71) + (-14.78)) / 3	- 14.62%

The overall change in stiffness of each storey based on the 5% noise SDF values from the 10 trials are presented in Table 4-4. The bracketed values in the ARMAX column represent the standard deviation of the 10 trials, with a lower standard deviation value signifying more stable results.

Table 4-4 Storey Stiffness Change (DC 1.1)

Storey	Stiffness Change (%)	
	Expected	ARMAX
1	**0**	**-0.56** (1.81)
2	**0**	**0.25** (1.66)
3	**0**	**0.11** (1.61)
4	**-17.13**	**-14.62** (0.87)

The ARMAX analysis successfully located and quantified the damage in the fourth storey while detecting no change in stiffness in all other storeys. The low standard deviation values for each storey (average value of 1.49) illustrates the stability of the results through the 10 trials even with added noise.

4.2.2. Damage Case 1.2 – Two Storey Damage (1st and 2nd Storeys)

The second damage case tested involved replacing two steel columns at the first storey and one steel column at the second storey with identically sized aluminum columns as shown in Figure 4-5.

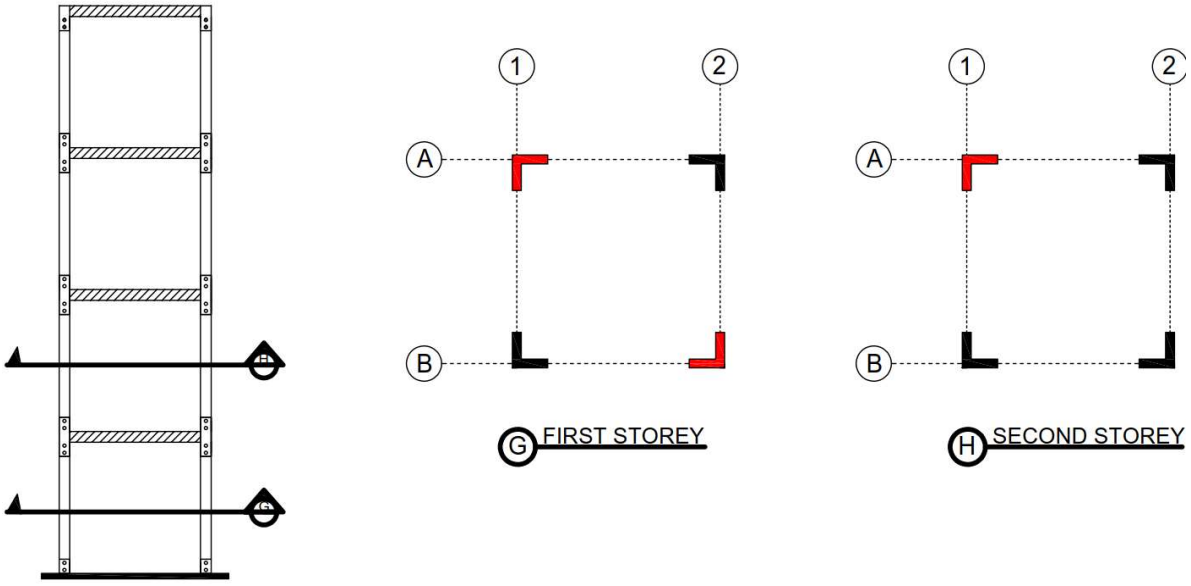

Figure 4-5 Damage Case 1.2

Similar to Damage Case 1.1, the damage ratios of the individual "damaged columns" is 0.685. SDF_{11}, which represents the change in stiffness of the combined first and second storey was calculated as [((5 x 0) - (3 x 0.685)) / 8] = -25.69%. The change in stiffness of the second story, as shown in SDF_{12} and SDF_{21} was calculated as [((3 x 0) - (1 x 0.685)) / 4] = -17.13% and SDF_{22} was calculated as [((7 x 0) – (1 x 0.315)) / 8] = -8.56%. For brevity, these calculations will not be shown for any further steel damage cases as the same process can be used for every damage case. In the results tables, each expected damage case result was completed by extracting the SAP2000 matrix, the hand calculations were only used as a second verification.

The expected SDFs and ARMAX SDFs are presented in Table 4-5.

Table 4-5 SDF Results (DC 1.2)

Damage			**SDFs (%) – Average of 10 Trials**											
Location	**Storey**	**Damage Ratio**	**SAP2000 Analysis (Expected)**				**ARMAX Analysis**							
							No Noise				**No Noise**			
A1	1	0.685	-25.69	-17.13	-	-	-26.29	-15.41	-	-	-23.11	-15.21	-	-
B2		0.685	-17.13	-8.56	0	-	-17.40	-7.21	-0.03	-	-17.72	-7.15	-0.12	-
A1	2	0.685	-	0	0	0	-	-3.10	-1.07	-0.50	-	-3.63	-3.77	-3.35
			-	-	0	0	-	-	-3.32	-2.32	-	-	-3.16	-2.01

The 5% noise effect did not have any significant impact on the ARMAX SDF values. The overall change in stiffness at each storey from both the expected results and the 5% noise ARMAX SDF are presented below as per Eq. 4.4.

Table 4-6 Storey Stiffness Change (DC 1.2)

Storey	Stiffness Change (%)	
	SAP2000	ARMAX
1	**-34.26**	**-29.75** (2.32)
2	**-17.13**	**-16.47** (1.45)
3	**0**	**-1.87** (1.34)
4	**0**	**-2.84** (0.87)

The ARMAX DDM successfully located the damage on the first and second storey while also measuring no substantial change in stiffness in the undamaged storeys. The degree of damage on the first floor was underestimated by 4.81%, however the degree of damage on the second storey was very close to the expected value. The low standard deviation values from the 10 trials illustrate the negligible impact that the 5% noise had on the ARMAX DDM.

4.2.3. Damage Case 1.3 – Three Storey Damage (1st, 2nd and 3rd Storeys)

The final damage case for the experimental steel structure represents a more severe case in which there is damage on the first, second and third storey with a total of six steel columns being replaced by aluminum columns as shown in Figure 4-6.

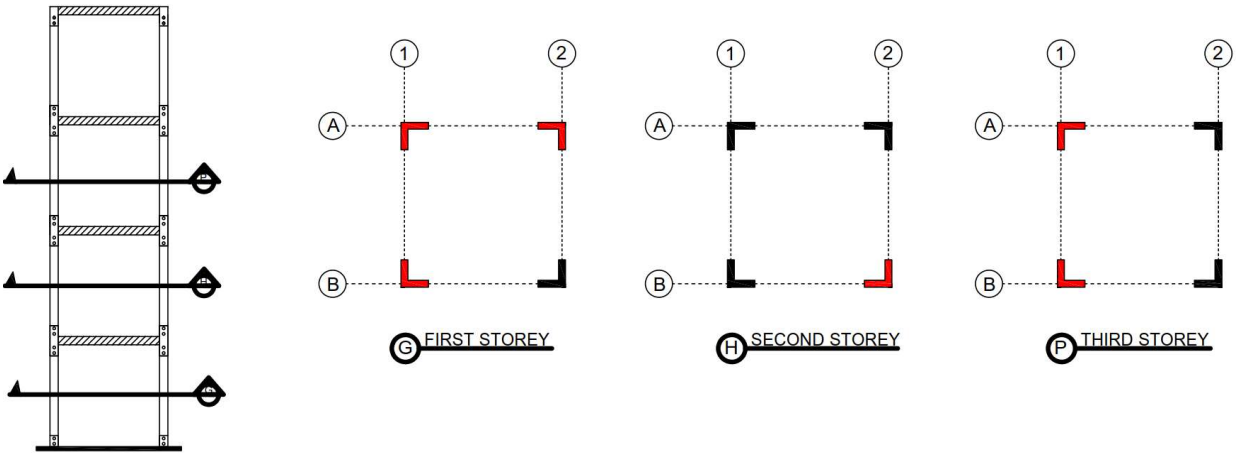

Figure 4-6 Damage Case 1.3

The expected SDFs along with the ARMAX Analysis results are presented in Table 4-7 below.

Table 4-7 SDF Results (DC 1.3)

Damage			SDFs (%) – Average of 10 Trials											
Location	Storey	Damage Ratio	SAP2000 Analysis				ARMAX Analysis							
							No Noise				5% Noise			
A1	1	0.685	-34.25	-17.13	-	-	-35.27	-18.60	-	-	-35.03	-18.24	-	-
A2		0.685	-17.13	-25.69	-34.25	-	-16.12	-22.37	-30.61	-	-16.75	-22.42	-31.30	-
B1		0.685	-	-34.25	-17.13	0	-	-33.77	-21.42	-4.63	-	-32.77	-18.72	-4.35
B2	2	0.685	-	-	0	0	-	-	-4.38	-4.71	-	-	-4.50	-3.70
A1	3	0.685												
B1		0.685												

Like the previous two damage cases, the 5% noise did not have any substantial effect on the ARMAX results. As the damage severity increased, the false negative SDF matrix values also increased. Damage Case 1.3 has false negative values as high as -4.71%, whereas the highest false negative SDF values in Damage Case 1.1 and Damage Case 1.2 were -1.60% and -3.32% respectively. The overall stiffness loss values for each storey are presented in Table 4-8.

Table 4-8 Storey Stiffness Change (DC 1.3)

Storey	Stiffness Change (%)	
	SAP2000	ARMAX
1	**-51.38**	**-52.57** (3.29)
2	**-17.13**	**-17.49** (1.45)
3	**-34.25**	**-32.04** (1.08)
4	**0**	**-4.18** (0.60)

The ARMAX DDM successfully located the damage at each storey with excellent correlation to the expected degree of damage and relatively small differences between each trial.

The ARMAX analysis results from the numerical modelling produced results very similar to the results which were measured through previous tests on the experimental structure built by Ngoan (2015). In each damage case, the ARMAX results successfully located and determined the degree of damage at each storey without yielding significant false negative or positive results. In some cases, however, the ARMAX model underestimated the severity of damage to a small degree.

4.3. Structure #2: Steel Structure - 10x Scale

With confirmation that the SAP2000 model can successfully replicate the behaviour of the experimental steel structure and that damage can be successfully located using the ARMAX DDM under MIF, the next step compared the results from MIF to results generated from wind forces.

Structure #1 was an experimental structure which only reached 1.7m in height. To properly incorporate wind forces, a larger structure was required. Structure #2 was modeled at a 10x scale to Structure #1.

The goal of Structure #2 was to compare the effects of wind loading to impulse loading, which was previously shown to be capable of successfully detecting damage. To test the validity of the wind loading compared to MIF, the identical damage cases from Structure #1 were used on Structure #2.

4.3.1. Damage Case 2.1 – Single Storey Damage (4th Storey)

The first damage case for Structure #2 involved replacing the steel column on the fourth storey with an aluminum column as shown in Figure 4-7.

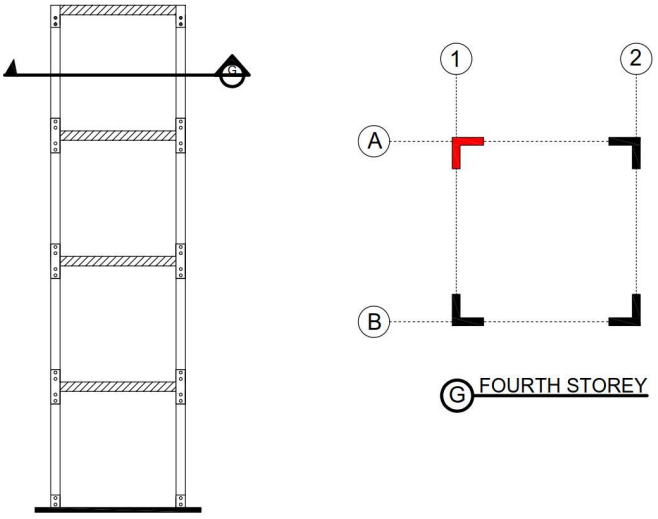

Figure 4-7 Damage Case 2.1

Similar to the Damage Cases in Structure #1, the expected SDFs extracted from SAP2000 and the ARMAX analysis are presented in Table 4-9.

Table 4-9 SDF Results (DC 2.1)

Damage			SDFs (%) – Average of 10 Trials											
Location	Storey	Damage Ratio	SAP2000 Analysis				ARMAX Analysis							
							No Noise				5% Noise			
A1	4	0.32	0	0	-	-	3.08	2.96	-	-	3.60	2.92	-	-
			0	0	0	-	3.59	2.06	1.48	-	0.00	-1.58	-2.84	-
			-	0	-8.56	-17.13	-	1.01	-7.94	-14.47	-	0.95	-7.64	-14.29
			-	-	-17.13	-17.13	-	-	-16.80	-16.57	-	-	-14.42	-14.80

The 5% noise appears to have more effect on the results when compared to the MIF loading cases. This is particularly prevalent in SDF_{21}, SDF_{22}, SDF_{23}, SDF_{43} and SDF_{44}. Also, the false negative and false positive results are slightly higher (average of 2% higher) than in the pulse loading case,

however they do not present a significant concern. The overall stiffness change at each storey is presented in Table 4-10.

Table 4-10 Storey Stiffness Change (DC 2.1)

Storey	Stiffness Change (%)	
	SAP2000	ARMAX
1	**0**	**5.73** (1.21)
2	**0**	**1.46** (1.10)
3	**0**	**-0.94** (0.85)
4	**-17.13**	**-14.50** (0.91)

The ARMAX damage detection model successfully located the damage at the fourth storey with a degree of damage almost identical to that calculated in Structure #1 (-14.50% vs -14.61%).

4.3.2. Damage Case 2.2 – 2 Storey Damage (1st and 2nd Storeys)

The second damage case involved replacing two steel columns on the first storey and one steel column on the second storey with aluminum columns as shown in Figure 4-8.

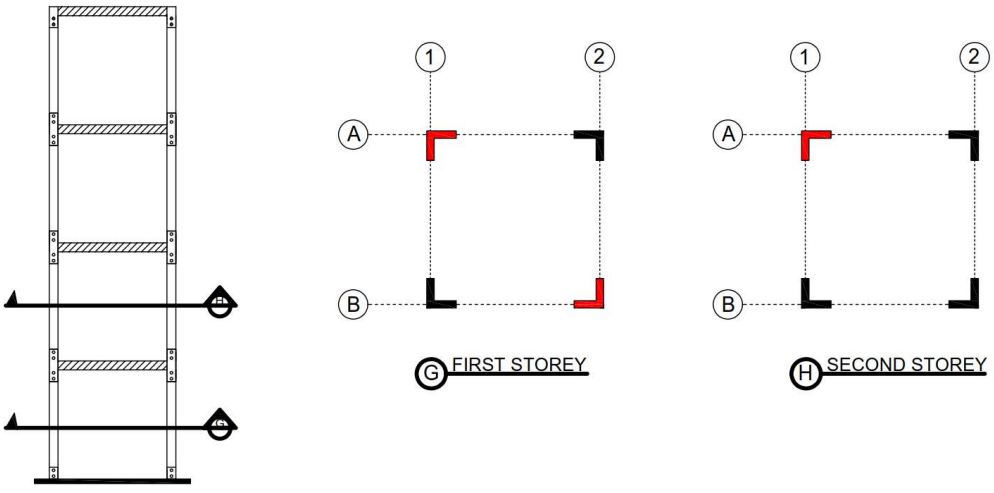

Figure 4-8 Damage Case 2.2

The expected SDFs extracted from SAP2000 and the ARMAX analysis are presented in Table 4-11.

Table 4-11 SDF Values (DC 2.2)

Damage			SDFs (%) – Average of 10 Trials											
Location	Storey	Damage Ratio	SAP2000 Analysis (Expected)				ARMAX Analysis							
							No Noise				5% Noise			
A1	1	0.685	-25.69	-17.13	-	-	-24.46	-15.24	-	-	-24.81	-15.51	-	-
B2		0.685	-17.13	-8.56	0	-	-15.39	-6.24	4.82	-	-17.75	-6.93	6.89	-
A1	2	0.685	-	0	0	0	-	4.98	2.11	-0.43	-	4.09	0.97	-1.04
			-	-	0	0	-	-	1.34	1.82	-	-	-1.48	-0.69

The SDF values appear to be more affected by the 5% noise effects and the false positive and negative results are higher compared to DC 1.2. The overall stiffness changes at each storey are presented in Table 4-12.

Table 4-12 Storey Stiffness Change (DC 2.2)

Storey	Stiffness Change (%)	
	SAP2000	ARMAX
1	**-34.26**	**-33.00** (0.47)
2	**-17.13**	**-16.63** (0.25)
3	**0**	**5.49** (0.99)
4	**0**	**-1.07** (0.42)

The ARMAX analysis successfully located the damage on the proper stories while producing negligible false positive and negative results at the undamaged stories. The degree of damage measured were very close to the expected results and unlike in DC 1.2, there was no large underestimation in the degree of damage in the first storey.

4.3.3. Damage Case 2.3 – 3 Storey Damage (1st, 2nd and 3rd Storeys)

The final damage case for the large scale experimental steel structure represented a more severe case in which there is damage on the first, second and third storey with a total of six steel columns being replaced by aluminum columns as shown in Figure 4-9.

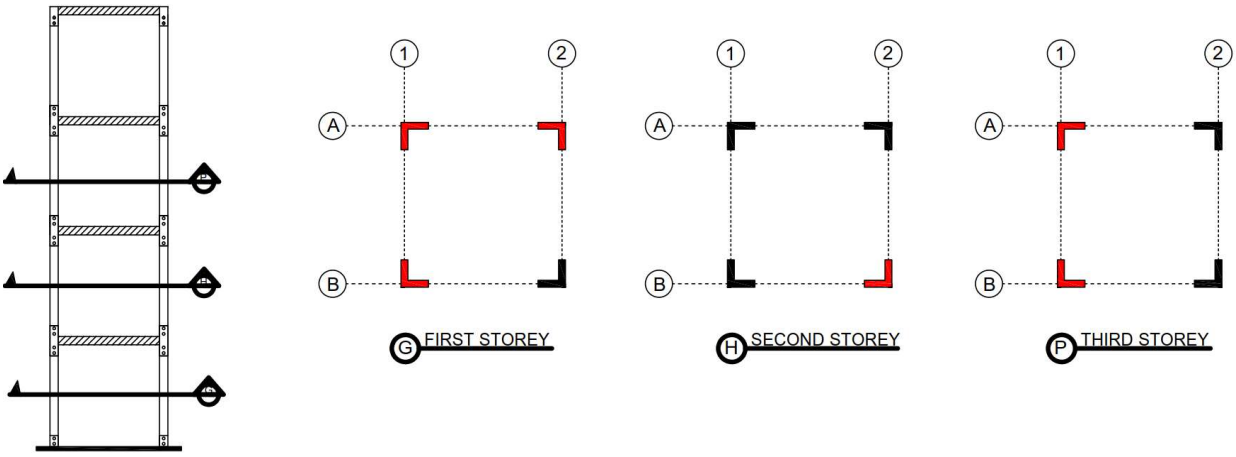

Figure 4-9 Damage Case 2.3

The expected SDFs extracted from Sap2000 and the ARMAX analysis are presented in Table 4-13.

Table 4-13 SDF Values (DC 2.3)

Damage			SDFs (%) – Average of 10 Trials											
Location	Storey	Damage Ratio	SAP2000 Analysis (Expected)				ARMAX Analysis							
							No Noise				5% Noise			
A1	1	0.685	-34.25	-17.13	-	-	-33.68	-15.62	-	-	-33.31	-15.52	-	-
A2		0.685	-17.13	-25.69	-34.25	-	-15.39	-21.39	-29.53	-	-15.79	-21.82	-29.38	-
B1		0.685	-	-34.25	-17.13	0	-	-30.79	-16.51	-2.88	-	-31.65	-16.50	-3.07
B2	2	0.685	-	-	0	0	-	-	5.40	4.91	-	-	3.70	3.37
A1	3	0.685												
B1		0.685												

The overall stiffness change at each storey and corresponding standard deviation is presented in Table 4-14.

Table 4-14 Storey Stiffness Change (DC 2.3)

Storey	Stiffness Change (%)	
	SAP2000	ARMAX
1	**-51.39**	**-50.97** (0.51)
2	**-17.13**	**-15.65** (0.37)
3	**-34.26**	**-30.52** (0.75)
4	**0**	**1.34** (0.53)

The damage trials in Structure #2 validated the use of wind loading for ARMAX damage detection as it yielded very similar results to the MIF damage cases. One difference between the two loading cases was that the wind loading has higher false positive and false negative SDFs ranging from 1-3% higher. The wind loading also yielded much more stable results, with the largest standard deviation from 10 trials being 1.21 compared to the largest MIF standard deviation being 3.29.

With the SAP2000 model parameters and wind loading both validated by Structure #1 and Structure #2, the next step involved testing the capability of the ARMAX DDM to detect damage in RC structures.

4.4. Structure #3: Reinforced Concrete Structure - 2 x 2 Column Layout

The next three buildings modeled were reinforced concrete frames, with the first building modeled being a four-storey structure with a 2x2 column layout as shown in Figure 4-10. The dimensions of the beams and columns were chosen to match the experimental steel structure as close as possible. These span lengths of the slabs and beams may be considered relatively small and the slab thickness may be considered relatively large for conventional building design, however different dimensioning would have no major effects on the numerical model as the beams and slabs are modeled as rigid in behaviour. Each column had identical rebar detailing and identical undamaged stiffness properties.

Unlike the steel structures, which incorporated aluminum columns as damage, the concrete structures reflected real life damage properties as they followed the simplified reinforced concrete damage model presented in Section 3.3. This was done through directly modifying the material properties of both the concrete and the steel in SAP2000.

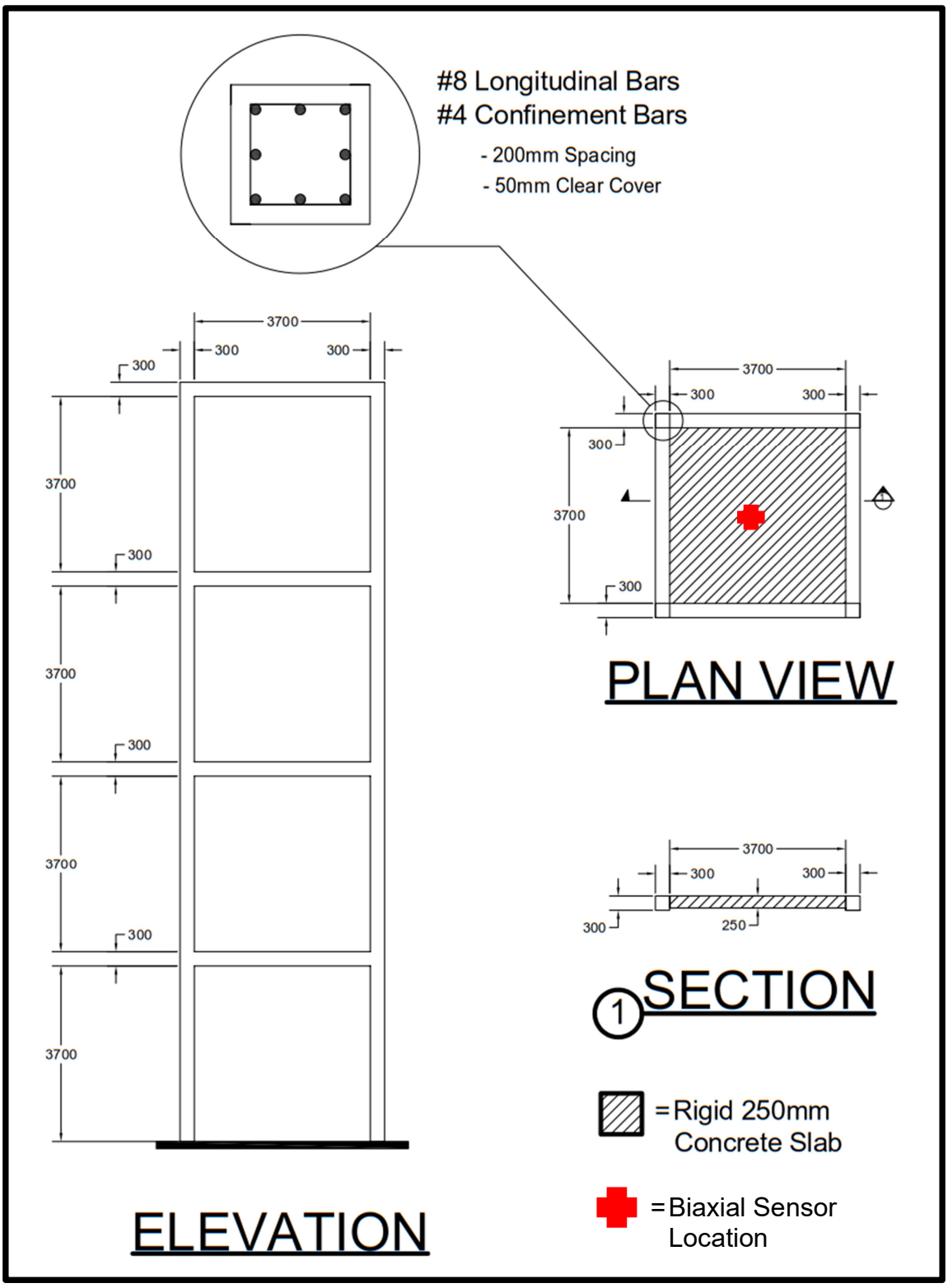

Figure 4-10 Structure #3

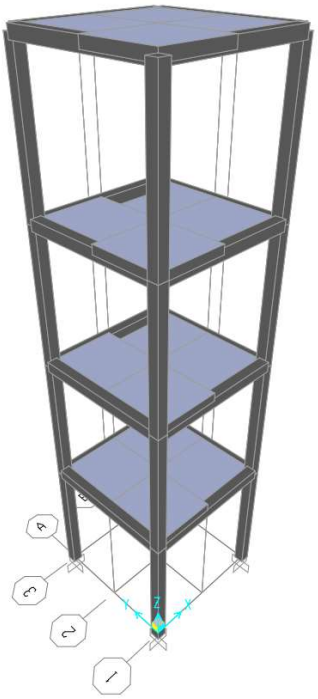

Figure 4-11 Structure #3 SAP2000 Model

4.4.1. Damage Case 3.1 – Single Storey Mild Damage (2nd Storey)

The first damage case involved applying slight damage (DR = 0.40) to one column on the third as illustrated in Figure 4-12.

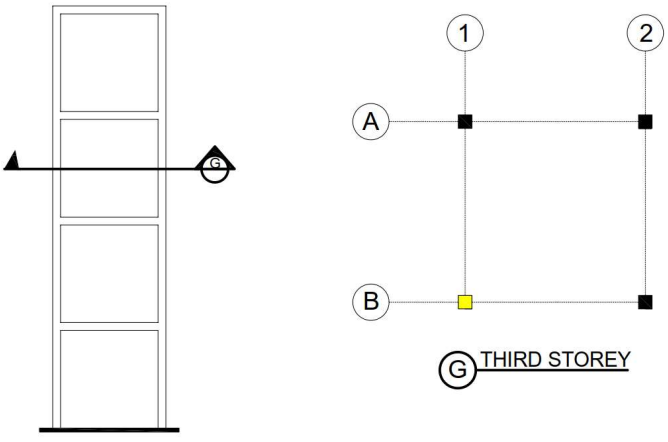

Figure 4-12 Damage Case 3.1

The overall loss in stiffness in the third storey was calculated by hand as [((3 x 0) - (1 x 0.4)) / 4] = -10.00% which would be reflected in SDF_{23} and SDF_{32}; SDF_{22} and SDF_{33} were similarly

calculated as [((7 x 0) – (1 x 0.4)) / 8] = -5.00%. The results from the SAP2000 show nearly identical results to the hand calculations as shown in Table 4-15.

In the following tables, the Damage Ratio refers to the change in initial modulus of elasticity in the concrete as in Eq. 3.33. The Damage Ratios of the steel rebar are not listed in the tables; however, they are still incorporated in the SAP2000 models.

Table 4-15 SDF Values (DC 3.1)

Damage			**SDFs (%) – Average of 10 Trials**											
Location	**Storey**	**Damage Ratio**	**SAP2000 Analysis (Expected)**				**ARMAX Analysis**							
							No Noise				**5% Noise**			
B1	3	0.4	0	0	-	-	-0.02	-0.16	-	-	0.02	0.37	-	-
			0	-5.00	-10.01	-	-0.25	-4.33	-10.77	-	-0.98	-3.27	-10.11	-
			-	-10.01	-5.00	0	-	-9.41	-4.93	0.26	-	-9.34	-4.86	0.52
			-	-	0	0	-	-	0.71	1.42	-	-	0.08	0.53

The SDF results from analyzing 10 trials of noisy data showed very good corroboration with the expected results. The model detected negligible false positive and negative values, with the largest false negative and false positive results being -0.97% and +0.63% respectively. The change in stiffness in each storey was calculated using Eq. 4.4 for all reinforced concrete damage building cases. An example of these calculations can be found in Damage Case 1.1. The change in stiffness in each storey is presented in Table 4-16.

Table 4-16 Storey Stiffness Change (DC 3.1)

Storey	Stiffness Change (%)	
	SAP2000	ARMAX
1	**0**	**0.34** (0.66)
2	**0**	**-0.31** (0.29)
3	**-10.01**	**-9.73** (0.33)
4	**0**	**0.37** (0.65)

The ARMAX results show that the DDM has the capability to detect very slight damage in a single column within a building. The stability of the ARMAX DDM was excellent with the largest standard deviation from 10 damage trials being 0.66.

4.4.2. Damage Case 3.2 – Single Storey Moderate Damage (2nd Storey)

The second damage case incorporated moderate damage to three columns on the second storey, with two columns having a DR of 0.50 and one column having a DR of 0.40 as illustrated in Figure 4-13.

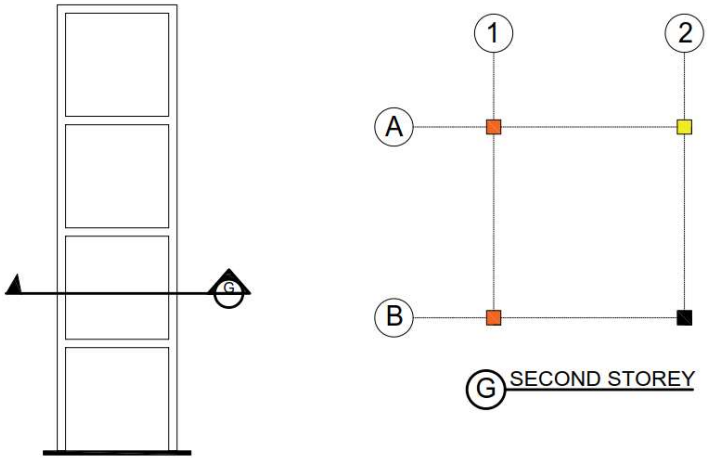

Figure 4-13 Damage Case 3.2

The overall loss in stiffness in the second storey was calculated by hand as [((1 x 0) - (2 x 0.5) – (1 x 0.4)) / 4]= -35.00% which would be reflected in SDF_{12} and SDF_{21}; SDF_{11} and SDF_{22} were similarly calculated as [((5 x 0) - (2 x 0.5) – (1 x 0.4)) / 8]= -17.50%. These hand calculations are nearly identical to the values which were extracted from the SAP2000 stiffness matrix as shown in Table 4-17.

Table 4-17 SDF Values (DC 3.2)

Damage			SDFs (%) – Average of 10 Trials											
Location	Storey	Damage Ratio	SAP2000 Analysis (Expected)				ARMAX Analysis							
							No Noise				5% Noise			
A1	2	0.5	-17.52	-35.03	-	-	-17.32	-35.00	-	-	-17.47	-34.66	-	-
A2		0.4	-35.03	-17.52	0	-	-34.12	-16.47	-1.58	-	-33.93	-17.80	-3.49	-
B1		0.5	-	0	0	0	-	-2.42	2.08	-3.47	-	-2.07	2.37	3.66
			-	-	0	0	-	-	-0.83	-0.17	-	-	1.62	1.65

The 5% noise had minimal effect on the SDFs of the ARMAX analysis. The overall change in stiffness at each storey is presented in Table 4-18.

Table 4-18 Storey Stiffness Change (DC 3.2)

Storey	Stiffness Change (%)	
	SAP2000	ARMAX
1	**0**	**-0.72** (0.42)
2	**-35.03**	**-34.72** (0.33)
3	**0**	**-1.59** (0.33)
4	**0**	**-0.13** (0.65)

The ARMAX analysis was able to locate the damage and calculate the severity with less than 1% error and with minimal standard deviations.

4.4.3. Damage Case 3.3 – Two Storey Damage (1st and 2nd Storeys)

The second damage case included severe damage on three columns on the first storey and moderate damage to two columns on the second storey as illustrated in Figure 4-14.

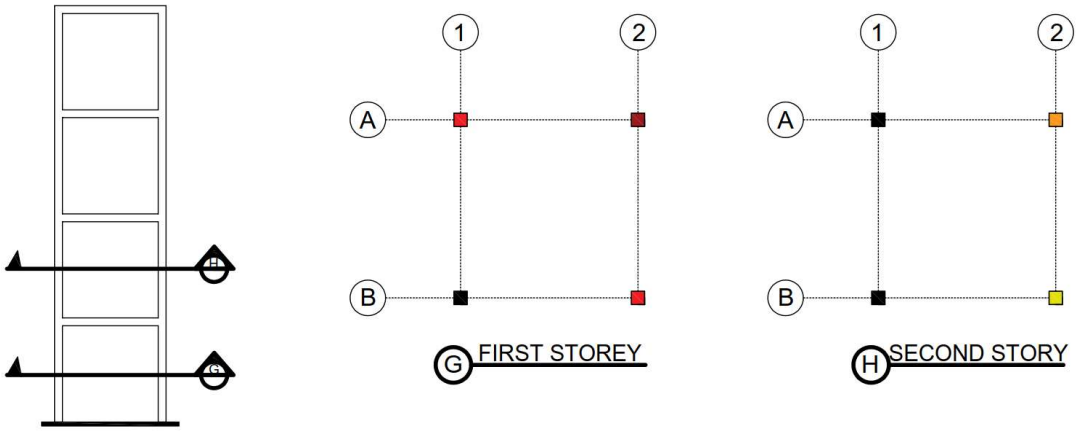

Figure 4-14 Damage Case 3.3

The expected SDFs extracted from Sap2000 and the results from 10 trials using the ARMAX DDM are presented in Table 4-19.

Table 4-19 SDF Values (DC 3.3)

Damage			**SDFs (%) – Average of 10 Trials**											
Location	**Storey**	**Damage Ratio**	**SAP2000 Analysis (Expected)**				**ARMAX Analysis**							
							No Noise				**5% Noise**			
A1	1	0.40	-35.08	-23.82	-	-	-33.50	-21.97	-	-	-33.97	-21.87	-	-
A2		0.35	-23.82	-11.91	0	-	-21.71	-10.90	-3.29	-	-20.56	-12.26	-3.53	-
B1		0.40	-	0	0	0	-	-4.07	2.06	5.17	-	-4.22	0.77	4.18
A2	2	0.50	-	-	0	0	-	-	-2.35	-0.86	-	-	-3.13	-2.16
B2		0.55												

The overall change in stiffness at each storey is presented in Table 4-20.

Table 4-20 Storey Stiffness Change (DC 3.3)

Storey	Stiffness Change (%)	
	SAP2000	ARMAX
1	**-46.34**	**-46.72** (0.90)
2	**-23.82**	**-21.21** (0.70)
3	**0**	**-3.88** (0.54)
4	**0**	**-0.37** (0.77)

The ARMAX analysis successfully located the damage on the proper stories while the overall change in stiffness on the undamaged floors remained very small. The degree of damage calculated for the first storey was nearly identical to the expected result, whereas the degree of damage on the second storey was calculated to be slightly smaller than expected.

4.4.4. Damage Case 3.4 – Three Storey Damage (1st, 2nd and 3rd Storeys)

The final damage case for Structure #3 reflects damage that a structure may undergo during a large magnitude earthquake. The first storey has critical damage (DR=0.65) in one column and severe damage (DR=0.60) in the other, the second storey incorporated moderate damage in two columns and the third storey contained two columns with slight damage as illustrated in Figure 4-15.

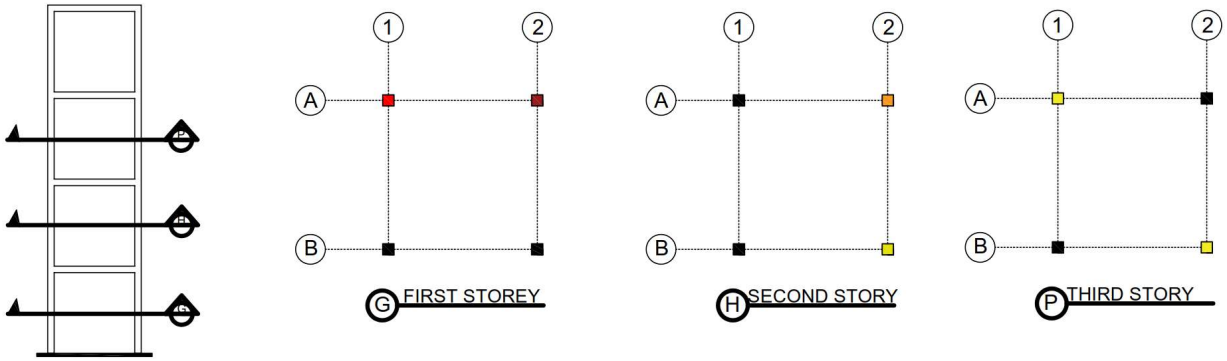

Figure 4-15 Damage Case 3.4

The expected SDFs extracted from Sap2000 and the ARMAX analysis are presented in Table 4-21.

Table 4-21 SDF Values (DC 3.4)

Damage			SDFs (%) – Average of 10 Trials											
Location	Storey	Damage Ratio	SAP2000 Analysis (Expected)				ARMAX Analysis							
							No Noise				5% Noise			
A1	1	0.60	-27.56	-23.82	-	-	-27.91	-23.78	-	-	-27.67	-23.97	-	-
A2		0.65	-23.92	-21.92	-20.02	-	-25.88	-24.51	-18.53	-	-25.14	-22.76	-19.42	-
A2	2	0.45	-	-20.02	-10.01	0	-	-21.76	-9.76	1.35	-	-20.74	-9.01	4.21
B2		0.50	-	-	0	0	-	-	3.31	3.01	-	-	1.16	0.75
A1	3	0.40												
B2		0.40												

The overall change in stiffness at each storey is presented in Table 4-22.

Table 4-22 Storey Stiffness Change (DC 3.4)

Storey	Stiffness Change (%)	
	SAP2000	ARMAX
1	**-31.31**	**-30.78** (1.23)
2	**-23.82**	**-24.55** (1.05)
3	**-20.02**	**-20.08** (1.20)
4	**0**	**2.04** (0.87)

The ARMAX analysis was able to locate the damage at each storey and measure the severity to with an average percentage error of 1.67%. The relatively small positive stiffness change at the fourth storey successfully indicates that there is no damage at that storey.

4.5. Structure #4: Concrete Structure – 3x3 Column Layout

The second reinforced concrete moment frame modeled was a 4-storey structure with a 3x3 column layout as shown in Figure 4-16. Each column had identical rebar detailing and identical undamaged stiffness properties. The building model was created to test the effects that additional columns would have on the ARMAX DDM. As that was the biggest variable that was intended to be changed between structure #3 and structure #4, the beams and slabs remained at 4-metre spans from centreline to centreline of columns.

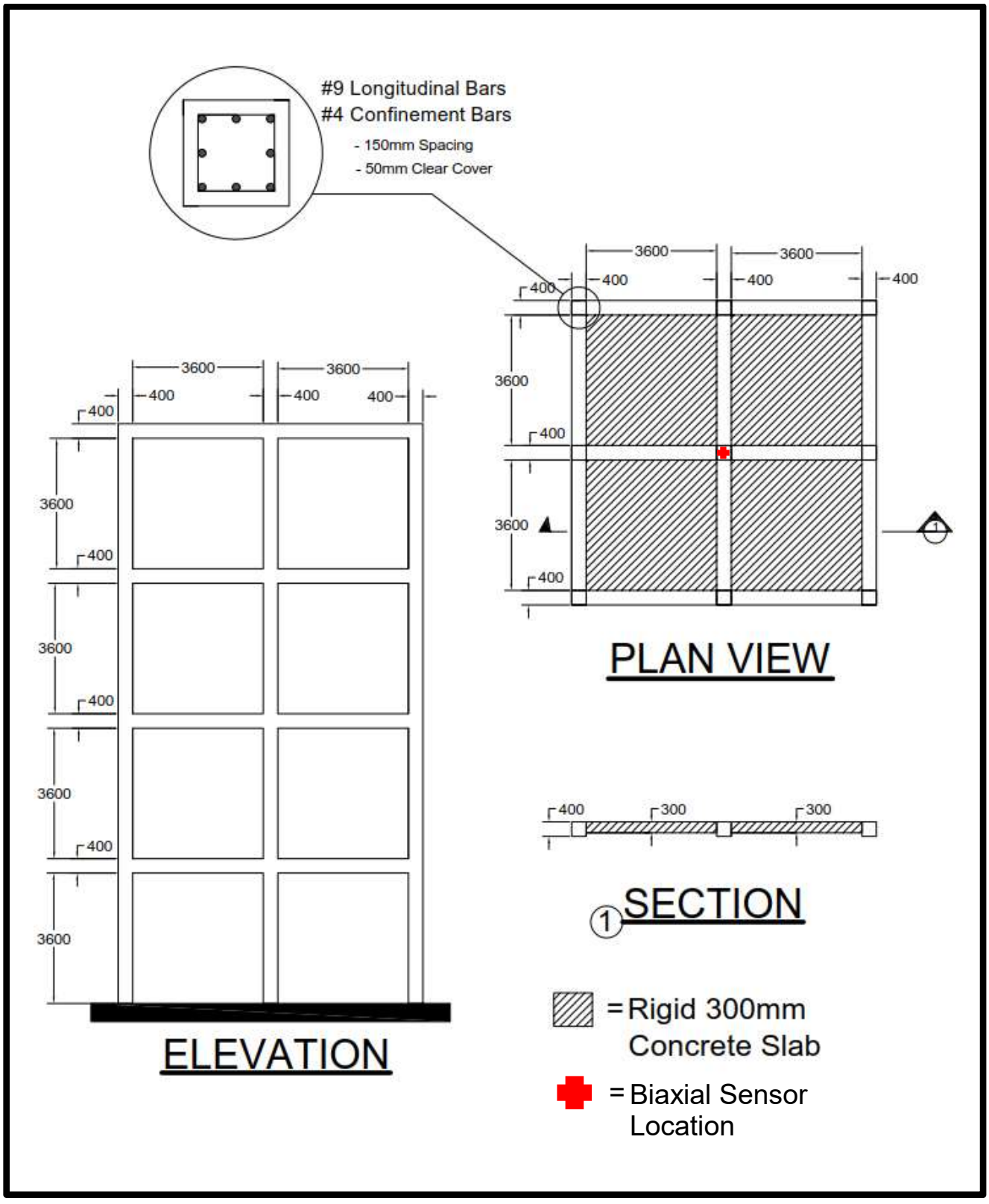

Figure 4-16 Structure #4

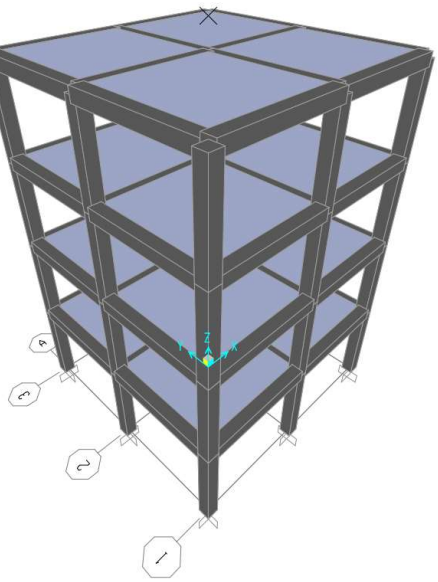

Figure 4-17 Structure #4 SAP2000 Model

4.5.1. Damage Case 4.1 – Single Storey (1st Storey)

The first damage case incorporated moderate damage to four columns on the first storey, each with a damage ratio of 0.50 as illustrated in Figure 4-18.

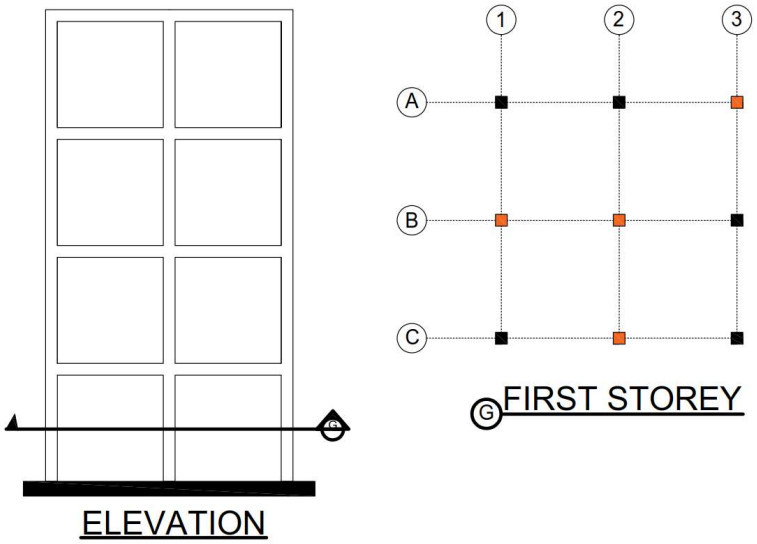

Figure 4-18 Damage Case 4.1

The expected SDFs along with the ARMAX SDF results are presented in Table 4-23.

Table 4-23 SDF Values (DC 4.1)

Damage			SDFs (%) – Average of 10 Trials											
Location	Storey	Damage Ratio	SAP2000 Analysis (Expected)				ARMAX Analysis							
							No Noise				5% Noise			
A3	1	0.50	-17.52	-35.03	-	-	-17.32	-35.00	-	-	-17.47	-34.66	-	-
B1		0.50	-35.03	-17.52	0	-	-34.12	-16.47	-1.58	-	-33.93	-17.80	-3.49	-
B2		0.50	-	0	0	0	-	-2.42	2.08	-3.47	-	-2.07	2.37	3.66
C2		0.50	-	-	0	0	-	-	-0.83	-0.17	-	-	1.62	1.65

The noise had a minor effect on some of the false positive and negative SDF values, however it had a negligible effect on the damaged SDFs (SDF_{11}, SDF_{12}, SDF_{21} and SDF_{22}). The overall stiffness changes at each storey are presented in Table 4-24.

Table 4-24 Storey Stiffness Change (DC 4.1)

Storey	Stiffness Change (%)	
	SAP2000	ARMAX
1	**-22.24**	**-22.30** (1.43)
2	**0**	**1.05** (0.49)
3	**0**	**0.13** (0.87)
4	**0**	**1.95** (0.90)

The ARMAX damage detection model successfully located the damage at the first storey while also presenting very small false positives on the other storeys. The degree of damage on the first storey nearly identical to the expected result and the standard deviations for each storey were minimal.

4.5.2. Damage Case 4.2 – Two Storey Damage (1st and 3rd Storeys)

The second damage case involved moderate damage to four columns on the first storey and slightly more severe damage to seven columns on the third storey as presented in Figure 4-19.

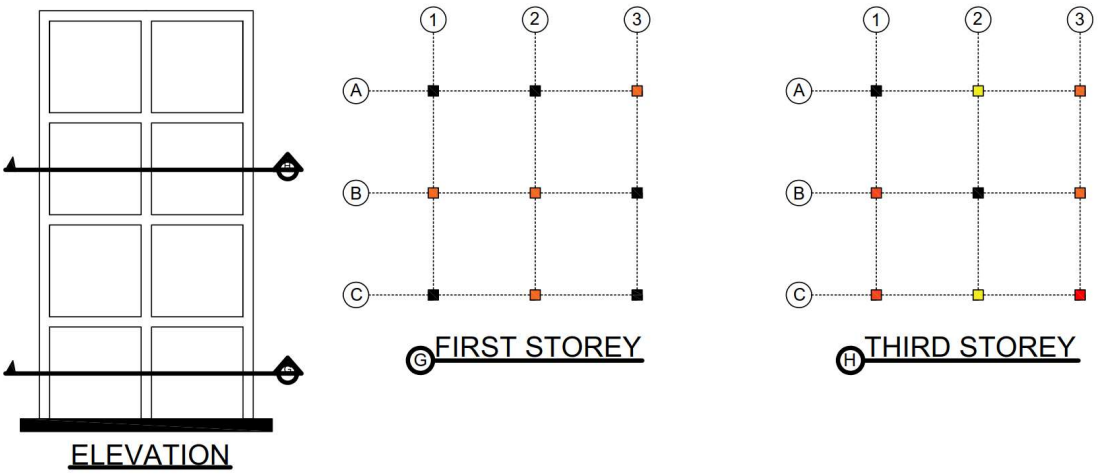

Figure 4-19 Damage Case 4.2

The expected SDFs along with the ARMAX results for Damage Case 4.2 are presented in Table 4-25.

Table 4-25 SDF Values (DC 4.2)

Damage			SDFs (%) – Average of 10 Trials											
Location	Storey	Damage Ratio	SAP2000 Analysis (Expected)				ARMAX Analysis							
							No Noise				5% Noise			
A3	1	0.50	-11.12	0	-	-	-8.62	-0.00	-	-	-9.29	-1.01	-	-
B1		0.50	0	-20.04	-40.08	-	-0.20	-14.25	-34.85	-	0.13	-14.48	-35.20	-
B2		0.50	-	-40.08	-20.04	0	-	-34.11	-18.59	-0.50	-	-34.30	-18.46	-0.12
C2		0.50	-	-	0	0	-	-	-0.98	-0.34	-	-	-1.24	2.28
A2	3	0.45												
A3		0.50												
B1		0.55												
B3		0.50												
C1		0.55												
C2		0.45												
C3		0.60												

The noise had no significant effect on the ARMAX SDF values as every value except one changed by less than +/- 1%. The overall stiffness change at each storey is presented in Table 4-26.

Table 4-26 Storey Stiffness Change (DC 4.2)

Storey	Stiffness Change (%)	
	SAP2000	ARMAX
1	**-22.24**	**-18.13** (0.81)
2	**0**	**-0.44** (0.66)
3	**-40.08**	**-34.75** (0.92)
4	**0**	**0.31** (0.53)

The ARMAX analysis was able to successfully locate the damage on the first and third storey, however at both storeys the degree of damage was underestimated by approximately 4% and 5% respectively.

4.5.3. Damage Case 4.3 - Three Storey Damage (1st, 2nd and 3rd Storeys)

Damage Case 4.3 included severe damage throughout the majority of the structure. The first storey was the most affected, with six columns being damaged and two of those columns approaching the critical damage level. The second storey had six columns severely damaged as well and the third storey had moderate damage to four columns. Damage Case 4.3 is presented in Figure 4-20.

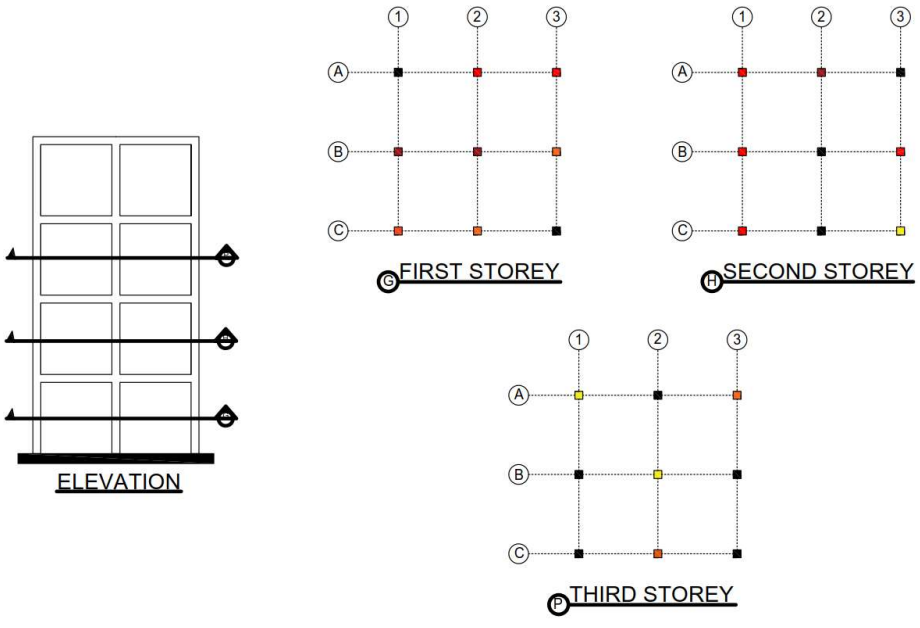

Figure 4-20 Damage Case 4.3

Table 4-27 SDF Values (DC 4.3)

Damage			SDFs (%) – Average of 10 Trials											
Location	Storey	Damage Ratio	SAP2000 Analysis (Expected)				ARMAX Analysis							
							No Noise				5% Noise			
A2	1	0.60	-42.03	-38.98	-	-	-37.81	-29.84	-	-	-38.66	-30.83	-	-
A3		0.60	-38.98	-30.35	-21.72	-	-31.71	-27.06	-16.94	-	-30.42	-27.00	-17.16	-
B1		0.65	-	-21.72	-10.86	0	-	-23.23	-12.11	1.70	-	-22.32	-11.44	2.08
B2		0.65	-	-	0	0	-	-	2.43	0.08	-	-	0.62	-1.62
B3		0.50												
C1		0.55												
C2		0.50												
A1	2	0.60												
A2		0.65												
B1		0.60												
B3		0.60												
C1		0.60												
C3		0.45												
A1	3	0.45												
A3		0.50												
B2		0.45												
C2		0.55												

The 5 % noise effects once again had minimal effects on the ARMAX SDF values. The overall stiffness changes at each storey based on the average SDF values from 10 trials are presented in Table 4-28.

Table 4-28 Storey Stiffness Change (DC 4.3)

Storey	Stiffness Change (%)	
	SAP2000	ARMAX
1	**-45.07**	**-46.72** (0.90)
2	**-38.98**	**-30.62** (0.53)
3	**-21.72**	**-19.74** (0.42)
4	**0**	**0.36** (0.98)

Although the ARMAX model successfully located the damage at each storey while also revealing negligible damage on the fourth storey, the degree of damage was underestimated on the second and third storey.

4.6. Structure #5: 10 Storey Concrete Structure – 4x4 Column Layout

The third reinforced concrete building tested was a 10-storey structure with a 4x4 column layout as shown in Figure 4-21. Each column had identical rebar detailing and identical undamaged stiffness properties. The main variables which were to be compared to the previous two structures were the effect of added columns at each storey and the effect of many more storeys. As such, the rigid beam and rigid slab spans remained identical to the previous two models. Both the vertical and longitudinal dimensions of the bays are identical to those in Structure #4.

Unlike the previous two models, the exact damage location for this building is not listed in tables for the sake of brevity. The precise location of damage at each storey can be found in detail in Appendix A.

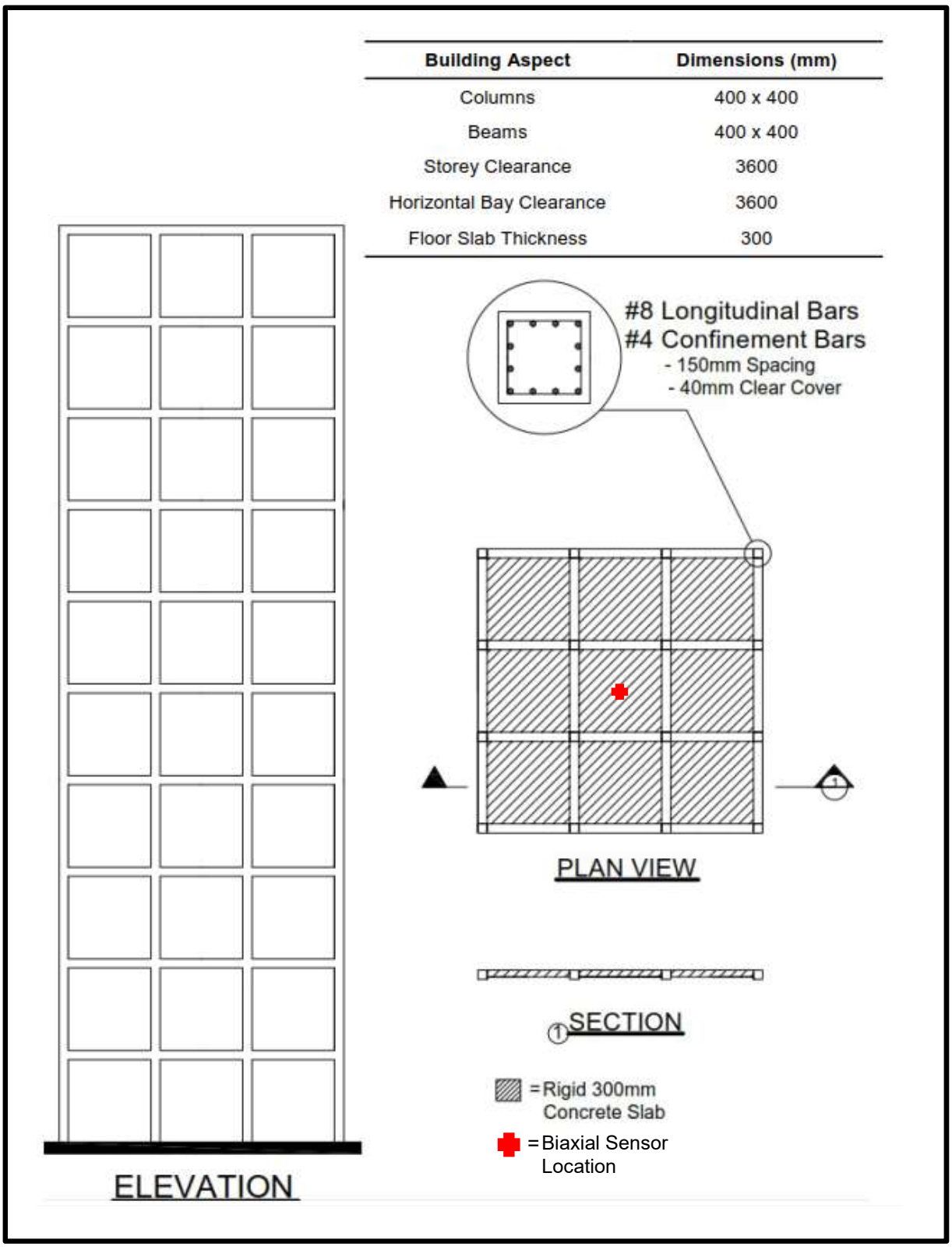

Figure 4-21 Structure #5

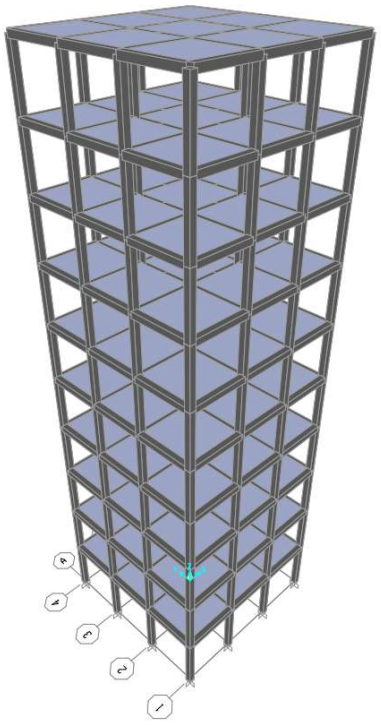

Figure 4-22 Structure #5 SAP2000 Model

4.6.1. Damage Case 5.1 – Two Storey Damage (2nd and 5th Storeys)

The first damage case incorporated moderate damage to eight columns; four columns with a DR of 0.50 and four columns with a DR of 0.55; at both the second and fifth storey. The location of the damage throughout the structure is illustrated in Figure 4-23 below, with a more detailed account being presented in Appendix A.

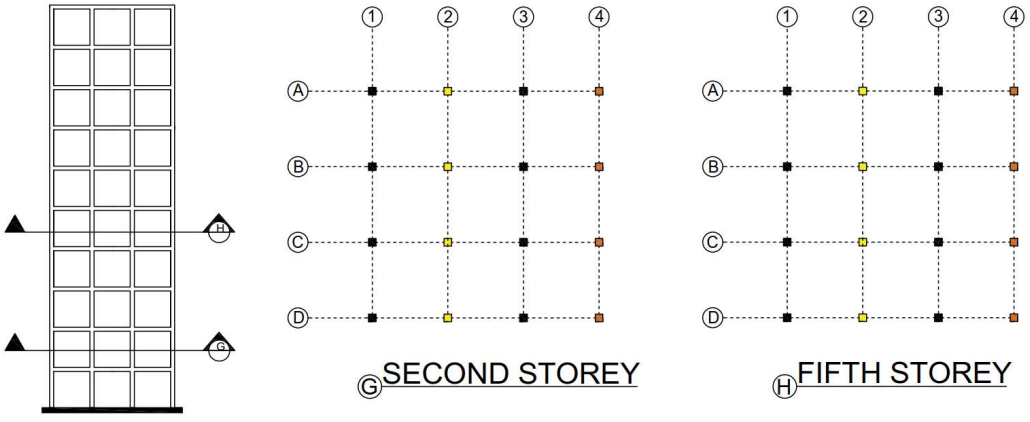

Figure 4-23 Damage Case 5.1

The expected SDFs extracted from SAP2000 and the ARMAX analysis with no noise and 5% noise are presented in Table 4-29

Table 4-29 SDF Values (DC 5.1)

Methodology	SDFs (%) – Average of 10 Trials									
SAP2000	-13.13	-26.25	-	-	-	-	-	-	-	-
	-26.25	-13.13	0	-	-	-	-	-	-	-
	-	0	0	0	-	-	-	-	-	-
	-	-	0	-13.13	-26.25	-	-	-	-	-
	-	-	-	-26.25	-13.13	0	-	-	-	-
	-	-	-	-	0	0	0	-	-	-
	-	-	-	-	-	0	0	0	-	-
	-	-	-	-	-	-	0	0	0	-
	-	-	-	-	-	-	-	0	0	0
	-	-	-	-	-	-	-	-	0	0
ARMAX (0% Noise)	-12.47	-25.56	-	-	-	-	-	-	-	-
	-21.48	-10.98	5.31	-	-	-	-	-	-	-
	-	-10.27	2.42	11.69	-	-	-	-	-	-
	-	-	-1.36	-15.66	-28.51	-	-	-	-	-
	-	-	-	-17.86	-9.98	-2.20	-	-	-	-
	-	-	-	-	-5.42	-1.70	2.25	-	-	-
	-	-	-	-	-	-8.69	-8.68	-7.14	-	-
	-	-	-	-	-	-	1.20	-0.86	-0.62	-
	-	-	-	-	-	-	-	1.87	-6.14	-9.9.
	-	-	-	-	-	-	-	-	1.27	0.16
ARMAX (5% Noise)	-12.18	-25.63	-	-	-	-	-	-	-	-
	-29.22	-15.54	0.89	-	-	-	-	-	-	-
	-	-10.14	0.21	7.87	-	-	-	-	-	-
	-	-	-2.21	-15.32	-27.23	-	-	-	-	-
	-	-	-	-20.79	-12.41	-1.50	-	-	-	-
	-	-	-	-	-5.22	-1.55	2.43	-	-	-
	-	-	-	-	-	-9.60	-8.79	-6.67	-	-
	-	-	-	-	-	-	0.27	-2.31	-2.45	-
	-	-	-	-	-	-	-	1.47	-5.95	-9.06
	-	-	-	-	-	-	-	-	0.57	-0.45

The noise had no significant effect on the SDF ARMAX values, however the false positive and negative SDF values are notably larger than those in Structure #3 and Structure #4. Equation 4.4

was used once again to calculate the storey stiffness change at each level and the results are presented in Table 4-30 along with the standard deviation from the 10 trials.

Table 4-30 Storey Stiffness Change (DC 5.1)

Storey	Stiffness Change (%)	
	SAP2000	ARMAX
1	**0**	**3.06** (1.19)
2	**-26.25**	**-27.42** (0.94)
3	**0**	**-4.63** (1.38)
4	**0**	**-3.22** (1.14)
5	**-26.25**	**-24.01** (0.91)
6	**0**	**-3.36** (0.62)
7	**0**	**-3.59** (0.82)
8	**0**	**-3.20** (1.56)
9	**0**	**-0.49** (1.53)
10	**0**	**-4.25** (0.41)

The ARMAX DDM successfully located the damage in the second and fifth storey. The severity of damage at each storey was very close to the expected values with minimal standard deviations. Although there were some false positive and false negative SDF values that were higher than in the previous structures, it did not result in any issues as the highest false negative storey stiffness change was calculated as -4.63%.

4.6.2. Damage Case 5.2 – Five Storey Damage (1st, 3rd, 4th, 7th and 9th Storeys)

The second damage case simulated a building which has undergone moderate to severe damage throughout with damage being applied to columns in five storeys. The first storey had five columns damaged with DRs ranging from 0.50 to 0.65. The second storey had five columns damaged as well with two columns having a DR of 0.55 and three columns having a DR of 0.60. The fourth storey incorporated damage in seven different columns with DRs ranging from 0.45 to 0.65. The seventh storey had three columns damaged: two with a DR of 0.55 and one with a DR of 0.50. The ninth storey had four columns damaged, each with a DR of 0.40. The location of the damaged columns is shown in Figure 4-24.

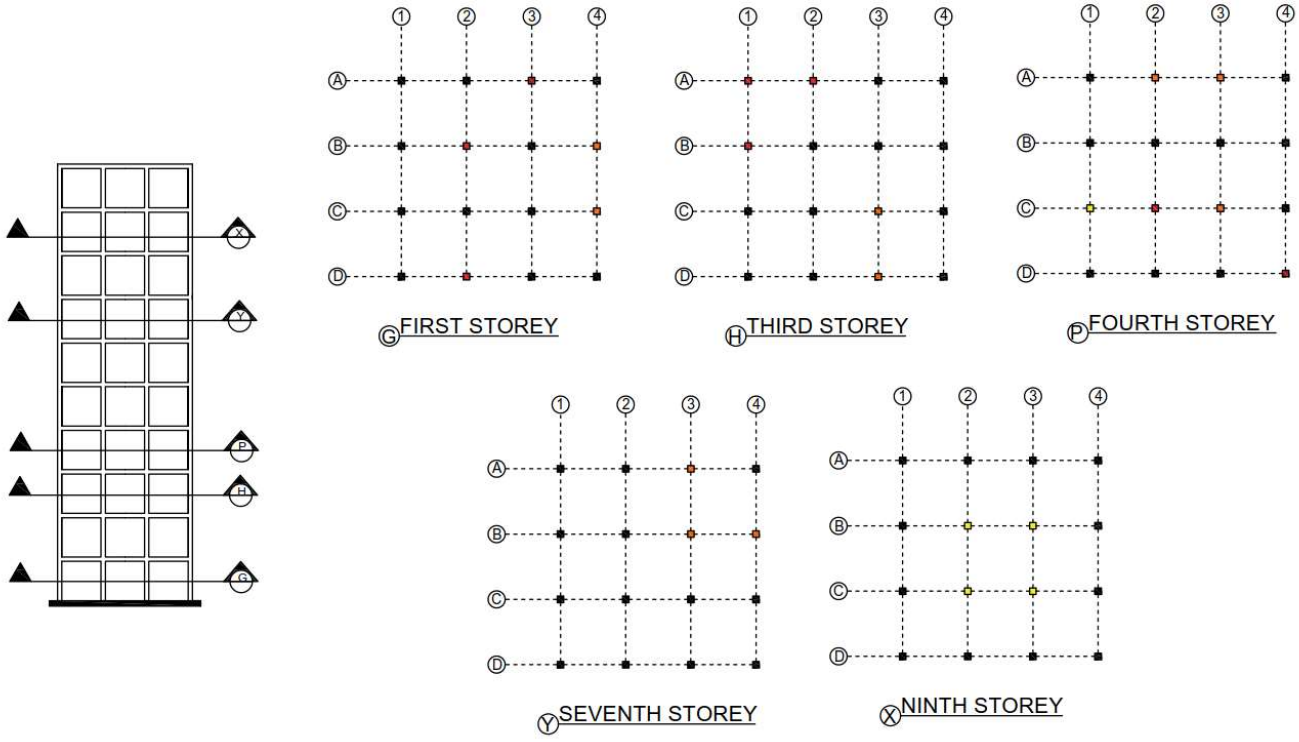

Figure 4-24 Damage Case 5.2

The average SDF values from 10 trials using the ARMAX DDM along with the extracted values from the SAP2000 analysis are shown in Table 4-31.

Table 4-31 SDF Values (DC 5.2)

Methodology	SDFs (%) – Average of 10 Trials									
SAP2000	-8.44	0	-	-	-	-	-	-	-	-
	0	-9.06	-18.12	-	-	-	-	-	-	-
	-	-18.12	-20.47	-22.82	-	-	-	-	-	-
	-	-	-22.82	-11.41	0	-	-	-	-	-
	-	-	-	0	0	0	-	-	-	-
	-	-	-	-	0	-9.22	-18.44	-	-	-
	-	-	-	-	-	-18.44	-9.22	0	-	-
	-	-	-	-	-	-	0	-5.00	-10.00	-
	-	-	-	-	-	-	-	-10.00	-5.00	0
	-	-	-	-	-	-	-	-	0	0
ARMAX (0% Noise)	-4.69	5.57	-	-	-	-	-	-	-	-
	-1.77	-6.99	-13.24	-	-	-	-	-	-	-
	-	-10.59	-19.31	-21.63	-	-	-	-	-	-
	-	-	-18.05	-5.00	9.76	-	-	-	-	-
	-	-	-	-0.99	1.60	5.38	-	-	-	-
	-	-	-	-	-3.31	-12.78	-19.33	-	-	-
	-	-	-	-	-	-8.88	-5.70	-0.65	-	-
	-	-	-	-	-	-	-0.27	-5.35	-8.84	-
	-	-	-	-	-	-	-	-13.31	-10.55	-10.70
	-	-	-	-	-	-	-	-	8.60	8.18
ARMAX (5% Noise)	-6.49	5.69	-	-	-	-	-	-	-	-
	1.52	-6.70	-15.59	-	-	-	-	-	-	-
	-	-13.38	-19.70	-21.42	-	-	-	-	-	-
	-	-	-18.32	-6.77	10.15	-	-	-	-	-
	-	-	-	-1.22	1.47	5.57	-	-	-	-
	-	-	-	-	-3.21	-12.11	-18.17	-	-	-
	-	-	-	-	-	-13.16	-6.33	-1.35	-	-
	-	-	-	-	-	-	-0.03	-5.46	-9.17	-
	-	-	-	-	-	-	-	-13.09	-11.39	-9.71
	-	-	-	-	-	-	-	-	5.03	4.62

Similar to Damage Case 5.1, the false negative and false positive SDF values are larger than in the previous building models. The noise, however, continues to not have a major influence on the damage detection model. Table 4-32 presents the overall change in stiffness calculated at each storey.

Table 4-32 Storey Stiffness Change (DC 5.2)

Storey	Stiffness Change (%)	
	SAP2000	ARMAX
1	**-16.88**	**-16.58** (1.12)
2	**0**	**3.60** (0.85)
3	**-18.12**	**-14.49** (0.76)
4	**-22.82**	**-19.87** (0.49)
5	**0**	**4.46** (0.66)
6	**0**	**1.18** (0.32)
7	**-18.44**	**-15.67** (0.45)
8	**0**	**-0.69** (0.30)
9	**-10.00**	**-11.13** (0.44)
10	**0**	**-0.02** (0.59)

The ARMAX DDM was successful in locating which five storeys were damaged without calculating significant false negative or false positive results at the undamaged locations. Like the previous building models, the ARMAX DDM slightly underestimated the severity of damage when the number of damaged storeys was increased.

4.6.3. Damage Case 5.3 – Seven Storey Damage (1st, 2nd, 3rd, 4th, 6th, 7th and 8th Storeys)

The final damage case tested represented a building that is in a critical state with damaged columns at seven different storeys. The most severe damage was incorporated on the four lowest storeys with the first, second, third and fourth storeys having ten, nine, nine and six columns damaged respectively. The sixth, seventh and eighth storeys each had seven columns damaged. The locations of the damaged columns are shown in Figure 4-25 below. A more detailed account of damage within each separate column can be found in Appendix A.

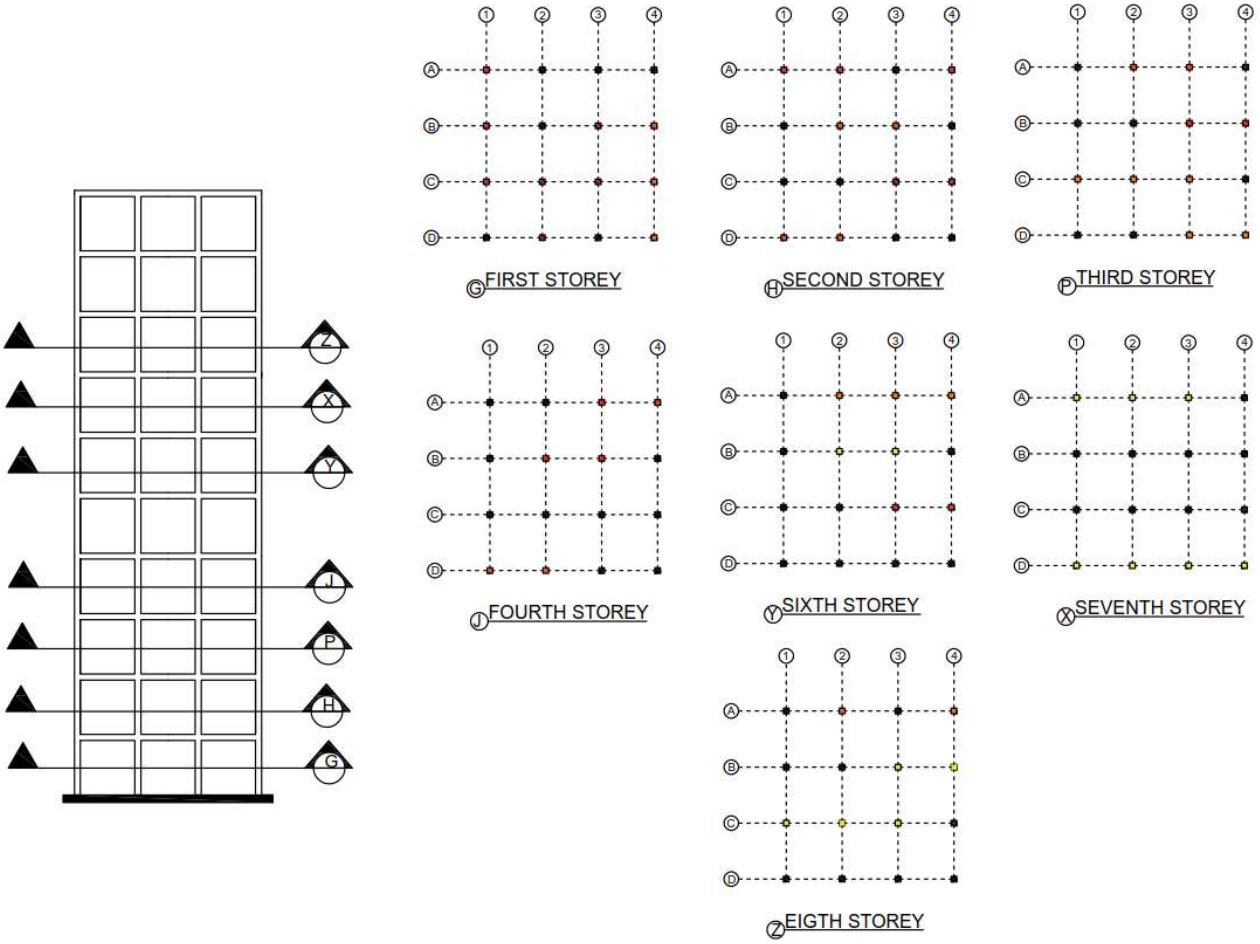

Figure 4-25 Damage Case 5.3

The SDF values from the ARMAX DDM along with the extracted values from the SAP2000 analysis are shown in Table 4-33.

Table 4-33 SDF Values (DC 5.3)

Analysis	SDFs (%) – Average of 10 Trials									
SAP2000	-35.47	-33.12	-	-	-	-	-	-	-	-
	-33.12	-31.56	-30.00	-	-	-	-	-	-	-
	-	-30.00	-25.94	-21.87	-	-	-	-	-	-
	-	-	-21.87	-10.94	0	-	-	-	-	-
	-	-	-	0	-11.25	-22.50	-	-	-	-
	-	-	-	-	-22.50	-20.47	-18.44	-	-	-
	-	-	-	-	-	-18.44	-18.60	-18.75	-	-
	-	-	-	-	-	-	-18.75	-9.38	0	-
	-	-	-	-	-	-	-	0	0	0
	-	-	-	-	-	-	-	-	0	0
ARMAX (0% Noise)	-35.55	-31.56	-	-	-	-	-	-	-	-
	-32.58	-31.90	-28.94	-	-	-	-	-	-	-
	-	-29.68	-23.71	-18.22	-	-	-	-	-	-
	-	-	-25.36	9.32	6.50	-	-	-	-	-
	-	-	-	-1.13	-4.09	-8.20	-	-	-	-
	-	-	-	-	-19.99	-21.72	-21.76	-	-	-
	-	-	-	-	-	-18.42	-19.57	-19.52	-	-
	-	-	-	-	-	-	-22.01	-10.11	-1.02	-
	-	-	-	-	-	-	-	-2.43	-5.43	-7.92
	-	-	-	-	-	-	-	-	-1.93	-2.04
ARMAX (5% Noise)	-35.81	-32.05	-	-	-	-	-	-	-	-
	-34.01	-34.13	-34.50	-	-	-	-	-	-	-
	-	-29.93	-23.72	-18.27	-	-	-	-	-	-
	-	-	-25.39	-9.55	5.90	-	-	-	-	-
	-	-	-	-2.82	-8.06	-14.18	-	-	-	-
	-	-	-	-	-20.05	-21.44	-21.28	-	-	-
	-	-	-	-	-	-18.23	-18.49	-19.85	-	-
	-	-	-	-	-	-	-23.50	-10.45	-1.14	-
	-	-	-	-	-	-	-	-2.88	-5.77	-8.14
	-	-	-	-	-	-	-	-	-0.18	-0.21

The SDF values calculated by the ARMAX DDM show excellent corroboration with the expected results from SAP2000, however there are still some false negative and false positive values present. The overall stiffness changes at each storey are presented in Table 4-34.

Table 4-34 Storey Stiffness Change (DC 5.3)

Storey	Stiffness Change (%)	
	SAP2000	ARMAX
1	**-37.81**	**-38.58** (0.87)
2	**-33.12**	**-33.03** (0.34)
3	**-30.00**	**-30.72** (1.18)
4	**-21.87**	**-21.78** (0.56)
5	**0**	**1.54** (0.80)
6	**-22.50**	**-17.15** (1.24)
7	**-18.44**	**-19.75** (0.56)
8	**-18.75**	**-21.68** (0.80)
9	**0**	**-2.01** (0.37)
10	**0**	**-4.16** (0.56)

The ARMAX DDM yielded excellent results by successfully locating the damage at each of the seven damaged storeys. The degree of damage was calculated with excellent precision in the first four storeys, however the model slightly underestimated the degree of damage in the three higher storeys.

4.7. Structure #6: 4 Storey Concrete Structure – Asymmetric Column Layout

The final reinforced concrete frame structure tested was a 4-storey building with an asymmetric column layout. All the previous buildings modeled have had symmetric layouts with the centre of rigidity matching the centre of mass. The final structure was implemented to verify the ARMAX DDM's capability to detect damage under significant torsional movements.

Each column had identical rebar detailing and identical undamaged stiffness properties. The slabs and beams were both considered rigid in behaviour.

Similar to the other reinforced concrete buildings tested, this structure's response was calculated using Newmark's direct integration method ($\gamma = 0.25$, $\beta = 0.50$) and incorporated proportional damping with a constant 7% damping coefficient for undamaged structures and a 5% damping coefficient for the damaged structures (Newmark & Hall, 1982). As this structure is asymmetric, it's numerical response simulation was not bound by any plane.

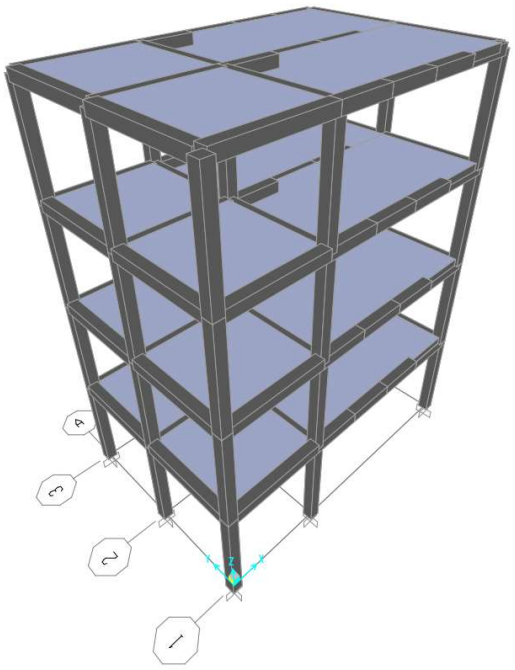

Figure 4-26 Structure #6 SAP2000 Model

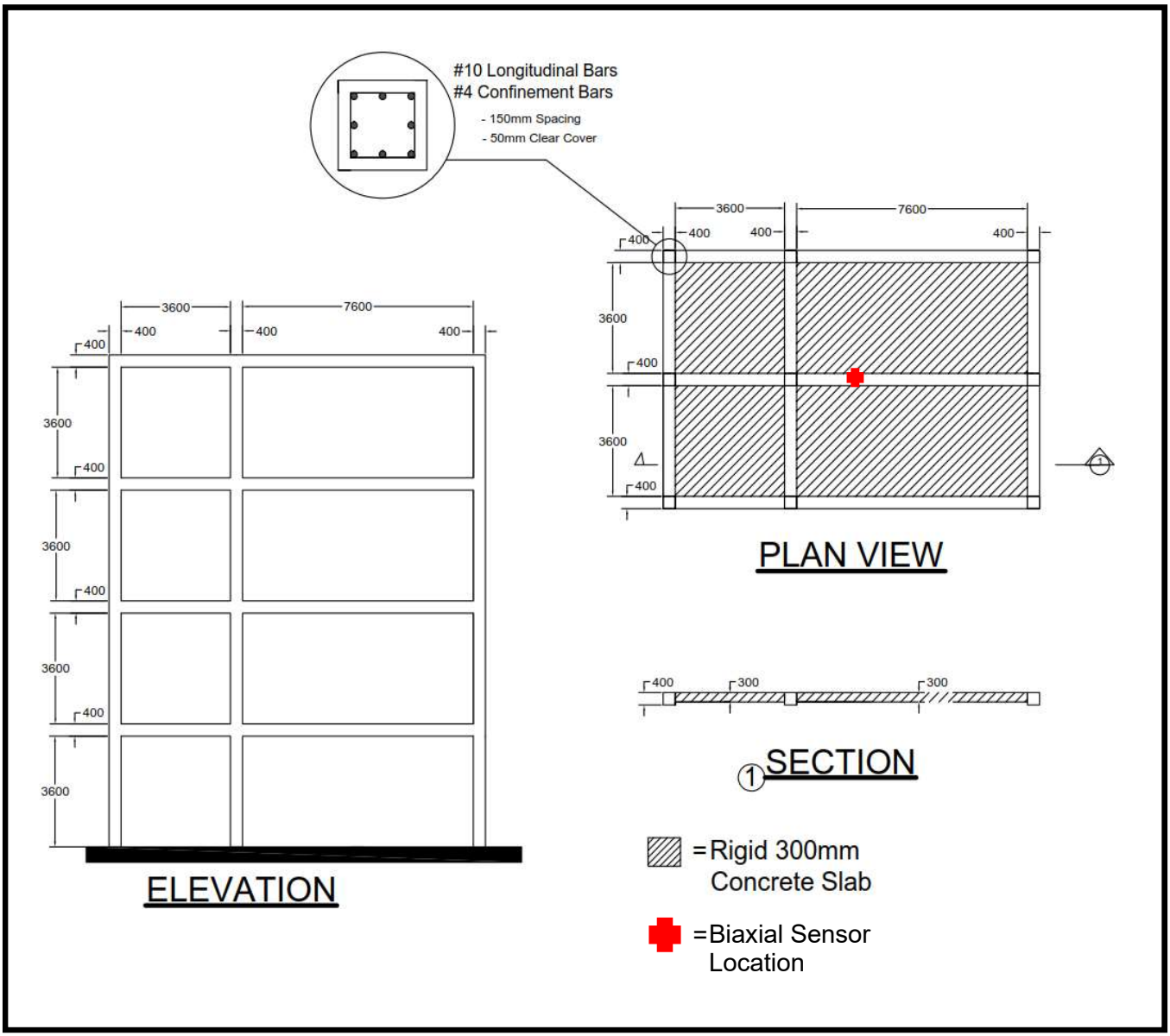

Figure 4-27 Structure #6

4.7.1. Damage Case 6.1 – Single Storey Damage (1st Storey)

The first damage case incorporated damage ranging from moderate to critical at five columns on the first storey; one column with a DR of 0.65, two columns with a DR of 0.60 and two columns with a DR of 0.55. The location of the damage at the first storey is illustrated in Figure 4-28 below.

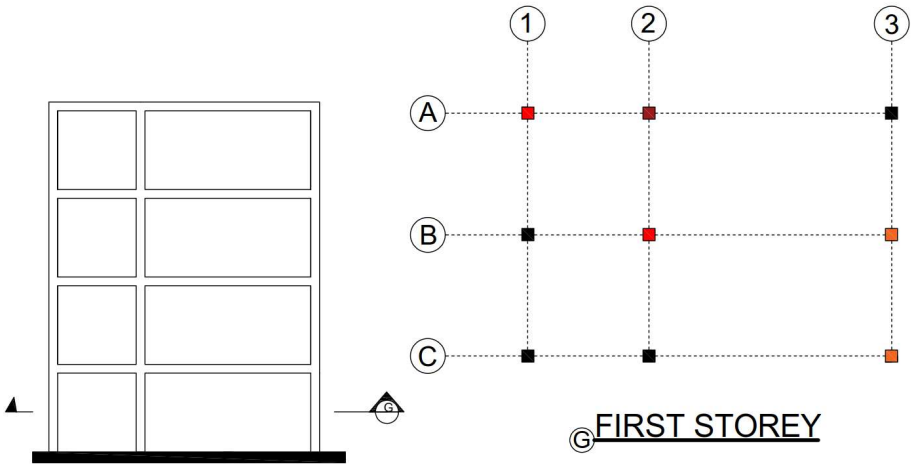

Figure 4-28 Damage Case 6.1

The SDF values from the ARMAX DDM along with the extracted values from the SAP2000 analysis are shown in Table 4-35.

Table 4-35 SDF Values (DC 6.1)

Damage			SDFs (%) – Average of 10 Trials											
Location	Storey	Damage Ratio	SAP2000 Analysis (Expected)				ARMAX Analysis							
							No Noise				5% Noise			
A1	1	0.60	-16.41	0	-	-	-14.22	2.27	-	-	-14.24	2.11	-	-
A2		0.65	0	0	0	-	0.15	0.18	-0.37	-	3.15	0.16	-1.37	-
B2		0.60	-	0	0	0	-	-2.34	0.20	-0.41	-	-1.33	0.54	-0.48
B3		0.55	-	-	0	0	-	-	-0.65	-0.48	-	-	0.53	0.52
C3		0.55												

The noise effects had minimal effects on the ARMAX SDF values. The overall stiffness changes at each storey based on the average SDF values from 10 trials are presented in Table 4-36.

Table 4-36 Storey Stiffness Change (DC 6.1)

Storey	Stiffness Change (%)	
	SAP2000	ARMAX
1	**-32.82**	**-30.03** (0.69)
2	**0**	**1.44** (0.52)
3	**0**	**-1.42** (0.47)
4	**0**	**-0.51** (0.43)

The ARMAX analysis was able to successfully locate the damage at the first with only a slight underestimation of 2.79 %. The results from the undamaged storeys show no significant false detection of damage with the largest false negative result being -1.42%.

4.7.2. Damage Case 6.2 – Three Storey Damage (1st , 2nd and 3rd Storeys)

The final damage case for this thesis reflects damage that the structure may undergo during a large magnitude earthquake with the first three storeys affected. The first storey had damage applied which was identical to Damage Case 6.1. The second storey had damage ranging from moderate to critical in four columns and the third storey had slight damage incorporated into three columns. The location and degree of damage in each individual column is listed in Table 4-37.

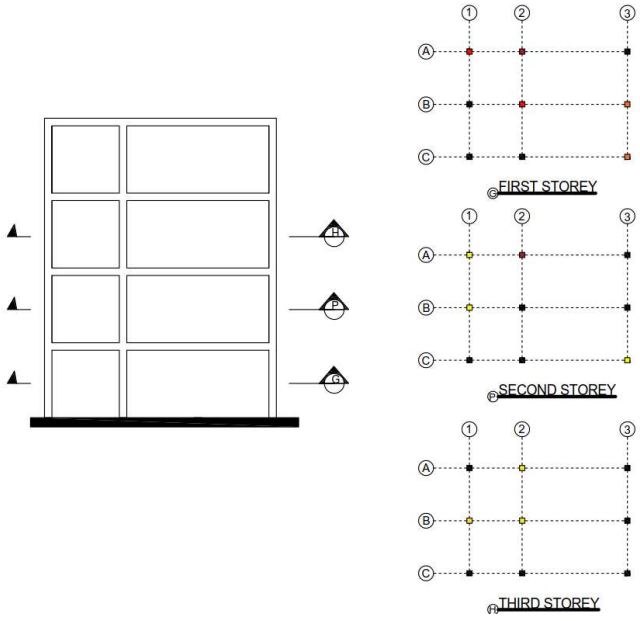

Figure 4-29 Damage Case 6.2

The expected SDFs along with the ARMAX SDF results are presented in Table 4-37.

Table 4-37 SDF Values (DC 6.2)

Damage			SDFs (%) – Average of 10 Trials											
Location	Storey	Damage Ratio	SAP2000 Analysis (Expected)				ARMAX Analysis							
							No Noise				5% Noise			
A1	1	0.60	-28.37	-23.92	-	-	-28.07	-19.93	-	-	-27.64	-19.46	-	-
A2		0.65	-23.92	-19.20	-14.49	-	-16.80	-22..17	-19.52	-	-16.39	-21.69	-18.03	-
B2		0.60	-	-14.49	-7.25	0	-	-12.69	-6.81	1.00	-	-12.90	-5.66	1.43
B3		0.55	-	-	0	0	-	-	2.18	2.16	-	-	-3.44	-3.02
C3		0.55												
A1	2	0.50												
A2		0.50												
B1		0.65												
C3		0.50												
A2	3	0.40												
B1		0.45												
B2		0.45												

The overall stiffness changes at each storey based on the average SDF values from 10 trials are presented in Table 4-38 below.

Table 4-38 Storey Stiffness Change (DC 6.2)

Storey	Stiffness Change (%)	
	SAP2000	ARMAX
1	**-32.82**	**-37.35** (1.16)
2	**-23.92**	**-17.93** (0.72)
3	**-14.49**	**-15.47** (1.23)
4	**0**	**1.08** (0.80)

The ARMAX DDM successfully located the damage at each storey, however the damage was overestimated at the first storey by 4.53% and the severity was underestimated in the second storey by 5.99%.

4.8. Discussion of Results

As the validation of this thesis is based on numerical modelling using SAP2000, it was imperative that the modelling parameters were correctly configured. Structure #1 was created to replicate previous experimental tests performed by Ngoan (2015). The ARMAX analysis results from the numerical modelling produced results very similar to the experimental results. In each damage case, the ARMAX results successfully located and determined the degree of damage at each storey without yielding significant false negative or positive results.

The forces applied to Structure #1 was a pair of Multiple Impulse Forces, however the main goal of the thesis was to detect damage using wind forces and therefore, Structure #2 was modelled as a 10x scale version of Structure #1 and wind forces were applied instead of MIF. The damage trials in Structure #2 validated the use of wind loading for ARMAX damage detection as it yielded very similar results to the MPF damage cases. The wind loading yielded slightly higher false positive and false negative SDFs, however the stability of the results improved.

With the SAP2000 parameters and wind loading validated, Structure #3 was created to attempt and locate damage within a reinforced concrete structure. In each of the damage cases, the ARMAX DDM successfully located the damaged storeys and measured the degree of damage accurately.

Structure #4 was created to add more columns and model a more realistic building. In each damage case, the damage was located, however the degree of damage was slightly underestimated in both the moderate and severe damage cases.

Structure #5 was a 10-storey building with a 4x4 column layout. Three damage cases were tested with the first, second and third damage cases incorporating two storey, five storey and seven storey damage respectively. The ARMAX DDM accurately located and quantified the damage in each case, however the degree of damage was slightly underestimated in both the moderate and severe damage cases.

The final structure tested was a four-storey reinforced concrete frame with an asymmetric column layout to incorporate torsional movements. The first damage case incorporated moderate to severe damage on the first storey and the damage was successfully located and with the degree of damage being underestimated by less than 3%. The second damage case involved applying damage to the

first three storeys, and although the damage was located, there was an overestimation in the degree of damage on the first storey and an underestimation of severity on the second storey.

Overall, the ARMAX DDM was shown to effectively locate the damaged storeys in every single model tested with no significant errors. For most of the damage cases, the ARMAX DDM accurately estimated the degree of damage, however, the DDM had slightly less accurate results in the building models with more columns. This was expected, as the ARMAX DDM relies on approximating buildings as simplified shear type structures, so the ARMAX DDM generated nearly identical results to the SAP2000 models when the structures themselves were simplified.

The DDM was also slightly less accurate in the building model which incorporated torsional movements, which once again is expected as the DDM relies on approximating each storey's dynamic response as a single degree of freedom. The results were more accurate with the cases that did not include torsion as that is where the single degree of freedom approximation holds the truest. The correlation between the torsional case and slight drop in accuracy when calculating the degree of damage is still being reviewed, however the level of inaccuracy was often so small that it does not warrant any major concerns.

Through rigorous numerical testing, the ARMAX DDM was proven to be an effective and consistent method for locating and quantifying damage.

CHAPTER 5: SUMMARY, CONCLUSIONS AND RECOMMENDATIONS

5.1. Summary and Conclusions

In this thesis, a new building damage detection model was proposed and developed using ARMAX analysis on the acceleration responses due to ambient wind loading. Through rigorous numerical modelling, it was demonstrated that damage can be identified at storey-level precision and the degree of damage can be accurately quantified based on floor accelerations due to wind forces.

The thesis can be categorized in two parts, with the first part including a detailed presentation of the damage detection model, outlining the ARMAX analysis procedure, sensor clustering technique, wind force simulation and numerical damage model. The second part of the thesis involved numerical modelling of a variety of structures to validate the ARMAX DDM.

Within the detailed description of the methodology, the ARMAX model, used in conjunction with a sensor clustering concept to analyze the dynamic responses of a structure was explored. By assuming the mass of a building can be grouped into the floors and incorporating mathematical approximations, the ARMAX time series model was transformed to represent the general equation of motion. Using a sensor clustering technique, the ARMAX DDM was able to create a baseline case and damaged case of a structure. With loop calculations, the two cases were evaluated to create a stiffness damage feature capable of locating and quantifying damage at storey-level precision.

Given that the intention of this thesis is to create an effective damage detection model that relies on wind forces, the next section was dedicated to demonstrating the process used to simulate the wind forces. To summarize, a reference level wind speed function was implemented which relied on stochastic procedures to generate 10 second wind speed intervals. Following that, a novel wind speed function was created for all other storeys which incorporated the reference level wind speed, the power law and wind speed correlation. Turbulence was then included at one second intervals using a white noise function. Finally, the wind speed was converted into a force through a pressure coefficient model which accounted for different characteristics of the building location.

It was imperative that the numerical damage model implemented in SAP2000 properly reflected real life behaviour of damaged reinforced concrete members. To ensure this, a stiffness degradation method was applied to reflect simplified damage effects on both the concrete and steel reinforcement material properties. The concrete damage was simulated through a dynamic reloading function based on a set of equations proposed by Chang and Mander (1994). This dynamic reloading function was capable of successfully modifying the reloading stiffness, ultimate strength and ultimate strain capacity based on the severity of damage. To account for damage in the steel reinforcement, fatigue loading was induced which lowers the ultimate strength of the steel based on the severity of damage.

With an accurate account of the analysis model, forcing function and numerical damage model, the second part of the thesis involved testing the capability of the ARMAX DDM in SAP2000. To accomplish this, six separate building models were created. The first was a previously built, experimental steel structure to which multiple impulse force loading was applied. The results from the ARMAX DDM effectively demonstrated that the model parameters used in SAP2000 accurately reflected real-life experimental behaviour. The second set of tests involved a structure that was 10x larger than the previous built steel structure. Wind loading was applied to damage cases identical to those in the first structure. The results proved that wind force is an effective tool for damage detection as it produced very similar results compared to using multiple impulse force loading.

With the SAP2000 model parameters and the wind forcing function being validated in tests of first two structures, the next four structures were created to test the ARMAX DDM's ability to detect damage in reinforced concrete frames. Structure #3; the first concrete structure tested; had a 2x2 column layout to which slight, moderate and severe damage cases were applied. In each case, the DDM was able to successfully locate the damage and estimate its severity. Structure #4 was a four-storey reinforced concrete frame with a 3x3 column layout with slight, moderate and severe damage cases applied. The ARMAX DDM was once again able to locate and quantify the damage within the structure, however occasionally the degree of damage was slightly under-estimated, particularly in the severe damage case. Structure #5 was a 10-storey frame with a 4x4 column layout. Damage was successfully located and quantified in the minor, moderate and severe damage cases. Similar to Structure #4, however, the structure slightly underestimated the degree of damage

in some storeys in the moderate and severe damage cases. The final building model created was a four-storey structure with an asymmetric column layout. This model was created to test the ARMAX DDM's capability to detect damage under torsional movements. In both the one storey and three storey damage cases, the DDM successfully located the damage without yielding significant false positive or false negatives on the undamaged storeys, however the degree of damage was less accurate in the more severe damage case.

Through rigorous numerical testing, the ARMAX DDM was shown to effectively locate the damaged storeys in every single building model tested. For most damage cases, the degree of damage was calculated very closely to the expected value, however in some cases the degree of damage was slightly underestimated; this was particularly true in the buildings with more columns and when torsional movements were incorporated. The level of underestimation, however, was small enough to not warrant any major concerns.

Overall, the ARMAX DDM was proven to be an effective and consistent method for locating and quantifying damage at storey-level precision.

5.2. Recommendations and Future Work

The ARMAX DDM has provided accurate results in multiple damage building scenarios, however there are still limitations that are worth mentioning and recommendations for future work.

One limitation of this thesis is that although it was validated through various numerical model testing, there have been no experimental structures tested using wind induced vibrations.

The numerical damage detection model incorporated a uniform change in material properties in only the columns, with the rigid beams and slabs being unaffected. It is recommended that tests be done which may simulate more realistic structural damage. This may include incorporating severe material property changes in the tops and bottoms of the columns while not affecting the middle elevation as much. This could also include not treating the beams and slabs as rigid members and instead applying damage to them and including plastic hinge effects.

Although the damage model was shown to be effective when replacing a steel column with an aluminum one, it is recommended that the ARMAX DDM be tested on a more realistic damage case for steel structures. It is also recommended that the timber buildings be tested.

REFERENCES

Ahmadian, H., Mottershead, J., & Friswell, M. (2000). Damage location indicators from substructure mode shapes. *Inverse Problems In Engineering*, *8*(4), 309-323. doi:10.1080/174159700088027733

Allemang, R. J., & Brown, D. L. (1982). A correlation coefficient for modal vector analysis. *1st International Modal Analysis Conference,*

American Society of Civil Engineers. (2007). *Seismic rehabilitation of existing buildings*. Reston, VA: American Society of Civil Engineers.

American Society of Civil Engineers. (2014). *ASCE standard ASCESEI 41-13 : American society of civil engineers : Seismic evaluation and retrofit of existing buildings*. Reston, Virginia: American Society of Civil Engineers.

Amri, F., Bouattane, O., Khalili, T., Raihani, A., & Bifadene, A. (2015). *Toward an evolutionary multi-criteria model for the analysis and estimation of wind potential* doi:10.4236/jpee.2015.311002

Andersen, P. (1997). *Identification of civil engineering structures using vector ARMA models.*

Applied Technology Council. (2005). *ATC-20-1 field manual: Postearthquake safety evaluation of buildings*. Oakland, California: R.P. Gallagher Associates, Inc.

Azad, K. A., Rasul, G. M., & Yusaf, T. (2014). *Statistical diagnosis of the best weibull methods for wind power assessment for agricultural applications* doi:10.3390/en7053056

Bañuelos-Ruedas, F., Angeles-Camacho, C., & Rios-Marcuello, S. (2010). Analysis and validation of the methodology used in the extrapolation of wind speed data at different heights. Renewable and Sustainable Energy Reviews, 14(8), 2383-2391. 10.1016/j.rser.2010.05.001

Bao, C., Hao, H., & Li, Z. (2013). *Integrated ARMA model method for damage detection of subsea pipeline system* doi:10.1016/j.engstruct.2012.09.033

Baumbach, G. (1994). *Luftreinhaltung* (3 ed.). Berlin [u.a]: Springer.

Bernal, D., & Beck, J. (2004). Preface to the special issue on phase I of the IASC-ASCE structural health monitoring benchmark. *Journal of Engineering Mechanics, 130*(1), 1-2.

Bodeux, J., & Golinval, J. (2000). ARMAV model technique for system identification and damage detection.

Box, G. E. P., Jenkins, G. M., & Reinsel, G. C. (1994). *Time series analysis : Forecasting and control*. Englewood Cliffs, N.J.: Prentice Hall.

Brown, B. G., Katz, R. W., & Murphy, A. H. (1984). Time series models to simulate and forecast wind speed and wind power. *Journal of Climate and Applied Meteorology, 23*(8), 1184-1195.

C. Nichita, D. Luca, B. Dakyo, & E. Ceanga. (2002). Large band simulation of the wind speed for real time wind turbine simulators. *IEEE Transactions on Energy Conversion, 17*(4), 523-529. doi:10.1109/TEC.2002.805216

Carpinteri, A., & Lacidogna, G. (2006). *Damage monitoring of an historical masonry building by the acoustic emission technique*

Carvalho, D., Rocha, A., Gómez-Gesteira, M., & Silva Santos, C. (2014). *WRF wind simulation and wind energy production estimates forced by different reanalyzes: Comparison with observed data for portugal* doi:10.1016/j.apenergy.2013.12.001

Catbas, F. N., Ciloglu, S. K., Hasancebi, O., Grimmelsman, K., & Aktan, A. E. (2007). Limitations in structural identification of large constructed structures. *Journal of Structural Engineering, 133*(8), 1051-1066.

Chae, M. J., Yoo, H. S., Kim, J. Y., & Cho, M. Y. (2012). Development of a wireless sensor network system for suspension bridge health monitoring. *Automation in Construction, 21*, 237-252. doi:10.1016/j.autcon.2011.06.008

Chang, G. A., & Mander, J. B. (1994). *Seismic energy based fatigue damage analysis of bridge columns: Part 1 - evaluation of seismic capacity*. NCEER.

Chang, G. A., Mander, John B., National Center for Earthquake Engineering Research (U.S.),. (1994). *Seismic energy based fatigue damage analysis of bridge columns. part I, evaluation of seismic capacity*. Buffalo, N.Y.: National Center for Earthquake Engineering Research.

Ching, J., Muto, M., & Beck, J. L. (2006). Structural model updating and health monitoring with incomplete modal data using gibbs sampler. *Computer-Aided Civil and Infrastructure Engineering, 21*(4), 242-257. doi:10.1111/j.1467-8667.2006.00432.x

Costa Rocha, P. A., de Sousa, R. C., de Andrade, C. F., & da Silva, Maria Eugênia Vieira. (2012). *Comparison of seven numerical methods for determining weibull parameters for wind energy generation in the northeast region of Brazil* doi:10.1016/j.apenergy.2011.08.003

Maity, D. & Tripathy, R. (2005). Damage assessment of structures from changes in natural frequencies using genetic algorithm. *Structural Engineering and Mechanics*, 21-42. doi:10.12989/sem.2005.19.1.021

De Boe, P., & Golinval, J. (2003). Principal component analysis of a piezosensor array for damage localization. *Structural Health Monitoring, 2*(2), 137-144. doi:10.1177/1475921703002002005

de Lautour, O.,R., & Omenzetter, P. (2010). Damage classification and estimation in experimental structures using time series analysis and pattern recognition. *Mechanical Systems and Signal Processing, 24*(5), 1556-1569.

Dharap, P., Koh, B.H., & Nagarajaiah, S.. (2006). Structural health monitoring using ARMarkov observers. *Journal of Intelligent Material Systems and Structures, 17*(6), 469-481. doi:10.1177/1045389X06058793

Do, N.T.. *Detection of stiffness and mass changes separately using output-only vibration data.*

Doebling, S. W., Farrar, C. R., & Prime, M. B. (1998). A summary review of vibration-based damage identification methods. *Shock & Vibration Digest, 30*(2), 91.

Ekelund, T. (1994). Speed control of wind turbines in the stall region. Paper presented at the *1994 Proceedings of IEEE International Conference on Control and Applications,* 232 vol.1. doi:10.1109/CCA.1994.381194

Fan, W., & Qiao, P. (2011). Vibration-based damage identification methods: A review and comparative study. *Structural Health Monitoring, 10*(1), 83-111. doi:10.1177/1475921710365419

Farrar, C. R., & Worden, K. (2007). An introduction to structural health monitoring. *Philosophical Transactions: Mathematical, Physical and Engineering Sciences,* (1851), 303. doi:10.1098/rsta.2006.1928

Federal Emergency Management Agency. *Evaluation of earthquake damaged concrete and masonry wall buildings: Technical resources / prepared by the applied technology council ; prepared for the partnership for response and recovery* (1999). Washington, D.C

Feijóo, A., & Villanueva, D. (2016). Assessing wind speed simulation methods. *Renewable and Sustainable Energy Reviews, 56*, 473-483. doi:10.1016/j.rser.2015.11.094

Fernandez-Bernal, F. (June 2012). Wind speed time series generation for dynamic analysis: A proposal. *12th International Conference on Probabilistic Methods Applied to Power Systems,* 404-449.

Fernandez-Bernal, F., & Alonso-Alonso, J. (2017). Wind speed generation for dynamic analysis. *Wind Energy, 20*(6), 1049-1068. doi:10.1002/we.2079

George, H., & Testa, R. B. (1991). Modal analysis for damage detection in structures. *Journal of Structural Engineering, 117*(10), 3042-3063.

Ghobarah, A., Abou-Elfath, H., & Biddah, A. (1999). Response-based damage assessment of structures. *Earthquake Engineering and Structural Dynamics, 28*(1), 79-104.

Goto, S., Suda, K., & Miyashita, K. (2002). Profiles of turbulence intensity on the basis of full scale measurements. *Summaries of Technical Papers of Annual Meeting;* 111-112.

Gualtieri, G., & Secci, S. (2012). *Methods to extrapolate wind resource to the turbine hub height based on power law: A 1-h wind speed vs. weibull distribution extrapolation comparison* doi:10.1016/j.renene.2011.12.022

Gul, M. (2009). *Investigation of damage detection methodologies for structural health monitoring*

Gul, M., & Catbas, F. N. (2011). *Structural health monitoring and damage assessment using a novel time series analysis methodology with sensor clustering* doi:10.1016/j.jsv.2010.09.024

Gul, M., & Necati Catbas, F. (2009). Statistical pattern recognition for Structural Health Monitoring using time series modeling: Theory and experimental verifications. *Mechanical Systems And Signal Processing*, *23*2192-2204. doi:10.1016/j.ymssp.2009.02.013

H. Bayem, Y. Phulpin, P. Dessante, & J. Bect. (2008). Probabilistic computation of wind farm power generation based on wind turbine dynamic modeling. Paper presented at the *Proceedings of the 10th International Conference on Probablistic Methods Applied to Power Systems,* 1-6.

Hamze, A., Gueguen, P., Roux, P., & Baillet, L. (2014). *Damage detection and localisation using mode-based method and perturbation theory*

Hola, J., & Schabowicz, K. (2010). *State-of-the-art non-destructive methods for diagnostic testing of building structures – anticipated development trends* doi:10.1016/S1644-9665(12)60133-2

Holmes, J. D. (2015). *Wind loading of structures* (Third ed.). Boca Raton: CRC Press.

Hong, Y. H., Kim, H., & Lee, H. S. (2010). *Reconstruction of dynamic displacement and velocity from measured accelerations using the variational statement of an inverse problem* doi:10.1016/j.jsv.2010.05.016

Hoon, S., & Charles, R.F. (2001). Damage diagnosis using time series analysis of vibration signals. *Smart Materials and Structures, 10*(3), 446.

Hoon, S., Czarnecki, J. A., & Farrar, C. R. (2000). Structural health monitoring using statistical process control. *Journal of Structural Engineering, 126*(11), 1356-1363.

Huang, Z., Liu, G. Todd, M. & Mao,Z. (2013). Damage detection using vector auto-regressive models. *8695* 10.

Hyun, M. S., & Yoon, S. W. (2015) Continuous vibration measurement of building horizontal vibration using mobile phone app. *Journal of Korean Spatial Structures, 15*(3), 77-83.

Ikeda, A., Minami, Y., Fujita, K., & Takewaki, I. (2014). *Smart system identification of super high-rise buildings using limited vibration data during the 2011 Tohoku earthquake*

Johnson, E. A., Lam, H. F., Katafygiotis, L. S., & Beck, J. L. (2004). Phase I IASC-ASCE structural health monitoring benchmark problem using simulated data. *Journal of Engineering Mechanics, 130*(1), 3-15.

Ju, F.,D., & Mimovich, M.,E. (1988). Experimental diagnosis of fracture damage in structures by the modal frequency method. *Journal of Vibration, Acoustics, Stress, and Reliability in.Design, 110*(4), 456-463. doi:10.1115/1.3269550

Jun, Z., Ivan, J. N., & DeWolf, J. T. (1998). Structural damage detection using artificial neural networks. *Journal of Infrastructure Systems, 4*(3), 93-101.

Karki, R., Hu, P. & Billinton, R. (2006). A simplified wind power generation model for reliability evaluation. *IEEE Transactions on Energy Conversion, 21*(2), 533-540. doi:10.1109/TEC.2006.874233

Karki, R., Thapa, S., & Billinton, R. (2012). Operating risk analysis of wind-integrated power systems. *Electric Power Components & Systems, 40*(4), 399-413. doi:10.1080/15325008.2011.639129

Kaya, Y., Kocakaplan, S., & Safak, E. (2015). *System identification and model calibration of multi-story buildings through estimation of vibration time histories at non-instrumented floors*

Kessler, S. S., Spearing, S. M., & Soutis, C. (2002). Damage detection in composite materials using lamb wave methods. *Smart Materials and Structures, 11*(2), 269.

Kim, H., & Melhem, H. (2004). *Damage detection of structures by wavelet analysis* doi:10.1016/j.engstruct.2003.10.008

Kim, J., Ryu, Y., Cho, H., & Stubbs, N. (2003). Damage identification in beam-type structures: Frequency-based method vs mode-shape-based method. *Engineering Structures, 25*, 57-67. doi:10.1016/S0141-0296(02)00118-9

Kim, Y.C., & Yoon, S.W. (2014). *Coherence of fluctuating wind speed and along-wind force power spectrum of tall building* Trans Tech Publications Ltd. doi:10.4028/www.scientific.net/AMR.1025-1026.922

Kim, Y. C., & Yoon, S. W. (2014). Coherence of fluctuating wind speed and along-wind force power spectrum of tall building. *Advanced Materials Research -Zug-, 1025/1026*, 922-925.

Kim, Y. C., Kanda, J., & Yoon, S. W. (2009). Characteristics of longitudinal turbulence fluctuations in strong winds. *Korea Society of Steel Construction, 21*, 40-45.

Ko, J. M., & Ni, Y. Q. (2005). Technology developments in structural health monitoring of large-scale bridges. *Engineering Structures, 27*(-), 1715-1725. doi:10.1016/j.engstruct.2005.02.021

Koo, K. Y., Brownjohn, J. M. W., List, D. I., & Cole, R. (2013). Structural health monitoring of the tamar suspension bridge. *Structural Control and Health Monitoring, 20*(4), 609-625. doi:10.1002/stc.1481

Krishnan-Nair, K., & Kiremidjian, A. S. (2006). Time series based structural damage detection algorithm using gaussian mixtures modeling. *Journal of Dynamic Systems, Measurement, and Control, 129*(3), 285-293.

Kullaa, J. (2003). *Damage detection of the z24 bridge using control charts* doi://dx.doi.org/10.1006/mssp.2002.1555

Kuwabara, M., Yoshitomi, S., & Takewaki, I. (2013). *A new approach to system identification and damage detection of high-rise buildings*

Lakshmi, K., & Rama, M. R. (2014). A robust damage-detection technique with environmental variability combining time-series models with principal components. *Nondestructive Testing and Evaluation, 29*(4), 357-376. doi:10.1080/10589759.2014.949709

Lee, U., & Shin, J. (2002). *A frequency response function-based structural damage identification method* doi:10.1016/S0045-7949(01)00170-5

Lei, Y.,C. (2008). In FAO of t. U. (Ed.), *Evaluation of three methods for estimating the weibull distribution parameters of chinese pine (pinus tabulaeformis)*

Lei, Y., Kiremidjian, A., Nair, K., Law, K.,H., Kenny, T.,W., Carryer, E., . . . Kottapalli, A. (2017). *Statistical damage detection using time series analysis on a structural health monitoring benchmark problem*

Liang Cheng, & Gui Yun Tian. (2012). Comparison of nondestructive testing methods on detection of delaminations in composites. *Journal of Sensors, 2012*, 1-7. doi:10.1155/2012/408437

Link, M., & Weiland, M. (2012). *Computational model updating based on stochastic test data and modeling parameters - a tool for structural health monitoring*

Liu, K., Law, S. S., Xia, Y., & Zhu, X. Q. (2014). *Singular spectrum analysis for enhancing the sensitivity in structural damage detection* doi:10.1016/j.jsv.2013.09.027

Ljung, L. (1999). *System identification*. Upper Saddle River, N.J.: Prentice Hall.

Lu, Y., & Gao, F. (2005). *A novel time-domain auto-regressive model for structural damage diagnosis* doi:10.1016/j.jsv.2004.06.030

Lynch, J.P., Sundararajan, A., Law, K.H., Kiremidjian, A.S., & Carryer, E. (2004). Embedding damage detection algorithms in a wireless sensing unit for operational power efficiency. *Smart Materials and Structures, 13*(4), 800.

Meyer, C., Roufaiel, M. S. L., & Arzoumanidis, S. G. (1983). Analysis of damaged concrete frames for cyclic loads. *Earthquake Engineering & Structural Dynamics, 11*(2), 207-228. doi:10.1002/eqe.4290110205

Minami, Y., Yoshitomi, S., & Takewaki, I. (2013). *System identification of super high-rise buildings using limited vibration data during the 2011 Tohoku (Japan) earthquake*

Monroig, E., & Fujino, Y.Damage identification based on a local physical model for small clusters of wireless sensors. *1st Asia-Pacific Workshop on Structural Health Monitoring,*

Mosavi, A. A., Dickey, D., Seracino, R., & Rizkalla, S. (2012). *Identifying damage locations under ambient vibrations utilizing vector autoregressive models and mahalanobis distances* doi:10.1016/j.ymssp.2011.06.009

Mujica, L., Ruiz, M., Pozo, F., Rodellar, J., & Guemes, A. (2014). *A structural damage detection indicator based on principal component analysis and statistical hypothesis testing* doi:10.1088/0964-1726/23/2/025014

Nair, K. K., Kiremidjian, A. S., & Law, K. H. (2006). *Time series-based damage detection and localization algorithm with application to the ASCE benchmark structure* doi:10.1016/j.jsv.2005.06.016

Necati, C. F., Brown, D. L., & Emin, A. A. (2006). Use of modal flexibility for damage detection and condition assessment: Case studies and demonstrations on large structures. *Journal of Structural Engineering, 132*(11), 1699-1712.

Newmark, N. M., & Hall, W. J. (1982). *Earthquake spectra and design*. Berkeley, Calif.: Earthquake Engineering Research Institute.

Noman, A. S., Farah, D., & Ashutosh, B. (2013). Health monitoring of structures using statistical pattern recognition techniques. *Journal of Performance of Constructed Facilities, 27*(5), 575-584. doi:10.1061/(ASCE)CF.1943-5509.0000346

Omenzetter, P., & William-Brownjohn, J.M. (2006). Application of time series analysis for bridge monitoring. *Smart Materials and Structures, 15*(1), 129.

Pandey, A. K., & Biswas, M. (1994). *Damage detection in structures using changes in flexibility* doi:10.1006/jsvi.1994.1002

Park, N., & Park, Y. (2003). *Damage detection using spatially incomplete frequency response functions* doi:10.1006/mssp.2001.1423

Peterson, E. W., & Hennessey, J. P. (1978). On the use of power laws for estimates of wind power potential. *Journal of Applied Meteorology, 17*(3), 390-394.

Qipei, M., & Gül, M. (2015). Novel sensor Clustering–Based approach for simultaneous detection of stiffness and mass changes using output-only data. *Journal of Structural Engineering, 141*(10), 04014237. doi:10.1061/(ASCE)ST.1943-541X.0001218

Rossi, R., Lazzari, M., & Vitaliani, R. (2004). Wind field simulation for structural engineering purposes. *International Journal For Numerical Methods In Engineering*, *61*(5), 738-763. doi:10.1002/nme.1083

Roy, K., Bhattacharya, B., & Ray-Chaudhuri, S. (2015). *ARX model-based damage sensitive features for structural damage localization using output-only measurements* doi:10.1016/j.jsv.2015.03.038

Ruigen Yao and Shamim, N Pakzad. (2014). Damage and noise sensitivity evaluation of autoregressive features extracted from structure vibration. *Smart Materials and Structures, 23*(2), 025007.

Rytter, A. (1993). *Vibrational based inspection of civil engineering structures*

Salawu, O. (1997). Detection of structural damage through changes in frequency: A review. *Engineering Structures*, *19*(9), 718-723.

Sampaio, R. P. C., Maia, N. M. M., & Silva, J. M. M. (1999). *Damage detection using the frequency-response-function curvature method* doi:10.1006/jsvi.1999.2340

Shamshad, A., Bawadi, M. A., Hussin, W. M. A., Majid, T. A., & Sanusi, S. A. M. (2005). First and second order markov chain models for synthetic generation of wind speed time series.*Energy, 30*, 693-708. doi:10.1016/j.energy.2004.05.026

Shih, C. Y., Tsuei, Y. G., Allemang, R. J., & Brown, D. L. (1988). *Complex mode indication function and its applications to spatial domain parameter estimation* doi:10.1016/0888-3270(88)90060-X

Shiradhonkar, S. R., & Shrikhande, M. (2011). *Seismic damage detection in a building frame via finite element model updating* doi:10.1016/j.compstruc.2011.06.006

Siebel, T., Friedmann, A., Koch, M., & Mayer, D. (2012). *Assessment of mode shape-based damage detection methods under real operational conditions*

Simulation of correlated wind speed data for economic dispatch evaluation. (2012). *IEEE Transactions on Sustainable Energy, Sustainable Energy, IEEE Transactions on, IEEE Trans.Sustain.Energy,* (1), 142. doi:10.1109/TSTE.2011.2165861

Sohn, H., Farrar, C. R., Hunter, N. F., & Worden, K. (2001). Structural health monitoring using statistical pattern recognition techniques. *Journal of Dynamic Systems, Measurement and Control, Transactions of the ASME, 123*(4), 706-711. doi:10.1115/1.1410933

Sohn, H. (2007). Effects of environmental and operational variability on structural health monitoring. *Philos Transact A Math Phys Eng Sci, 365*(1851), 539.

Sohn, H., Worden, K., & Farrar, C. R. (2002). Statistical damage classification under changing environmental and operational conditions. *Journal of Intelligent Material Systems and Structures, 13*(9), 561-574. doi:10.1106/104538902030904

Taha, M. R. (2010). *A neural-wavelet technique for damage identification in the ASCE benchmark structure using phase II experimental data* doi:10.1155/2010/675927

Toussi, S., & Yao, J. T. P. (1983). Hysteresis identification of existing structures. *Journal of Engineering Mechanics, 109*(5), 1189-1202. doi:5(1189)

Trendafilova, I., & Manoach, E. (2008). Vibration-based damage detection in plates by using time series analysis. *Mechanical Systems and Signal Processing, 22*(5), 1092-1106. doi:10.1016/j.ymssp.2007.11.020

Van Zwol, T. R., & University of Alberta. (2005). *Long-term structural health monitoring of the crowchild trail bridge*

Van, d. H. (1957). Power spectrum of horizontal wind speed in the frequency range from 0.0007 to 900 cycles per hour. *Journal of Meteorology, 14*(2), 160-164.

Wang, Y., Ligon, D., Creegan, E., Williamson, C., Klipp, C., Felton, M., & Calhoun, R. (2004). 6.3 turbulence characteristics over an urban domain observed by doppler lidars.

Welfonder, E., Neifer, R., & Spanner, M. (1997). *Development and experimental identification of dynamic models for wind turbines* doi:10.1016/S0967-0661(96)00208-0

West, W. M. (1986). *Illustration of the use of modal assurance criterion to detect structural changes in an orbiter test specimen*. United States: NASA Center for Aerospace Information (CASI).

Wind speed simulation in wind farms for steady-state security assessment of electrical power systems. (1999). *IEEE Transactions on Energy Conversion, Energy Conversion, IEEE Transactions on, IEEE Trans.Energy Convers.,* (4), 1582. doi:10.1109/60.815109

Wong, K. (2004). Instrumentation and health monitoring of cable-supported bridges. *Structural Control and Health Monitoring, 11*(2), 91-124. doi:10.1002/stc.33

Xing, Z., & Mita, A. (2012). A substructure approach to local damage detection of shear structure. *Structural Control and Health Monitoring, 19*(2), 309-318. doi:10.1002/stc.439

Yazgan, U., & Dazio, A. (2012). Post-earthquake damage assessment using residual displacements. *Earthquake Engineering and Structural Dynamics, 41*(8), 1257-1276. doi:10.1002/eqe.1184

Yue, J., Qian, J., & Beskos, D. E. (2016). A generalized multi-level seismic damage model for RC framed structures. *Soil Dynamics and Earthquake Engineering, 80*, 25-39. doi:10.1016/j.soildyn.2015.10.005

Zhang, D., & Johnson, E. A. (2013). *Substructure identification for shear structures I: Substructure identification method*

Zhong, S., Oyadiji, S. O., & Ding, K. (2008). Response-only method for damage detection of beam-like structures using high accuracy frequencies with auxiliary mass spatial probing.*Journal of Sound and Vibration, 311*, 1075-1099. doi:10.1016/j.jsv.2007.10.004

Zongming, G., Zhang, Y., Jiezhi, L., & Jian, F. (2016). Stiffness degradation-based damage model for RC members and structures using fiber-beam elements. *Earthquake Engineering & Engineering Vibration, 15*(4), 697-714. doi:10.1007/s11803-016-0359-4

APPENDIX A

Detailed SAP2000 Results

Modelling Parameters

Structure ID	Sampling Time	# of Trials	Location of Sensor
#1	10	10	Center of Floor Slab
#2	30	10	Center of Floor Slab
#3	30	10	Center of Floor Slab
#4	30	10	Center Column
#5	30	10	Center of Floor Slab

Material Properties

Structural Steel

Yield Strength	380	MPa
Ultimate Strength	450	MPa
Modulus of Elasticity	200,000	MPa
Poisson Ratio	0.3	
Density	7850	kg/m^3

Concrete

Ultimate Strength	40	MPa
Modulus of Elasticity	32,900	MPa
Poisson Ratio	0.2	
Density	2403	kg/m^3

Reinforcing Steel

Yield Strength	455	MPa
Ultimate Strength	683	MPa
Modulus of Elasticity	200,000	MPa
Density	7850	kg/m^3

Structure #1

Case #	Damage			SAP2000 Analysis		Stiffness Loss Matrix (Noise Level)	
	Location		DR				
	X-Y	Storey		K Loss	Stiffness Loss Matrix (%)	0%	5%
1.1	A1	4	0.685	0	0 0 NaN NaN	-0.0913 -0.6787 NaN NaN	-0.1563 -0.4951 NaN NaN
				0	0 0 0 NaN	0.7572 1.0663 1.2221 NaN	0.9977 1.2360 1.8215 NaN
				0	NaN 0 -8.5625 -17.1250	NaN -0.8986 -7.5182 -14.1160	NaN -1.5992 -7.4972 -14.3859
				-17.125	NaN NaN -17.1250 -17.1250	NaN NaN -14.8663 -14.7952	NaN NaN -14.7060 -14.7814
1.2	A1	4	0.685	0	0 0 NaN NaN	-0.1304 -1.0434 NaN NaN	-0.2253 -1.1615 NaN NaN
	A2	4	0.685	0	0 0 0 NaN	3.2491 2.2719 1.5773 NaN	3.9700 3.2749 3.0424 NaN
				0	NaN 0 -17.1250 -34.2500	NaN -1.8544 -15.6746 -29.9519	NaN -2.4134 -15.6590 -30.1421
				-34.25	NaN NaN -34.2500 -34.2500	NaN NaN -29.7508 -29.4255	NaN NaN -30.0738 -29.4042
1.3	A1	2	0.685	0	-8.5625 -17.1250 NaN NaN	-6.9054 -14.2710 NaN NaN	-6.7910 -14.8503 NaN NaN
				-17.125	-17.1250 -8.5625 0 NaN	-14.9193 -8.3221 -1.6005 NaN	-15.3484 -7.5027 -1.1945 NaN
				0	NaN 0 0 0	NaN -2.6682 -1.6855 -1.6550	NaN -1.6005 -1.2004 -1.3790
				0	NaN NaN 0 0	NaN NaN 0.7914 0.6080	NaN NaN -0.1399 -0.0306
1.4	A1	2	0.685	0	-17.1250 -34.2500 NaN NaN	-13.4220 -27.7092 NaN NaN	-13.0864 -28.4785 NaN NaN
	A2	2	0.685	-34.25	-34.2500 -17.1250 0 NaN	-29.8384 -15.8073 -3.6222 NaN	-30.0627 -15.7662 -2.6019 NaN
				0	NaN 0 0 0	NaN -3.2647 -3.9027 -3.6947	NaN -3.3321 -3.2189 -3.8808
				0	NaN NaN 0 0	NaN NaN -0.2248 0.1617	NaN NaN -0.7935 -0.3558
2.1	A1	2	0.685	0	-17.1250 -34.2500 NaN NaN	-13.9208 -28.1025 NaN NaN	-13.2751 -27.9139 NaN NaN
	A2	2	0.685	-34.25	-34.2500 -17.1250 0 NaN	-29.7032 -15.0949 -1.3291 NaN	-26.9275 -14.1427 -0.6463 NaN
	B1	4	0.685	0	NaN 0 -17.1250 -34.2500	NaN -2.6165 -15.4377 -29.0286	NaN -3.2153 -16.7093 -30.5669
	B2	4	0.685	-34.25	NaN NaN -34.2500 -34.2500	NaN NaN -29.6895 -29.8237	NaN NaN -28.8591 -28.8822
2.2	A1	1	0.685	-34.25	-25.6875 -17.1250 NaN NaN	-26.2949 -15.4081 NaN NaN	-23.1137 -15.2118 NaN NaN
	B2	1	0.685	-17.125	-17.1250 -8.5625 0 NaN	-17.4028 -7.2125 -0.0307 NaN	-17.7194 -7.1507 -0.1220 NaN
	A1	2	0.685	0	NaN 0 0 0	NaN -3.0950 -1.0739 -0.5032	NaN -3.6277 -3.7719 -3.3538
				0	NaN NaN 0 0	NaN NaN -3.3152 -2.3163	NaN NaN -3.1554 -2.0130
3.1	A1	1	0.685	-51.375	-34.2500 -17.1250 NaN NaN	-35.2661 -18.6035 NaN NaN	-35.0338 -18.2351 NaN NaN
	A2	1	0.685	-17.125	-17.1250 -25.6875 -34.2500 NaN	-16.1203 -22.3747 -30.6125 NaN	-16.7512 -22.4150 -31.3041 NaN
	B1	1	0.685	-34.25	NaN -34.2500 -17.1250 0	NaN -33.7714 -20.4206 -4.6314	NaN -32.7742 -18.7177 -4.3458
	B2	2	0.685	0	NaN NaN 0 0	NaN NaN -4.3798 -4.7101	NaN NaN -4.5040 -3.7011
	A1	3	0.685				
	B1	3	0.685				

Structure #2

Case #	Wind		Damage			SAP2000 Analysis		Stiffness Loss Matrix (Noise Level)		
			Location		DR					
	Base	Dam	X-Y	Storey		K Loss	Stiffness Loss Matrix (%)	0%	5%	10%
1.1	7	5	A1	4	0.685	0	0 0 NaN NaN	3.0753 2.9597 NaN NaN	3.5970 2.9175 NaN NaN	3.1434 2.6984 NaN NaN
						0	0 0 0 NaN	3.5881 2.0619 1.4835 NaN	0.0033 -1.5803 -2.8440 NaN	-0.6755 -0.2585 -1.0958 NaN
						0	NaN 0 -8.5646 -17.1293	NaN 1.0121 -7.9406 -14.4735	NaN 0.9545 -7.6375 -14.2931	NaN -0.8043 -7.8659 -15.2176
						-17.1293	NaN NaN -17.1293 -17.1293	NaN NaN -16.7998 -16.5704	NaN NaN -14.4155 -14.7957	NaN NaN -14.2207 -14.6907
1.2			A1	4	0.685	0	0 0 NaN NaN	3.2576 3.3354 NaN NaN	2.2998 1.6716 NaN NaN	2.0549 1.2651 NaN NaN
			A2	4	0.685	0	0 0 0 NaN	0.3708 -2.6129 -4.3043 NaN	0.4604 -3.0011 -4.0912 NaN	-1.5698 -3.1267 -4.5861 NaN
						0	NaN 0 -17.1293 -34.2586	NaN -1.0414 -15.3796 -29.7916	NaN -4.5819 -16.8387 -30.3168	NaN -3.2347 -16.6880 -30.5673
						-34.2586	NaN NaN -34.2586 -34.2586	NaN NaN -29.6671 -30.1066	NaN NaN -28.7842 -29.4402	NaN NaN -29.1858 -29.7450
1.3	3	5	A1	2	0.685	0	-8.5646 -17.1293 NaN NaN	-8.2050 -14.2041 NaN NaN	-7.3304 -12.6513 NaN NaN	-7.1956 -13.9511 NaN NaN
						-17.1293	-17.1293 -8.5646 0 NaN	-14.8461 -7.1557 0.3584 NaN	-12.2972 -6.4493 -0.2710 NaN	-13.0293 -6.9881 -0.6917 NaN
						0	NaN 0 0 0	NaN 2.7568 3.8615 5.0016	NaN 1.8750 2.4661 3.1562	NaN 2.4854 3.9494 3.4812
						0	NaN NaN 0 0	NaN NaN -1.4660 -1.0633	NaN NaN -1.6041 -1.6196	NaN NaN -2.6525 -2.5320
1.4			A1	2	0.685	0	-17.1293 -34.2586 NaN NaN	-16.3326 -30.7507 NaN NaN	-15.1463 -29.6660 NaN NaN	-15.4319 -29.9954 NaN NaN
			A2	2	0.685	-34.2586	-34.2586 -17.1293 0 NaN	-27.1853 -14.5971 2.2686 NaN	-25.7874 -13.7294 3.7262 NaN	-26.9756 -14.1601 4.4772 NaN
						0	NaN 0 0 0	NaN 4.5629 2.7231 0.5143	NaN 5.5033 2.9183 0.9812	NaN 5.0961 4.1264 3.1021
						0	NaN NaN 0 0	NaN NaN -3.1910 -3.6657	NaN NaN -3.3382 -3.7365	NaN NaN -3.3298 -2.9227
2.1	3	6	A1	2	0.685	0	-17.1293 -34.2586 NaN NaN	-14.6779 -29.0992 NaN NaN	-15.5871 -29.8660 NaN NaN	-16.8195 -31.2288 NaN NaN
			A2	2	0.685	-34.2586	-34.2586 -17.1293 0 NaN	-28.3379 -13.4232 7.2093 NaN	-29.8969 -14.1215 3.8344 NaN	-28.3660 -14.4221 4.0218 NaN
			B1	4	0.685	0	NaN 0 -17.1293 -34.2586	NaN 1.7498 -15.8056 -28.5642	NaN -3.1026 -17.4443 -30.5021	NaN -4.5958 -17.9006 -30.3422
			B2	4	0.685	-34.2586	NaN NaN -34.2586 -34.2586	NaN NaN -30.6548 -30.7285	NaN NaN -31.2144 -31.2634	NaN NaN -30.6063 -30.5651
2.2	7a	7b	A1	1	0.685	-34.2586	-25.6939 -17.1293 NaN NaN	-24.4575 -15.2406 NaN NaN	-24.8138 -15.5054 NaN NaN	-24.6801 -15.2174 NaN NaN
			B2	1	0.685	-17.1293	-17.1293 -8.5646 0 NaN	-17.2471 -6.2474 4.8184 NaN	-17.7464 -6.9340 6.8854 NaN	-17.4356 -7.3747 4.3194 NaN
			A1	2	0.685	0	NaN 0 0 0	NaN 4.9838 2.1120 -0.4270	NaN 4.0914 0.9673 -1.0384	NaN 4.6553 2.0329 -1.8467
						0	NaN NaN 0 0	NaN NaN 1.3422 1.8151	NaN NaN -1.4780 -0.6891	NaN NaN -0.1875 0.4855
3.1	7	2	A1	1	0.685	-51.3879	-34.2586 -17.1293 NaN NaN	-33.6769 -15.6166 NaN NaN	-33.3142 -15.5178 NaN NaN	-34.0973 -16.1927 NaN NaN
			A2	1	0.685	-17.1293	-17.1293 -25.6939 -34.2586 NaN	-15.3943 -21.3860 -29.5276 NaN	-15.7911 -21.8201 -29.3840 NaN	-17.3830 -22.7346 -29.9130 NaN
			B1	1	0.685	-34.2586	NaN -34.2586 -17.1293 0	NaN -30.7945 -16.5115 -2.8782	NaN -31.6463 -16.5039 -3.0712	NaN -29.5976 -16.9132 -3.5407
			B2	2	0.685	0	NaN NaN 0 0	NaN NaN 5.4045 4.9116	NaN NaN 3.7027 3.3740	NaN NaN 5.1729 4.5347
			A1	3	0.685					
			B1	3	0.685					

Structure #3

Case #	Wind		Damage			SAP2000 Analysis		Stiffness Loss Matrix (%) (Noise Level)		
	Base	Dam	Location X-Y	Location Storey	DR	K Loss	Stiffness Loss Matrix (%)	0%	5%	10%
1.1	4	2	A3	1	0.4	-20.0228	-10.0114 0 NaN NaN	-10.6004 -0.9798 NaN NaN	-10.9321 -1.1102 NaN NaN	-10.5557 0.3020 NaN NaN
			C1	1	0.4	0	0 0 0 NaN	3.7901 -0.5079 -3.2336 NaN	3.6321 -0.7318 -3.2732 NaN	3.7168 0.0504 -0.6762 NaN
						0	NaN 0 0 0	NaN 3.1937 4.6603 4.2396	NaN 3.7377 4.5280 4.3071	NaN 3.2762 2.9927 3.6577
						0	NaN NaN 0 0	NaN NaN 3.2231 3.2958	NaN NaN 0.7603 0.7400	NaN NaN -1.7903 -1.8096
1.2	4	6	A1	2	0.5	0	-17.5171 -35.0342 NaN NaN	-17.3183 -35.0012 NaN NaN	-17.7207 -34.8263 NaN NaN	-17.4657 -34.6759 NaN NaN
			A3	2	0.4	-35.0342	-35.0342 -17.5171 0 NaN	-34.1217 -16.4677 -1.5800 NaN	-34.6132 -16.1999 -1.5161 NaN	-33.9279 -17.7954 -3.4930 NaN
			C1	2	0.5	0	NaN 0 0 0	NaN -2.4210 2.0791 3.4739	NaN -1.6555 1.8237 3.1133	NaN -2.0677 2.3720 3.6581
						0	NaN NaN 0 0	NaN NaN -0.8324 -0.1689	NaN NaN -2.1383 -1.3637	NaN NaN 1.6161 1.6545
1.3	3	5	C1	3	0.6	0	0 0 NaN NaN	-0.5919 -1.1750 NaN NaN	-0.0553 -0.7142 NaN NaN	2.3003 0.3990 NaN NaN
			C3	3	0.45	0	0 -13.1659 -26.3317 NaN	-2.9887 -12.4863 -23.7706 NaN	-2.5523 -13.6560 -25.1853 NaN	-3.2811 -13.6250 -24.6195 NaN
						-26.3317	NaN -26.3317 -13.1659 0	NaN -25.3470 -14.5126 -3.6343	NaN -24.9811 -14.4733 -3.9979	NaN -24.5185 -14.7376 -3.1061
						0	NaN NaN 0 0	NaN NaN -4.4280 -4.7738	NaN NaN -3.6974 -4.2142	NaN NaN -3.5945 -3.4452
1.4	5	6	C1	3	0.4	0	0 0 NaN NaN	-0.0155 -0.1566 NaN NaN	0.0176 0.3695 NaN NaN	0.6325 1.1091 NaN NaN
						0	0 -5.0557 -10.0114 NaN	0.2495 -4.3317 -10.7657 NaN	-0.9863 -3.2669 -10.1140 NaN	0.9039 -4.4997 -10.9214 NaN
						-10.0114	NaN -10.0114 -5.0057 0	NaN -9.4110 -4.9308 0.2627	NaN -9.3370 -4.8572 0.5150	NaN -9.7007 -4.7626 0.7081
						0	NaN NaN 0 0	NaN NaN 0.7140 1.4206	NaN NaN 0.0819 0.5267	NaN NaN 1.0964 0.5155
2.1	6	5	A3	1	0.4	-20.0228	-10.0114 0 NaN NaN	-8.7739 -0.2157 NaN NaN	-9.0823 0.7512 NaN NaN	-9.4739 0.6346 NaN NaN
			C1	1	0.4	0	0 -13.1659 -26.3317 NaN	0.1486 -15.6159 -26.2810 NaN	-3.7758 -14.3885 -27.7103 NaN	-2.7975 -14.3052 -26.4499 NaN
			C1	3	0.6	-26.3317	NaN -26.3317 -13.1659 0	NaN -24.2345 -14.0072 -2.0764	NaN -25.8330 -13.9536 -2.1059	NaN -25.2666 -14.1566 -1.5670
			C3	3	0.45	0	NaN NaN 0 0	NaN NaN -2.6452 -1.5845	NaN NaN -5.0499 -3.8806	NaN NaN -4.8696 -4.1098
2.2	6	4	A1	1	0.6	-46.3416	-35.0787 -23.8157 NaN NaN	-33.4994 -21.9685 NaN NaN	-33.9668 -21.8671 NaN NaN	-33.7302 -20.6299 NaN NaN
			A3	1	0.65	-23.8157	-23.8157 -11.9079 0 NaN	-21.7120 -10.9002 -3.2880 NaN	-20.5599 -12.2608 -3.5342 NaN	-21.3797 -13.0282 -3.6761 NaN
			C3	1	0.6	0	NaN 0 0 0	NaN -4.0673 2.0573 5.1712	NaN -4.2179 0.7741 4.1819	NaN -4.3630 0.4754 5.7077
			A3	2	0.5	0	NaN NaN 0 0	NaN NaN -2.3520 -0.8612	NaN NaN -3.1269 -2.1596	NaN NaN -2.6818 -4.3030
			C3	2	0.45					
3.1	3	4	A1	1	0.6	-31.3142	-27.5650 -23.8157 NaN NaN	-27.9121 -23.7879 NaN NaN	-27.6666 -23.9656 NaN NaN	-27.3709 -23.5519 NaN NaN
			A3	1	0.65	-23.8157	-23.8157 -21.9193 -20.0228 NaN	-25.8820 -24.5089 -18.5253 NaN	-25.1417 -22.7616 -19.4169 NaN	-25.1428 -24.3816 -19.9202 NaN
			A3	2	0.5	-20.0228	NaN -20.0228 -10.0114 0	NaN -20.7611 -9.7588 1.3510	NaN -20.7398 -9.0081 4.2074	NaN -21.4449 -9.3176 2.9002
			C3	2	0.45	0	NaN NaN 0 0	NaN NaN 3.3063 3.0143	NaN NaN 1.1618 0.7546	NaN NaN -2.6123 -2.6578
			A1	3	0.4					
			C3	3	0.4					

Structure #4

Case #	Wind		Damage			SAP2000 Analysis		Stiffness Loss Matrix (%) (Noise)		
	Base	Dam	Location X-Y	Location Storey	DR	K Loss	Stiffness Loss Matrix (%)	0%	5%	10%
1.1	5	3	A3	1	0.5	-22.2425	-11.1212 0 NaN NaN	-11.2253 1.6779 NaN NaN	-10.6223 2.6022 NaN NaN	-10.7631 2.7013 NaN NaN
			B1	1	0.5	0	0 0 0 NaN	-0.4918 -3.5215 -0.8096 NaN	-0.4981 -4.1605 -1.7775 NaN	1.9486 -2.9581 -0.8832 NaN
			B2	1	0.5	0	NaN 0 0 0	NaN 1.3481 -0.0456 1.1010	NaN 2.0398 0.1767 1.2487	NaN -0.0448 -0.8852 0.5639
			C2	1	0.5	0	NaN NaN 0 0	NaN NaN 0.3462 -0.3084	NaN NaN 2.8817 1.7064	NaN NaN 4.3284 2.8116
1.2	5	6	A2	2	0.45	0	-20.0500 -40.1000 NaN NaN	-16.8327 -34.4421 NaN NaN	-17.6372 -34.9925 NaN NaN	-18.3158 -35.7016 NaN NaN
			B2	2	0.6	-40.1	-40.1000 -20.0500 0 NaN	-35.9670 -17.6677 1.0748 NaN	-36.1337 -17.2214 1.7691 NaN	-35.5458 -17.1039 1.0844 NaN
			B3	2	0.6	0	NaN 0 0 0	NaN 4.1738 0.1803 0.2597	NaN 5.0319 0.5357 0.4868	NaN 7.4189 1.9961 1.7176
			C1	2	0.65	0	NaN NaN 0 0	NaN NaN 1.9811 0.8348	NaN NaN 6.4322 5.3424	NaN NaN 7.8905 8.4549
			C2	2	0.65					
			C3	2	0.65					
1.3	5	7	A2	3	0.45	0	0 0 NaN NaN	4.2057 -1.0849 NaN NaN	3.0952 -2.3874 NaN NaN	3.4850 -3.1030 NaN NaN
			A3	3	0.5	0	0 -20.0382 -40.0763 NaN	-6.6226 -15.3466 -35.7426 NaN	-4.0096 -15.8215 -36.7432 NaN	-3.2330 -14.6475 -34.7669 NaN
			B1	3	0.55	-40.0763	NaN -40.0763 -20.0382 0	NaN -34.5697 -16.9163 -1.2852	NaN -33.8742 -16.1882 -0.1043	NaN -32.2678 -15.8638 -0.8749
			B3	3	0.5	0	NaN NaN 0 0	NaN NaN -0.2645 -0.3367	NaN NaN -0.4956 -0.5695	NaN NaN 2.0567 1.3405
			C1	3	0.55					
			C2	3	0.45					
			C3	3	0.6					
2.1	3	7	A3	1	0.5	-22.2425	-11.1212 0 NaN NaN	-8.6240 -0.0043 NaN NaN	-9.2850 -1.0148 NaN NaN	-9.7466 -2.9264 NaN NaN
			B1	1	0.5	0	0 -20.0382 -40.0763 NaN	-0.2017 -14.2446 -34.8489 NaN	0.1305 -14.4816 -35.1955 NaN	2.1280 -13.3801 -33.9353 NaN
			B2	1	0.5	-40.0763	NaN -40.0763 -20.0382 0	NaN -34.1072 -18.5912 -0.5046	NaN -34.2993 -18.4562 -0.1181	NaN -33.7334 -18.2103 -0.2692
			C2	1	0.5	0	NaN NaN 0 0	NaN NaN -0.9775 2.4189	NaN NaN -1.2351 2.2828	NaN NaN 12.5916 16.6274
			A2	3	0.45					
			A3	3	0.5					
			B1	3	0.55					
			B3	3	0.5					
			C1	3	0.55					
			C2	3	0.45					
			C3	3	0.6					
2.2	3	4	A2	1	0.6	-43.3938	-36.7386 -30.0834 NaN NaN	-34.1592 -21.3613 NaN NaN	-34.7245 -22.2204 NaN NaN	-35.0794 -22.2349 NaN NaN
			A3	1	0.6	-30.0834	-30.0834 -15.0417 0 NaN	-22.1838 -14.5446 -0.7927 NaN	-20.6272 -15.2834 -2.0493 NaN	-22.2383 -15.4595 -1.4084 NaN
			B1	1	0.5	0	NaN 0 0 0	NaN 2.8774 -1.2001 -0.2846	NaN 3.1853 -0.2962 1.0189	NaN 6.0726 1.4458 2.6826
			B2	1	0.65	0	NaN NaN 0 0	NaN NaN 2.1741 0.1050	NaN NaN 4.2879 1.9390	NaN NaN 8.8333 6.9310
			B3	1	0.5					
			C1	1	0.55					
			C2	1	0.5					
			A2	2	0.6					
			A3	2	0.6					
			B3	2	0.6					
			C1	2	0.45					
			C3	2	0.45					
3.1	3	2	A2	1	0.6	-45.0728	-42.0256 -38.9784 NaN NaN	-37.1177 -28.3625 NaN NaN	-37.4689 -28.8099 NaN NaN	-38.0622 -29.4908 NaN NaN
			A3	1	0.6	-38.9784	-38.9784 -30.3503 -21.7222 NaN	-30.0308 -26.3641 -14.2967 NaN	-30.1702 -26.2712 -14.0109 NaN	-29.4621 -27.0917 -15.5664 NaN
			B1	1	0.65	-21.7222	NaN -21.7222 -10.8611 0	NaN -11.4032 -11.0980 -2.0113	NaN -10.1920 -10.8471 -2.0957	NaN -12.8859 -9.3792 0.1040
			B2	1	0.65	0	NaN NaN 0 0	NaN NaN 2.2942 0.2302	NaN NaN -1.1063 -3.2095	NaN NaN -2.9186 -5.4237
			B3	1	0.5					
			C1	1	0.55					
			C2	1	0.5					
			A1	2	0.6					
			A2	2	0.65					
			B1	2	0.6					
			B3	2	0.6					
			C1	2	0.6					
			C3	2	0.45					
			A1	3	0.45					
			A3	3	0.5					
			B2	3	0.45					
			C2	3	0.55					

Structure #5

Case #	Wind		Damage				Stiffness Loss Matrix (%)																									
	Base	Dam	Location		DR	K Loss	SAP2000	ARMAX Analysis																								
			X-Y	Storey				0%														5%										
1	2	4	A2	2	0.55	0	-13.1264 -26.2527 NaN NaN NaN NaN NaN NaN NaN NaN;	-12.47	-25.56	NaN	NaN	NaN	NaN	NaN	NaN	NaN	NaN	-12.18	-25.63	NaN	NaN	NaN	NaN	NaN	NaN	NaN	NaN
			B2	2	0.55	-26.25	-26.2527 -13.1264 0 NaN NaN NaN NaN NaN NaN NaN;	-21.48	-10.98	5.31	NaN	NaN	NaN	NaN	NaN	NaN	NaN	-29.22	-15.54	0.89	NaN	NaN	NaN	NaN	NaN	NaN	NaN
			C2	2	0.55	0	NaN 0 0 0 NaN NaN NaN NaN NaN NaN;	NaN	-10.27	2.42	11.69	NaN	NaN	NaN	NaN	NaN	NaN	NaN	-10.14	0.21	7.87	NaN	NaN	NaN	NaN	NaN	NaN
			D2	2	0.55	0	NaN NaN 0 -13.1264 -26.2527 NaN NaN NaN NaN NaN;	NaN	NaN	-1.36	-15.66	-28.51	NaN	NaN	NaN	NaN	NaN	NaN	NaN	-2.21	-15.32	-27.23	NaN	NaN	NaN	NaN	NaN
			A4	2	0.5	-26.25	NaN NaN NaN -26.2527 -13.1264 0 NaN NaN NaN NaN;	NaN	NaN	NaN	-17.86	-9.98	-2.20	NaN	NaN	NaN	NaN	NaN	NaN	NaN	-20.79	-12.41	-1.50	NaN	NaN	NaN	NaN
			B4	2	0.5	0	NaN NaN NaN NaN 0 0 0 NaN NaN NaN;	NaN	NaN	NaN	NaN	-5.42	-1.70	2.25	NaN	NaN	NaN	NaN	NaN	NaN	NaN	-5.22	-1.55	2.43	NaN	NaN	NaN
			C4	2	0.5	0	NaN NaN NaN NaN NaN 0 0 0 NaN NaN;	NaN	NaN	NaN	NaN	NaN	-8.69	-8.68	-7.14	NaN	NaN	NaN	NaN	NaN	NaN	-9.60	-8.79	-6.67	NaN	NaN
			D4	2	0.5	0	NaN NaN NaN NaN NaN NaN 0 0 0 NaN;	NaN	NaN	NaN	NaN	NaN	NaN	1.20	-0.86	-0.62	NaN	NaN	NaN	NaN	NaN	NaN	NaN	0.27	-2.31	-2.45	NaN
						0	NaN NaN NaN NaN NaN NaN NaN 0 0 0;	NaN	NaN	NaN	NaN	NaN	NaN	NaN	1.87	-6.14	-9.93	NaN	NaN	NaN	NaN	NaN	NaN	NaN	1.47	-5.95	-9.06
			A2	5	0.55	0	NaN NaN NaN NaN NaN NaN NaN NaN 0 0	NaN	NaN	NaN	NaN	NaN	NaN	NaN	NaN	1.27	0.16	NaN	NaN	NaN	NaN	NaN	NaN	NaN	0.57	-0.45
			B2	5	0.55																									
			C2	5	0.55																									
			D2	5	0.55																									
			A4	5	0.5																									
			B4	5	0.5																									
			C4	5	0.5																									
			D4	5	0.5																									
2	5	6	A3	1	0.65	-16.8755	-8.4377 0 NaN NaN NaN NaN NaN NaN NaN NaN	-4.693	5.57114	NaN	NaN	NaN	NaN	NaN	NaN	NaN	NaN	-6.4913	5.68724	NaN	NaN	NaN	NaN	NaN	NaN	NaN	NaN
			B2	1	0.6	0	0 -9.0611 -18.1221 NaN NaN NaN NaN NaN NaN NaN	-1.7681	-6.9921	-13.24	NaN	NaN	NaN	NaN	NaN	NaN	NaN	1.5126	-6.6967	-15.588	NaN	NaN	NaN	NaN	NaN	NaN	NaN
			B4	1	0.5	-18.1221	NaN -18.1221 -20.4697 -22.8172 NaN NaN NaN NaN NaN NaN	NaN	-10.589	-19.31	-21.63	NaN	NaN	NaN	NaN	NaN	NaN	NaN	-13.384	-19.703	-21.424	NaN	NaN	NaN	NaN	NaN	NaN
			C4	1	0.5	-22.8172	NaN NaN -22.8172 -11.4086 0 NaN NaN NaN NaN NaN	NaN	NaN	-18.048	-5.0033	9.75913	NaN	NaN	NaN	NaN	NaN	NaN	NaN	-18.32	-6.7653	10.1452	NaN	NaN	NaN	NaN	NaN
			D2	1	0.6	0	NaN NaN NaN 0 0 0 NaN NaN NaN NaN	NaN	NaN	NaN	-0.9921	1.60021	5.383	NaN	NaN	NaN	NaN	NaN	NaN	NaN	-1.2159	1.47341	5.57162	NaN	NaN	NaN	NaN
						0	NaN NaN NaN NaN 0 -9.2214 -18.4429 NaN NaN NaN	NaN	NaN	NaN	NaN	-3.3104	-12.783	-19.334	NaN	NaN	NaN	NaN	NaN	NaN	-3.2066	-12.111	-18.165	NaN	NaN	NaN
			A1	3	0.6	-18.4429	NaN NaN NaN NaN NaN -18.4429 -9.2214 0 NaN NaN	NaN	NaN	NaN	NaN	NaN	-8.8771	-5.6987	-0.6463	NaN	NaN	NaN	NaN	NaN	NaN	-13.165	-6.3329	-1.3524	NaN	NaN
			A2	3	0.6	0	NaN NaN NaN NaN NaN NaN 0 -5.0011 -10.0021 NaN	NaN	NaN	NaN	NaN	NaN	NaN	-0.2729	-5.3484	-8.8444	NaN	NaN	NaN	NaN	NaN	NaN	-0.0315	-5.4616	-9.1669	NaN
			B1	3	0.6	-10.0021	NaN NaN NaN NaN NaN NaN NaN -10.0021 -5.0011 0	NaN	NaN	NaN	NaN	NaN	NaN	NaN	-13.307	-10.554	-10.698	NaN	NaN	NaN	NaN	NaN	NaN	-13.087	-11.387	-9.7143
			C3	3	0.55	0	NaN NaN NaN NaN NaN NaN NaN NaN 0 0	NaN	NaN	NaN	NaN	NaN	NaN	NaN	NaN	8.60167	8.18115	NaN	NaN	NaN	NaN	NaN	NaN	NaN	5.0269	4.62405
			D3	3	0.55																									
			A2	4	0.5																									
			A3	4	0.5																									
			C1	4	0.45																									
			C2	4	0.6																									
			C3	4	0.5																									
			D4	4	0.65																									
			A3	7	0.5																									
			B3	7	0.55																									
			B4	7	0.55																									
			B2	9	0.4																									
			B3	9	0.4																									
			C2	9	0.4																									
			C3	9	0.4																									

Structure #5

Case #	Wind		Damage			Stiffness Loss Matrix (%)																											
	Base	Dam	Location		DR	K Loss	SAP2000										ARMAX Analysis																	
			X-Y	Storey													0%										5%							
3	4	8	A1	1	0.6	-37.8101	-35.4662	-33.1223	NaN	NaN	NaN	NaN	NaN	NaN	NaN	NaN	-35.547	-31.564	NaN	NaN	NaN	NaN	NaN	NaN	NaN	NaN	-35.808	-32.054	NaN	NaN	NaN	NaN	NaN	NaN	NaN	NaN
			B1	1	0.6	-33.1223	-33.1223	-31.5620	-30.0018	NaN	NaN	NaN	NaN	NaN	NaN	NaN	-32.576	-31.902	-28.944	NaN	NaN	NaN	NaN	NaN	NaN	NaN	-34.011	-34.125	-31.5	NaN	NaN	NaN	NaN	NaN	NaN	NaN
			B3	1	0.65	-30.0018	NaN	-30.0018	-25.9365	-21.8712	NaN	NaN	NaN	NaN	NaN	NaN	NaN	-29.676	-23.71	-18.216	NaN	NaN	NaN	NaN	NaN	NaN	NaN	-29.933	-23.716	-18.271	NaN	NaN	NaN	NaN	NaN	NaN
			B4	1	0.55	-21.8712	NaN	NaN	-21.8712	-10.9356	0	NaN	NaN	NaN	NaN	NaN	NaN	NaN	-25.356	-9.3247	6.49605	NaN	NaN	NaN	NaN	NaN	NaN	NaN	-25.293	-9.5495	5.89688	NaN	NaN	NaN	NaN	NaN
			C1	1	0.6	0	NaN	NaN	NaN	0	-11.2518	-22.5036	NaN	NaN	NaN	NaN	NaN	NaN	NaN	-1.1323	-4.0862	-8.1973	NaN	NaN	NaN	NaN	NaN	NaN	NaN	-2.8227	-8.0646	-14.179	NaN	NaN	NaN	NaN
			C2	1	0.65	-22.5036	NaN	NaN	NaN	NaN	-22.5036	-20.4740	-18.4444	NaN	NaN	NaN	NaN	NaN	NaN	NaN	-19.993	-21.715	-21.758	NaN	NaN	NaN	NaN	NaN	NaN	NaN	-20.053	-21.448	-21.275	NaN	NaN	NaN
			C3	1	0.65	-18.4444	NaN	NaN	NaN	NaN	NaN	-18.4444	-18.5993	-18.7542	NaN	NaN	NaN	NaN	NaN	NaN	NaN	-18.418	-19.571	-19.519	NaN	NaN	NaN	NaN	NaN	NaN	NaN	-18.233	-18.49	-19.85	NaN	NaN
			C4	1	0.55	-18.7542	NaN	NaN	NaN	NaN	NaN	NaN	-18.7542	-9.3771	0	NaN	NaN	NaN	NaN	NaN	NaN	NaN	-22.01	-10.106	-1.0249	NaN	NaN	NaN	NaN	NaN	NaN	NaN	-23.503	-10.449	-1.1415	NaN
			D2	1	0.65	0	NaN	NaN	NaN	NaN	NaN	NaN	NaN	0	0	0	NaN	NaN	NaN	NaN	NaN	NaN	NaN	-2.4313	-5.435	-7.9204	NaN	NaN	NaN	NaN	NaN	NaN	NaN	-2.8772	-5.7672	-8.1392
			D4	1	0.55	0	NaN	NaN	NaN	NaN	NaN	NaN	NaN	NaN	0	0	NaN	NaN	NaN	NaN	NaN	NaN	NaN	NaN	-1.9336	-2.0374	NaN	NaN	NaN	NaN	NaN	NaN	NaN	NaN	-0.1765	-0.2131
			A1	2	0.6																														
			A2	2	0.6																														
			A4	2	0.6																														
			B2	2	0.55																														
			B3	2	0.55																														
			C3	2	0.65																														
			C4	2	0.65																														
			D1	2	0.55																														
			D2	2	0.55																														
			A2	3	0.55																														
			A3	3	0.55																														
			B3	3	0.6																														
			B4	3	0.6																														
			C1	3	0.5																														
			C2	3	0.5																														
			C3	3	0.5																														
			D3	3	0.5																														
			D4	3	0.5																														
			A3	4	0.6																														
			A4	4	0.6																														
			B2	4	0.6																														
			B3	4	0.6																														
			D1	4	0.55																														
			D2	4	0.55																														
			A2	6	0.5																														
			A3	6	0.5																														
			A4	6	0.5																														
			B2	6	0.45																														
			B3	6	0.45																														
			C3	6	0.6																														
			C4	6	0.6																														
			A1	7	0.45																														
			A2	7	0.45																														
			A4	7	0.45																														
			D1	7	0.4																														
			D2	7	0.4																														
			D3	7	0.4																														
			D4	7	0.4																														
			A2	8	0.5																														
			A4	8	0.5																														
			B3	8	0.4																														
			B4	8	0.4																														
			C1	8	0.4																														
			C2	8	0.4																														
			C3	8	0.4																														

Structure #6

Case #	Wind		Damage			SAP2000 Analysis		Stiffness Loss Matrix (%)					
			Location		DR					(Noise)			
	Base	Dam	X-Y	Storey		K Loss	Stiffness Loss Matrix (%)	K Loss	Std Dev	0%		5%		10%	
1	2	6	A1	1	0.6	-32.8197	-16.410 0 NaN NaN	-30.0344	0.6925	-14.2228 2.2743 NaN NaN		-14.2971 2.3093 NaN NaN		-14.2447 2.1110 NaN NaN	
			A2	1	0.65	0	-23.9152 -19.2030 -14.4907 NaN	1.4401	0.519	0.1483 0.1754 -0.3720 NaN		0.5710 0.1970 -0.5519 NaN		3.1496 0.1561 -1.3671 NaN	
			B2	1	0.6	0	NaN -14.4907 -7.2454 0	-1.4215	0.4741	NaN -2.3367 0.1969 -0.4057		NaN -2.2911 -0.0108 -0.8767		NaN -1.3304 0.5356 -0.4756	
			B3	1	0.55	0	NaN NaN 0 0	-0.5073	0.4331	NaN NaN -0.6479 -0.4817		NaN NaN -0.3718 -0.2735		NaN NaN 0.5261 0.5193	
			C3	1	0.55										
3	5	3	A1	1	0.6	-32.8197	-28.3675 -23.9152 NaN NaN	-37.3488	1.1634	-28.0745 -19.9333 NaN NaN		-27.6383 -19.4648 NaN NaN		-27.1791 -18.8838 NaN NaN	
			A2	1	0.65	-23.9152	-23.9152 -19.2030 -14.4907 NaN	-17.93	0.7242	-16.7993 -22.1695 -19.5188 NaN		-16.3911 -21.6866 -18.0338 NaN		-16.2322 -19.5751 -16.0566 NaN	
			B2	1	0.6	-14.4907	NaN -14.4907 -7.2454 0	-15.47	1.2282	NaN -12.6856 -6.8105 0.9974		NaN -12.9024 -5.6604 2.6006		NaN -12.6141 -6.6050 1.4335	
			B3	1	0.55	0	NaN NaN 0 0	1.08	0.8017	NaN NaN 2.1758 2.1624		NaN NaN 0.2528 0.3893		NaN NaN -3.4356 -3.0197	
			C3	1	0.55										
			A1	2	0.5										
			B1	2	0.5										
			A2	2	0.65										
			C3	2	0.5										
			B1	3	0.4										
			A2	3	0.45										
			B2	3	0.45										